Volume 20, Number 5
May, 1966

SOVIET ATOMIC ENERGY

АТОМНАЯ ЭНЕРГИЯ
(ATOMNAYA ÉNERGIYA)

TRANSLATED FROM RUSSIAN

c/b CONSULTANTS BUREAU

SOVIET ATOMIC ENERGY

Soviet Atomic Energy is a cover-to-cover translation of *Atomnaya Énergiya*, a publication of the Academy of Sciences of the USSR.

An arrangement with Mezhdunarodnaya Kniga, the Soviet book export agency, makes available both advance copies of the Russian journal and original glossy photographs and artwork. This serves to decrease the necessary time lag between publication of the original and publication of the translation and helps to improve the quality of the latter. The translation began with the first issue of the Russian journal.

Subscription
(12 Issues): $95

Single Issue: $30
Single Article: $15

Order from:

CONSULTANTS BUREAU
227 West 17th Street, New York, New York 10011

SOVIET ATOMIC ENERGY

A translation of *Atomnaya Énergiya*

Volume 20, Number 5 May, 1966

CONTENTS

CONTENTS

(continued)

NOTE

The Table of Contents lists all material that appeared in the original Russian journal. Items originally published in English or generally available in the West are not included in the translation and are shown in brackets. Whenever possible, the English-language source containing the omitted items is given.

The Russian press date (podpisano k pechati) of this issue was 5/14/1966. Publication therefore did not occur prior to this date, but must be assumed to have taken place reasonably soon thereafter.

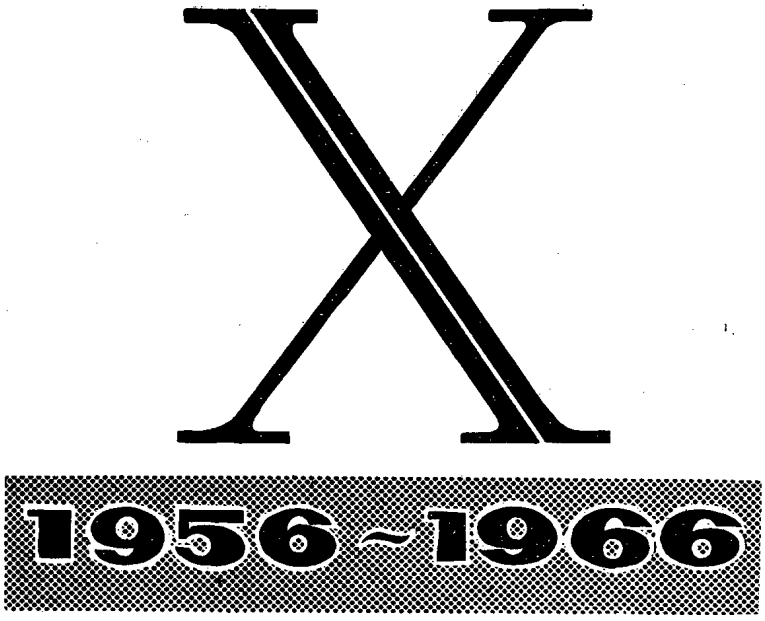

The periodical Atomnaya Énergiya is ten years old. It is only two years younger than the worldwide nuclear power industry itself. Its pages have reflected the progress of nuclear power—from 5000 kilowatts at the world's first power station to 10 million kilowatts, from laboratory experiments to completion of work on several types of scaled-up nuclear power installations competitive economically with "classical" electric power generating stations. The solution of the fundamental problem of fuel breeding, including Th and U^{238} in nuclear fuel and expanding fuel reserves a thousand-fold, is embodied in the Soviet Union, in the construction of a fast reactor with industrial power capability.

The third issue of our periodical (1956) published a report by Academician I. V. Kurchatov which set the basis for the wide-open worldwide discussion of work on controlled thermonuclear fusion of light elements. The periodical has shed light on the subsequent development of this work and the discussion of results of these endeavors at many international conferences. The complexity of the problem, obvious from the very outset, is now understood in a more concrete and more fundamental way. Even though the most optimistic forecasts have not been validated by the decade elapsed since then, confidence in ultimate success has broadened and gained strength.

The periodical's pages have also reflected achievements in the field of accelerator practice, nuclear chemistry, nuclear geology, the production and application of isotopes, radiation safety and health physics.

The volume of information published over the ensuing years since the start of our publication fills almost 1400 printing folios.

The editorial staff of the periodical takes this occasional to greet its contributing authors, readers, and all those involved in nuclear power and related fields of science and industry, and to wish them renewed creative successes accelerating technical progress.

Translated from Atomnaya Énergiya, Vol. 20, No. 5, p. 378, May, 1966.

ECONOMIC INCENTIVES IN THE NUCLEAR POWER FIELD

V. V. Batov and Yu. I. Koryakin

UDC 338.4:621.039.516

Payments on fixed productive capital and on circulating capital in nuclear power installations are reconsidered in the light of decisions adopted at the September (1965) Plenum of the Central Committee of the Communist Party of the Soviet Union. The discussion centers on circulating capital tied up in nuclear fuel procurement and inventory. Qualitative considerations on rates of payment for productive capital in nuclear power are outlined. Equations are derived for calculating the specific payment relating to reactor performance data.

The basic decision adopted at the September (1965) Plenum of the Central Committee of the Communist Party of the Soviet Union on payability of productive capital assigned to fuel-cycle enterprises prompts a review of these economic incentives within the context of the nuclear power picture. The decision on the quantitative value of profit write-off in budgeting, as related to the value of basic capital and circulating capital tied up in nuclear-fueled power generating stations and in other fuel-cycle installations, is of enormous importance for the nuclear power industry of the USSR, and especially for nuclear electric power stations producing marketable electric power and characterized by certain specific costs features. These costs features are determined primarily by the familiar economic dualism inherent in fuel inventorying which exhibits certain features of fixed capital on the one hand, viz., in the way it functions (in view of the long operating period T_k/φ where T_k is the length of the reactor run, φ is the utilization factor of the power station installed capacity), and the cost (reaching 40% of the direct capital investments in nuclear power stations), and on the other hand exhibits certain features of circulating capital, viz. in the way costs are assigned to the salable commodity (electric power) over the production period and the uncompleted nature of the production (the spent fuel serves as a semifinished product useful for further production operations, in view of the fissionable isotopes remaining and accumulated in the fuel). Nevertheless, assigment of fuel inventory to circulating capital (i.e., long-term circulating capital) would still be a more correct procedure, especially if we bear in mind that, in contrast to the fixed capital tied up in the nuclear generating station, the fuel inventory is essentially a less conservative item in its initial cost relationship as a part of the nuclear power station, compared to other parts and components of the power station, and the fact that fuel inventory value is capable of a wide range of variation during the operating process. In effect, nuclear power development practice has demonstrated that there is not a single operating power reactor in which each subsequent fuel inventory did not differ markedly from its predecessors in regard to engineering costs. Moreover, the fuel inventory is such a flexible and dynamic part of the reactor picture that its costs characteristics vary markedly even during the fuel dwell time in the reactor (during the reactor run). A highly intriguing and unique property of the fuel inventory, in the costs sense, a property bearing little resemblance if any to other forms of production, is its ability in certain cases (as for instance in fast breeders) to increase in value over the initial cost during a single reactor run. This can of course be held accountable to the buildup of secondary fissionable material of high power-producing value. A consequence of this property of the fuel inventory is, in some instances, the approximation of the fuel components of the nuclear power generating costs to zero or even the appearance of a paradoxical negative fuel component in the nuclear electric power generating costs.

Without wishing to prejudge the question of payments on the fuel costs, we can nevertheless state that a contribution to the correct solution of this problem will be made by an objective understanding of the effectiveness of utilizing the circulating capital invested in the fuel inventory.

The values of the nuclear fuel on hand at a nuclear power station account for most of the power station circulating capital. The circulating capital associated with the fuel inventory includes the value of fresh fuel (in the form of hot channels, fuel assemblies, fuel clusters, fuel elements, etc.), and the value of the nuclear fuel after drainage from the reactor and core reloading, to be regarded in fact as a semifinished product for further reprocessing

Translated from Atomnaya Énergiya, Vol. 20, No. 5, pp. 379-384, May, 1966. Original article submitted January 29, 1966.

(fuel recovery). This article considers only that portion of the power station operating capital which is tied up in the fuel inventory.

At the present the accepted criterion for the economic effectiveness of fixed capital is given by what we term the calculated expenditures Z, defined as

$$Z = C + E_n K, \tag{1}$$

where C is the net cost; E_n is the standard economic effectiveness factor of the fixed capital; K is the fixed capital.

An attempt to take into account that portion of the surplus labor corresponding to social expenditures made in the production of the end commodity is undertaken by adding the $E_n K$ term to the net generating cost. The use of the calculated expenditures category as a criterion for the economic effectiveness of nuclear fuel utilization leaves room for a more correct evaluation of the costs savings achievable than the use of the net cost category alone.

It is generally acknowledged that one of the basic tendencies in current power reactor design is the constant striving to increase nuclear fuel burnup, resulting in a lower fuel costs component C_T as part of the total net generating costs; the fuel component is related to the average burnup $\bar{B}$ as:

$$C_T \sim \frac{\sum_i C_i}{\bar{B}\eta}, \tag{2}$$

where η is the net efficiency of the nuclear power stations; $\sum_i C_i$ is the sum of the fuel cycle costs (planned profits not taken into account).

As a rule, increased burnup of nuclear fuel realizable by way of improvements in the fabrication technology of fuel elements and improved durability of fuel elements is brought about by increasing the initial fuel enrichment. This, plus certain additional expenditure involved in routinizing the fabrication technology of improved fuel elements and in designing additional excess reactivity compensating facilities leads to a higher cost of the new fuel charges, which can amount to rather considerable sums in some instances. This raises the question of whether any and every lowering of the fuel component in the electric power generating costs at a nuclear power station will prove economically effective. Currently available procedures [1] indicate that lowering net generating costs (in the specific case of the fuel component of the electric power generating costs) is economically effective only in the case where the size of the cost drop ΔC_T obeys the constraint

$$\Delta C_T \geqslant E_n \Delta K_{fi}, \tag{3}$$

where ΔK_{fi} is additional operating capital invested in the fuel inventory.

It would be ill advised to base the approach solely on lowering the fuel component of the generating costs at a nuclear power station, since in that case the monetary expression of the fuel component would end up expressing nothing more than specific expenditures in means of production and in the necessary labor expended in the fuel cycle, and would not reflect labor expenditures in the production of the surplus product for social use. A part of the surplus product previously made available to society and directed to the production of new surplus product constitutes productive capital, as we known from economic theory, but in this concrete case it refers to the additional circulating capital invested in the fuel inventory. In this instance the standard economic effectiveness factor E_n expresses the ratio of the surplus product involved in the use of nuclear fuel to the value of the surplus product, at the given moment. In other words, the economic category of the fuel component of calculated expenditures on electric power generation [2] takes into account the addition to the fuel component of the electric power generating costs of the value of precisely that surplus product in the fuel cycle (expressed in money terms) which is formed per unit electric power generated at the nuclear power station.

A part of the surplus product finds a real monetary expression, with the introduction of the concept of payment of productive capital. Since the rate of payment for the use of productive capital will reflect only the value of a part of the surplus product, the sum of the generating costs and rate of payment for the use of productive capital cannot be regarded as a necessary and sufficient criterion of economic effectiveness.

Nevertheless there are some engineering costs problems in which this sum does constitute a necessary and sufficient criterion of economic effectiveness. Here, we have in mind all optimization problems in which only the basic productive capital and the circulating capital vary, other conditions being equal.

Setting a scientifically justified payment rate for both fixed capital and circulating capital in a nuclear power plant is a matter acquiring fundamental importance. In the view of the present authors, the rate of payment in the nuclear power industry must be arrived at on the basis of two factors: the relative capital consumption in production and the interchangeability of nuclear-fuel and fossil-fuel electric power generation. We know that nuclear electric power has been called upon to replace "conventional" or fossil-fuel electric power primarily in those districts of the USSR where this is most feasible, i.e., in the European sector of the USSR. In addition, studies carried out in the USSR indicate that the relative capital consumption of nuclear and fossil-fuel power generation (on the scale of several tens of millions of kilowatts) is about on the same level in those districts [3]. This means that the rate of payment of fixed capital in the nuclear power industry must be the same as (or at least not below) the rate prevailing in the fossil-fuel and hydroelectric sector. The high relative capital consumption of production typical of nuclear and conventional power generation possibly calls for a rate of payment on fixed capital lower than that set for branches of the national economy which eat up less capital. On the whole, however, it is worth noting that the question of whether the capital payments can be written off on the basis of unit rates or differentiated rates requires further discussion.

Of course, the rate of payment on fixed capital cannot be viewed as invariant in the nuclear power industry. With growth in technical process and changes in payment on fixed capital, the rate of payment will have to be reviewed periodically, remaining constant over each planning period in nuclear power development. It is indicated in the proceedings of the September (1965) Plenum of the Central Committee of the Communist Party of the Soviet Union that payment on capital purports to be a crucial part of the state budget revenues.

The rate of payment on circulating capital in the nuclear power industry is a question meriting special attention. The overwhelming bulk of the circulating capital in nuclear power is the value of the nuclear fuel on hand. While the amount of operating capital tied up in fuel inventory in a modern coal-fired electric power generating station is no greater than 1-2% of the fixed productive capital of the power station, in the case of nuclear power stations the amount of operating capital tied up in fuel inventory can run to 20-40% of the power station fixed capital assets. In addition, for a number of obvious reasons the rate of turnover of capital tied up in conventional fuel, or the rate of turnover of any other forms of operating capital, runs tens of times higher than the rate of turnover of the working capital tied up in fuel procurement and fuel inventory for nuclear power generating stations.

This means that the circulating capital tied up in fuel inventory for nuclear power stations shares certain common features with basic fixed capital, both in the relative size and in rate of turnover. These features must govern the approach to setting the standard rate of payment for the use of nuclear fuel. In the view of the present authors, the rate of payment must be set close to the rate of payment on fixed capital in the nuclear power industry, and in any case must be not lower than the rate of payment for conventional circulating assets.

It is clear that the payment on the use of nuclear fuel must be collected during the time the fuel is still in the fuel cycle. The rate of payment must be assumed unitary for all links in the fuel cycle over a sufficiently long time interval (not less than three to five complete periods of the fuel cycle, or about two decades). Hence, the introduction of a unit rate of payment for the use of nuclear fuel covering an entire branch of the national economy (those enterprises involved in the fuel cycle) will provide an incentive for the routinization and use of those technological methods of nuclear fuel reprocessing which provide the least residence time of the fuel in all links of the fuel cycle (from the standpoint of hitting upon a method of spent fuel recovery which would be preferable, for example a method requiring no previous protracted radiation cool-down of the spent fuel elements). In a formal sense, we could set a unit rate of payment for the use of nuclear fuel based on the assumption that the circulating capital (price of the fuel inventory) is paid out over the fuel cycle duration, and since the terminal useful product of the nuclear power industry is electric power, payment for the use of nuclear fuel over the entire fuel cycle would be included in the cost of electric power delivered by the nuclear power generating station.

We see readily that if this payment is to be collected solely from the nuclear power station, all the remaining enterprises involved in the fuel cycle will be indifferent to accelerated conversion of the nuclear fuel in the fuel cycle. Further, in that case, uneven consumer costs in the fuel inventory will be levelled out in the various links of the fuel cycle. Despite the unequal amounts of valuable products embodied in a unit of spent fuel, and the cost of extracting them, the payment for the time of residence of the fuel in the fuel cycle will be determined by the cost of fresh fuel, and this is wrong. It obviously makes no difference for society as a whole whether the cost of the spent fuel is realized or not. In other words, for the state as a whole any nuclear power station is in essence always seen as at least a dual-purpose utility. The cost of the nuclear fuel varies as it moves through the fuel cycle. As the nuclear raw materials are converted to fuel elements (reactor channels), the cost of reprocessing will be added to the

cost of the nuclear raw materials in all links of the fuel cycle. It is typical of the utilization of fuel in nuclear power stations that the spent fuel always has a certain finite value and, in some instances (this should be stressed), this value can be higher than the initial value, or higher than the value of fresh fuel.*

If the average value of the nuclear fuel in the i-th link in the fuel cycle is denoted as $\bar{C}_i$ (in rubles per kg U), then the total specific charge for use of the fuel (during the fuel cycle) can be expressed as

$$P = p_t \sum_i \bar{C}_i T_i \text{ rubles/kg U}, \tag{4}$$

where P_t is the standard effectiveness factor for circulating capital tied up in nuclear fuel, or the payment rate for the use of nuclear fuel, in units per year; T_i is the holdup time of the fuel in the i-th link of the fuel cycle.

The unique rate of payment for the use of nuclear fuel in all links of the fuel cycle is a precondition, in the view of the present authors, for economic stimulation of the nuclear power industry. The optimum performance of individual enterprises involved in the fuel cycle in the nuclear power industry must be determined by the optimum performance of the fuel cycle taken as a whole (the optimum performance of the entire branch of industry). The introduction of a single payment rate for the use of nuclear fuel in all links of the fuel cycle is, therefore, a precondition for economic incentives to speed up the movement of fuel through the fuel cycle. Additional holdup of nuclear fuel, e.g., values at K rubles over a time of T years in any link in the fuel cycle, will have to be expressed in a surcharge amounting to P_tKT rubles.

If the amount of fuel on hand in the reactor is G† (kg U per reactor), then the total budget deductions for the use of nuclear fuel by enterprises involved in the fuel cycle (during the fuel cycle) will be

$$P_p = p_t G \sum_i \bar{C}_i T_i \text{ rubles/reactor}. \tag{5}$$

The charges accruing to the nuclear power station in that sum come to

$$P_{NPS} = p_t G \bar{C}_{NPS} T_{NPS} \text{ rubles/reactor}. \tag{6}$$

This raises the question of how budget deductions should be related to a given level of circulating assets tied up in nuclear fuel, i.e., what should be considered the average value $\bar{C}_{NPS}$ of the nuclear power station fuel inventory over the in-pile residence time of the fuel.

Since only the initial and final states of the nuclear fuel are realized from the standpoint of consumer value, the average value of the fuel inventory during the in-pile residence time must be taken as the arithmetic-mean value of its initial and final values:

$$\bar{C}_{NAS} = \frac{1}{2}(C_{fr.f} + C_{sp.f}) \text{ rubles/kg U}, \tag{7}$$

where $C_{fr.f}$ is the value of the fresh fuel in the form of fuel elements (hot channels, in rubles per kg U); $C_{sp.f}$ is the value of the spent fuel, or the value of the fuel remaining or accumulated after holdup charges, transportation charges, and nuclear fuel reprocessing charges have been deducted, and with losses due to freezing of assets in these links of the fuel cycle, in rubles per kg U, taken into account. $C_{sp.f} \geq 0$ of course in every case, since if the holdup, transportation, and spent-fuel recovery charges were greater than the cost of the extracted and reprocessed fuel, then fuel recovery would be economically unfeasible.

This means that the result of the cost calculations is independent of the variation pattern of cost indices of the fuel inventory during the reactor run, which is to be determined by the special features of the processes taking place in the reactor. Only the initial and final values of the fuel inventory cost are important.

*E. g., fuel located in the shields of fast reactors.

†Added to the necessary reserves of fuel stocks on hand at the nuclear power generating station.

In particular cases where there is complete burnup of the nuclear fuel (if the innumerable value fission fragments or radioactive isotopes are neglected) or where there is no recovery of spent fuel (the consumer value of the spent fuel will be zero in that case)

$$_{\text{NPS}} = \frac{1}{2} C_{\text{fr.f}} \text{ rubles/kg U.} \tag{8}$$

Since the time the fuel is in the reactor is related to the reactor run by the formula

$$T_{\text{NPS}} = T_{\text{к}}/\varphi,$$

the nuclear power station payment for the use of nuclear fuel is given by the formula

$$P_t = \frac{1}{2} p_t G (C_{\text{fr.f}} + C_{\text{sp.f}}) \frac{T_{\text{к}}}{\varphi} \text{ rubles/reactor.} \tag{9}$$

The variable P_t characterizes that part of the surplus product created by the nuclear power station labor force and associated with the use of the power station nuclear fuel inventory over a period of T_k/φ years.

The value (cost) of the electric power generated by the nuclear power station during the run must therefore include payment for the use of circulating capital tied up in the fuel, to the extent indicated by formula (9). The size of the specific payment (payment per kilowatt-hour of electric power delivered to consumers) is

$$P_t = \frac{100 p_t}{8760 \varphi \bar{J}_{\text{eff}} \eta} \cdot \frac{C_{\text{fr.f}} + C_{\text{sp.f}}}{2} \text{ kopecks/kW} \cdot \text{h,} \tag{10}$$

where $\bar{J}_{\text{eff}}$ is the average specific fuel irradiation at the power station, including the required fresh fuel reserves, or the effective average specific irradiation of the fuel, in kW(th) per kg U.

If reserves of fresh fuel sufficient to fuel the power station on full power for t_{res} years are on hand at the power generating station, then

$$\bar{J}_{\text{eff}} = \bar{J} \left(1 + \frac{\varphi t_{\text{res}}}{T_{\text{к}}}\right)^{-1}, \tag{11}$$

where $\bar{J}$ is the average specific irradiation of the fuel present in the reactor.*

We realize from formula (10), that the size of the payments must be inversely proportional to the utilization factor of the nuclear power station installed plant capacity, the effective average specific irradiation of the nuclear fuel, the thermodynamic efficiency of the nuclear power station, and directly proportional to the average value of the fuel present at the nuclear power station, when we introduce the concept of payability of circulating assets.

Remember that the size of the fuel component in the electric power generating costs figured for the nuclear power station is expressed in the general case by the formula

$$C_{\text{т}} = \frac{100}{24} \cdot \frac{C_{\text{fr.f}} - C_{\text{sp.f}}}{\bar{B}\eta} \text{ kopecks/kW} \cdot \text{h.} \tag{12}$$

i.e., in contrast to the payment for the use of nuclear fuel, the fuel component in the electric power generating costs is inversely proportional not to the effective fuel irradiation (10), but to the fuel burnup. The difference in the values of the fresh fuel and spent fuel is transferred to the electric power value in this case.

The sum of the fuel component in the electric power generating costs and the payment for the use of circulating capital tied up in nuclear fuel inventory is given, hence, by the formula

*In this case we ignore any spent fuel present at the power station, since the spent-fuel storage basin built for spent fuel holdup can be viewed in principle as an independent enterprise participating in the fuel cycle in its own right, sharing the same premises as the nuclear power generating station proper.

$$C_{\text{T}}^{*}=\frac{100}{24}\cdot\frac{C_{\text{fr.f}}-C_{\text{sp.f}}}{\bar{B}\eta}+$$
$$+\frac{100p_{\text{t}}}{8760\varphi\bar{J}_{\text{eff}}\eta}\cdot\frac{C_{\text{fr.f}}+C_{\text{sp.f}}}{2}, \tag{13}$$

which reduces to

$$C_{\text{T}}^{*}=\frac{100}{24\bar{B}\eta}\left[(C_{\text{fr.f}}-C_{\text{sp.f}})+\right.$$
$$\left.+p_{\text{t}}\left(\frac{T_{\text{K}}}{\varphi}+t_{\text{res}}\right)\frac{C_{\text{fr.f}}+C_{\text{sp.f}}}{2}\right], \tag{14}$$

where $\bar{B}$ is the average fuel burnup, in kW(th)days/kg U.

The most efficient (optimum) utilization of the nuclear fuel corresponds to the minimized C_{T}^{*} in problems in which variations in the payroll and fixed productive capital can be safely neglected. The optimum utilization of nuclear fuel is achieved when the independent nuclear power station parameters are optimized, in which case the equations

$$\frac{\partial C_{\text{T}}^{*}}{\partial x_i}=0 \qquad (i=1, 2, \ldots, n), \tag{15}$$

where n is the number of independent nuclear power station performance parameters, are satisfied.

It is important to emphasize the fact that conditions (15) are valid (to a sufficient degree of exactness in most cases) only when a variation of the core parameters does not entail any variation in other performance characteristics of the nuclear power station (and, hence, does not entail any further expenditures).

In the most general case (this applies to problems in which payroll variations can be neglected), optimality conditions for the independent parameters can be stated in the form of a system of equations

$$\frac{\partial C^{*}}{\partial x_i}=0 \qquad (i=1, 2, \ldots, n), \tag{16}$$

where $C^{*} = C + P$; C is the generating cost of the electric power delivered to the consumers; P is the payment for the use of the nuclear power station fixed capital and circulating capital.

In the most general case, finally, the optimality condition of the independent power station performance parameters is stated in the form of a system of equations

$$\frac{\partial P_{\text{W}}}{\partial x_i}=0 \qquad (i=1, 2, \ldots, n), \tag{17}$$

where P_{W} is the wholesale price of the electric power generated.

It is readily seen that conditions (15) and (16) are particular cases of the general condition (17), since the wholesale price is made up of the generating costs and the surplus product, one part of which is calculated as proportional to the payroll, the other part as proportional to the productive capital.

Strictly speaking, as a consequence of the fact that the basic or independent performance parameters of nuclear power generating stations are quasi-independent, practical optimization of the cost indices of nuclear power stations is an exceedingly complicated and cumbersome undertaking, but nevertheless a crucially important one, the solution of which could yield important benefits to the national economy. The development of optimization techniques, one of the most important problems in nuclear power work, is particularly needed under present conditions where transitions to new techniques of economic management are in progress.

The introduction of payability of productive capital is an important economic incentive for more rational use of nuclear fuel in the fuel cycle, and smoothes the way for a new and more profound review of fuel cycle economics.

Such important questions as optimum time of introduction and productivity of enterprises participating in the fuel cycle can be solved with economic benefits only by taking the payability of productive capital into account. On comparing various types of reactors, we see that the circulating capital tied up in the formation of secondary nuclear fuel takes on the role of a factor displacing capital investments into the mining industry and to a partial extent into uranium reprocessing plants incorporated in the fuel cycle. Hence, the mathematical tools for investigating the comparative economic effectiveness different reactor types can include concepts of negative capital investments, and the introduction of the payability concept makes it possible to gain a correct understanding of the economic significance of the rate of turnover of recovered fuel.

The present article of course makes no pretense to an exhaustive coverage of the entire scope of topics arising in nuclear power economics with the introduction of payability of fixed productive capital and circulating assets. The utilization of this economic incentive, combined with others such as profit incentives which take into account some natural conditions (alienation of territories for nuclear power station construction sites and for other fuel-cycle operations), can bring about a change in concepts held on the economic indices of nuclear power, and will, therefore, require further study.

LITERATURE CITED

1. Basic Techniques for Power Engineering Costs Calculations [in Russian], Moscow, State Tech. Lit. Press (1959).
2. Yu. I. Koryakin, V. V. Batov, and V. G. Smirnov, Atomnaya énergiya, 17, 94 (1964).
3. N. M. Sinev, B. B. Baturov, and V. M. Shmelev, Third Geneva International Conference on the Peaceful Uses of Atomic Energy, Paper No. 294 (1964).

HEAVY-CURRENT ACCELERATOR BASED ON A TRANSFORMER

E. A. Abramyan and V. A. Gaponov

UDC 621.384.60

The operating principles of a direct-action accelerator designed to accelerate electrons to an energy of 1.5 MeV with a mean beam power of tens of kilowatts and an efficiency of around 90% are described. The electron–current pulse length can be varied from 0 to 5 msec, and the repetition frequency up to 50 times per sec. The mean current i_m may reach 1/6 of the maximum current in the pulse. Magnetic lenses are installed in order to focus electron currents of up to 100 mA into a beam a few mm in diameter in the accelerating tube. Heavy-metal screens are placed close to the axis of the tube in order to protect the gas gaps and other electrically-stressed parts of the accelerator from radiation arising inside the tube.

The construction of a system for producing an electron beam with an energy of 1.5 MeV and a mean power of 25 kW (i_m = 17 mA) is described.

Accelerators producing 1 MeV electrons and upward find wide application in both physical investigations and various applied systems. Accelerators are used as radiation sources in chemistry, for the sterilization of medical appliances, and for the conservation of products. Electron beams with energy densities of tens of kW/cm^2 enable melting, welding, and other metal-treatment processes to be carried out. For energies of many hundreds of keV, the electrons can be brought out of the vacuum chamber in which acceleration takes place and used in air or an inert-gas medium at atmospheric pressure or higher.

In 1963, on the initiative of G. I. Budker, in the Institute of Nuclear Physics of the Siberian Branch of the Academy of Sciences, USSR, work was begun on setting up a high-efficiency, high beam-power accelerator for applied purposes. Of the many known and possible means of accelerating charged particles, acceleration by means of a transformer [1] was selected. In 1964, the first experimental ÉIT-1.5 apparatus was constructed and prepared, this being an electron transformer for accelerating electrons to energies of 1.5 MeV. We here present the main components of the apparatus and its operating principles.

Arrangement of the Apparatus

The main constructional arrangement of the apparatus is shown in Fig. 1. The primary winding of the transformer, 1, and a section of the secondary winding, 2, are placed coaxially. The central part of the magnetic circuit consists of individual, mutually-insulated discs 3, and is completed on the high-voltage side by the head 4. The magnetic flux also passes through the outer components 5, 6, 14 of the magnetic circuit and through the base 16. Sections 2 are connected in series (every two sections fixed to a disc 3), and the middle point of two neighboring sections is electrically connected to the disc. The accelerating tube 8 is mounted on the transformer and its electrodes are connected to the discs 3. The injector 10 has a control electrode 9, which enables the electron current through the tube to be varied as far as complete cutoff. Heating of the cathode and the voltage on the control electrode are provided by the injector supply system 11, fed from coil 7, which forms part of the secondary winding. Capacity divider 13 serves to regulate the voltage on electrode 9. In addition to the control system, the head 4 carries a condenser battery 12 connected to coil 7 (the purpose of the condensers will be explained in a moment). The whole transformer is placed in the vessel 15, filled with compressed gas. The vacuum pump 17 ensures a vacuum of 10^{-5} to 10^{-6} mm Hg in the tube. For scanning the beam and releasing electrons into the atmosphere, we have a magnet 18 and a "trumpet" 19 carrying a foil. The dimensions and position of the beam are determined by probes 21, and the current is measured with a screened Rogowski belt 20.

Operating Principles and Characteristics of the Transformer

Figure 2 shows the equivalent circuit of the transformer, where L is the inductance of the transformer, L_{Is} is the stray inductance of the primary winding, C is the total capacity of the transformer, and R_L is the load resistance.

Translated from Atomnaya Énergiya, Vol. 20, No. 5, pp. 385-392, May, 1966. Original article submitted January 25, 1966.

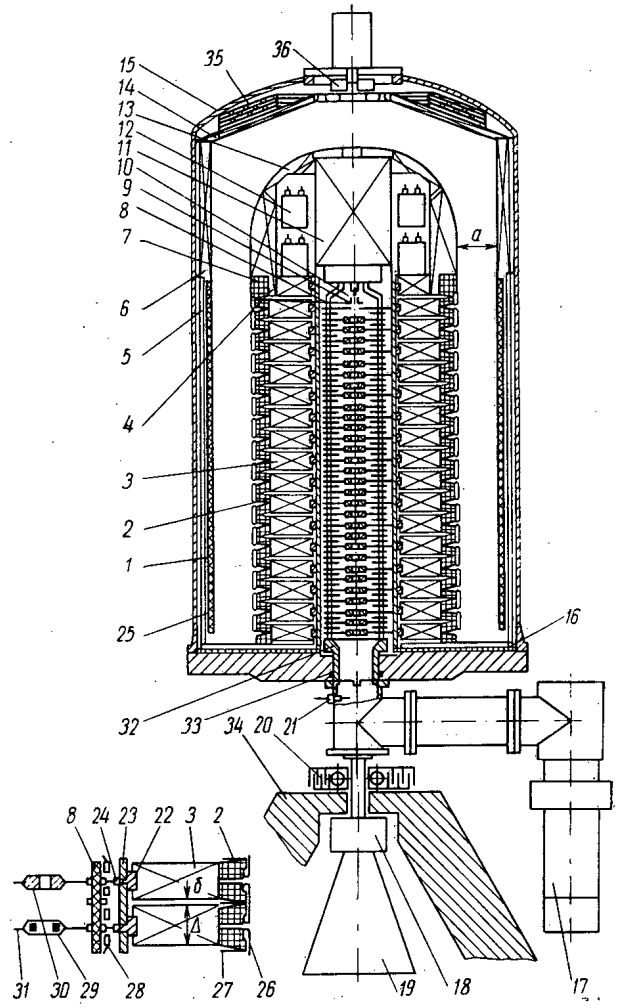

Fig. 1. Construction of the apparatus. 1) Primary winding of the transformer; 2) section of secondary winding; 3) disc of magnetic circuit; (head); 5, 6, 14) components of magnetic circuit; 7) head coil); 8) accelerator tube; 9) control electrode; 10) injector; 11) injector supply system; 12) condenser battery; 13) capacitive element of head; 15) vessel; 16) principal magnetic circuit; 17) vacuum pump; 18) rotating magnet; 19) "trumpet" with outlet window; 20) Rogowski belt; 21) probe; 22) copper rings; 23) support cylinders; 24) elastic contacts of accelerator tube; 25) primary-winding screen; 26) screen for section of secondary winding; 27) protective discharge tubes; 28) ohmic divider; 29) magnetic lenses; 30) radiation screens; 31) electrodes of accelerating tube; 32) ball-bearing support for tube; 33) tube sealing; 34) radiation shield; 35) cooling radiator; 36) ventilator.

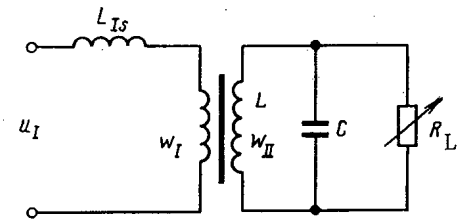

Fig. 2. Simplified transformer circuit: L = transformer inductance; L_{Is} = stray inductance of primary winding; C = capacity of transformer, R_L = load resistance.

Let us consider the case in which the power lost in the transformer is much smaller than the useful power $\bar{P}$. Let us also suppose that the natural frequency of the LC circuit equals the frequency of variation of the voltage u_I applied to the primary winding. As already indicated, thanks to the presence of a control electrode on the injector, the current through the tube can be zero even in those half-periods in which the polarity of the voltage on the secondary winding corresponds to acceleration of the electrons (minus on the high-voltage end of the tube). While there is no current in the tube, the transformer operates under no-load conditions and the current i_I in the primary winding is

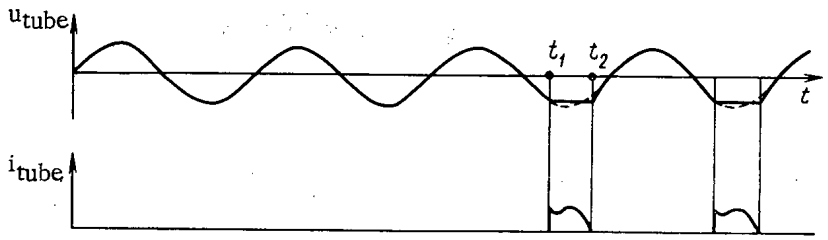

Fig. 3. Voltage and current variation in tube: u_{tube} = voltage on accelerating tube; i_{tube} = current of accelerated electrons.

small. Let us suppose that the control electrode begins to open at a moment t_1 (Fig. 3). It is easily seen that, for a particular law of variation of the current i_{tube} in the accelerating tube, the voltage u_{tube} on the latter may remain constant. Let us call w_I and w_{II} the number of turns in the primary and secondary windings and $k = w_I/w_{II}$ the transformation factor; then for the time interval $t_1 < t < t_2$ we may write: $u_{Im} \sin\omega t = L_{Is}(di_I)/dt + ku_{tube}$. Integrating both sides of the equation, putting u_{tube} = const, and considering that $u_{im}/k = u_{IIm}$, we obtain

$$i_I = u_{tube}\frac{k}{L_{Is}}\left[\frac{u_{IIm}}{\omega u_{tube}}(\cos\omega t_1 - \cos\omega t) - (t - t_1)\right]. \tag{1}$$

During the time $t_1 < t < t_2$, the voltage in the inductance L is also constant $L(di_L)/dt = u_{tube}$, whence, the current in the inductance is $i_L = u_{tube}/L(t-t_1) + i_L(t_1)$. The value of $i_L(t_1)$ can be found by considering the no-load condition:

$$L\frac{di_L}{dt} = u_{IIm}\sin\omega t; \quad i_L(t_1) = -\frac{u_{IIm}}{\omega L}\cos\omega t_1.$$

For constant voltage on the capacity C, the current $i_C = 0$, and the current in the tube $i_{tube} = ki_I - i_L$. Denoting $u_{tube}/u_{IIm} = \sin\omega t_1 = \alpha$ and $L_{Is}/L = \nu$, we obtain

$$\begin{aligned} i_{tube} = \frac{u_{IIm}}{\omega L_{Is}}&[(k^2+\nu)\cos\omega t \\ &-\alpha\omega(k^2+\nu)(t-t_1) - k^2\cos\omega t]. \end{aligned} \tag{2}$$

For $i_{tube} = 0$, at the moment t_2, Eq. (2) takes the form

$$\begin{aligned} (k^2+\nu)\cos\omega t_1 - \alpha\omega(k^2+\nu)(t_2-t_1) \\ -k^2\cos\omega t_2 = 0. \end{aligned} \tag{3}$$

We may find t_2 from Eq. (3).

The mean power in the beam $P = fu_{tube}\int_{t_1}^{t_2} i_{tube}dt$, or

$$\begin{aligned} \overline{P} = \frac{u^2_{tube}}{2\pi\alpha L_{Is}}&\left[(k^2+\nu)(t_2-t_1)\cos\omega t_1\right. \\ &\left.-\frac{\alpha\omega}{2}(k^2+\nu)(t_2-t_1)^2 - \frac{k^2}{\omega}(\sin\omega t_2 - \sin\omega t_1)\right]. \end{aligned} \tag{4}$$

The formula obtained in P is approximate and reflects the qualitative dependence of useful power on the pulse length $t_2 - t_1$, the stray inductance L_{Is}, and the ratio $\nu = L_{Is}/L$. A more exact relationship between P and all the parameters in the steady-state condition, allowing for the distributed parameters of the transformer, was found from models. For the apparatus described in this paper P = 25 kW for $t_2 - t_1$ = 5 msec, $L_{Is} = 4.6 \cdot 10^{-4}$ H, L = 40,000 H and $\nu = 1.15 \cdot 10^{-8}$.

The method here considered for keeping a constant voltage on the tube by controlling the tube current may also be used in order to produce any other desired form of voltage, $u_{tube}(t)$, by due choice of the law governing the variation of i_{tube} during the pulse.

As indicated earlier, the natural frequency of the circuit was chosen to be equal to that of the voltage supplying the transformer. Thus, for the apparatus here described $f = \frac{1}{2\pi\sqrt{LC}} = 50$ cps, and the supply for the primary winding is taken directly from the mains.

In order to ensure constancy of the electric-potential gradient along the central part of the magnetic circuit, the number of ampere turns in each air (or more strictly gas) gap should be proportional to the corresponding magnetic resistance $R\left(R_i = \frac{l_i}{\mu_i S_i}\right)$. There are two sections 2 in each gap δ between the discs (see Fig. 1). The gap between the highest disc and the head 4 is half as wide and, therefore, contains only one section 2. The same holds for the gap between the lowest disc and the base of the magnetic circuit 16. The ratio of the number of ampere turns in coil 7 to the total number in all the sections equals $R_a/16R_\delta$, where R_a is the magnetic resistance of section a to which the whole voltage is applied, and R_δ is the magnetic resistance of the gap δ between discs. The equivalent circuit of the magnetic system with the secondary winding is shown in Fig. 4, where $\mathcal{E}$ and e are the number of ampere turns on the coil 7 and section 2 respectively. On the basis of the condition that there should be approximately the same electric field in the gas gaps, the value of a equals the sum of all the interdisc gaps (or a little more than this), so that $R_a \gg R_\delta$. The peak value of the ampere turns in coil 7 is $i_{7m}w_7 = \Phi_m R_a$, where Φ_m is the amplitude of the principal flux. In order to ensure the necessary calue of $i_{7m}w_7$ for a relatively small voltage, a current several orders larger than that passing through sections 2 is passed through the turns of coil 7. In order to obtain the desired value of i_{7m}, a condenser battery 12 is connected to coil 7; the capacity of the battery is determined from the relation $C_{12} = \frac{i_{7m}}{\omega u_{7m}}$, where $u_{7m} = u_{IIm}\frac{w_7}{w_{II}}$. On satisfying these conditions, the amplitudes of the magnetic energy in the gap a and the electric energy in the capacity 12 will be equal, which follows from the identity existing between the conditions $i_{7m}w_7 = \Phi_m R_a$, $i_{7m} = \omega C_{12} u_m$ on the one hand and $C_{12}\mu_{7m}^2 = \Phi^2_m R_a$ on the other.

One of the peculiarities of the transformer described is the large number of gaps in the magnetic circuit. It is easy to show that this arrangement will have a maximum Q factor for a certain ratio δ/Δ, where Δ is the height of the discs 3. As we know, the Q factor is determined from the relation $Q = P_r/(P_c + P_s)$, where P_r is the reactive power of the transformer, and P_c and P_s are the copper and steel losses respectively. If the operating frequency, the magnetic-circuit material and the material of the windings, and the dimensions of the magnetic circuit (over-all length and cross section at each point) are given, then

$$P_r = k_1 \frac{i_L^2}{R}, \quad P_c = k_2 i_L^2 \text{ and } P_s = k_3 \frac{i_L^2}{R^2},$$

where $R = \sum \frac{l_i}{\mu_i S_i}$ is the total magnetic resistance (reluctance), and k_1, k_2, and k_3 are coefficients constant under the given conditions. It follows from this that

$$Q = \frac{k_1 R}{k_2 R + k_3}. \tag{5}$$

We see from Eq. (5), that Q is a function of the magnetic resistance of the circuit, R. From the condition $dQ/dR = 0$ we find the value of $R^* = \sqrt{\frac{k_3}{k_2}}$, corresponding to maximum Q factor of the transformer. The values of δ and Δ, giving $\sum \frac{l_i}{\mu_i S_i} = R^* = \sqrt{\frac{k_3}{k_2}}$, are easy to calculate. It is not difficult to see that for $R = R^*$ we have $P_c = P_s$, i.e., when the losses in the windings and in the steel of the transformer are equal the Q factor reaches its maximum.

Thus, in the apparatus here described the size of the gaps δ between the discs is determined by the electric strength required and by the condition corresponding to maximum Q factor.

Parameters of the ÉlT-1.5

Before describing the structural characteristics of the ÉlT-1.5 accelerator, let us give its principal parameters:

Supply voltage of primary winding	220/380 V, 50 cps
Maximum voltage on secondary winding for no-load running	1.7 mV
Maximum accelerating voltage on tube	1.5 mV
Range of variation of accelerating voltage	400 kV to 1.5 mV
Stability of accelerating voltage	up to 2%
Mean power of electron beam in the main operation condition (u_{tube} = 1.5 mV)	25 kW
Range of variation of mean power	0 to 25 kW
Value of α for the principal operating condition	0.88
Current pulse length for the principal condition	5 msec
Mean current for the principal condition	~17 mA
Maximum current in the pulse for the principal condition	100 mA
Total losses in the windings and magnetic circuit of the transformer, the injector, and its supply system for the principal condition	~2.5 kW
Transformer inductance L	$4 \cdot 10^4$ H
Total transformer capacity C	$250 \cdot 10^{-12}$F
Natural frequency of the LC circuit	50 cps
Stray inductance of the primary windings in the principal conditions	$4.6 \cdot 10^{-4}$ H
Dimensions of accelerator with outlet device and vacuum pump	height 3.3 m width 1.3 m
Dimensions of containing vessel	height 2.1 m diam. 1.2 m
Gas pressure in vessel	15 atm
Weight of accelerator	8 tons

Construction of the ÉlT-1.5

Transformer. The magnetic circuit of the transformer is made of É43 transformer-steel plates 0.35 mm thick cemented with epoxy resin. The discs 3 (16 of these in all), the head 4, and other components of the magnetic circuit are formed of plates arranged radially; after applying the resin, the end surfaces are specially treated to give a good finish. The voltage on the gaps δ (in our apparatus δ = 6 mm) is around 100 kV for a nominal voltage of 1.5 mV on the accelerator. The gap a = 120 mm; the maximum field in the gas is about 160 kV/cm for a voltage of 1.5 mV on the secondary winding. The head 4 (Fig. 5) and other components of the magnetic circuit are treated after cementing in order to obtain the desired shape and finish of the surface. In order to avoid short-circuiting the plates in the course of machining, the insulation between the plates is made up to 0.15 mm thick. The discs and head have central openings with built-in closed copper rings 22 (see Fig. 1). The bearing insulating cylinders 23 are supported on the rings. The transformer-iron places of the discs are electrically connected to the rings 22, which almost entirely screens out the magnetic field of the transformer in the tube region.

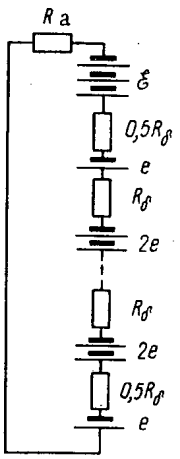

Fig. 4. Equivalent electrical circuit of the magnetic circuit; ℰ ampere turns of the head coil; e ampere turns of the section of secondary winding; R_a magnetic resistance between the head and outer components of the magnetic circuit; R_δ magnetic resistance of the gap between the discs.

The primary winding 1 is mounted on a copper screen 25; glass ribbon and epoxy resin serve for insulation. Each section 2 of the secondary winding consists of 3550 turns of copper conductor 0.1 mm^2 in cross section. The sections are connected in series. The operating voltage on each section is about 50 kV. We see from Fig. 1 that the gap between neighboring sections 2 varies with radius, thus, ensuring an approximately uniform electric field between sections. The value of the test voltage on the sections is greater than the operating voltage by a factor of 1.5 to 2. The screens 26 protect the secondary winding from damage in electrical breakdown, and the discharge tubes 27 from overvoltage on

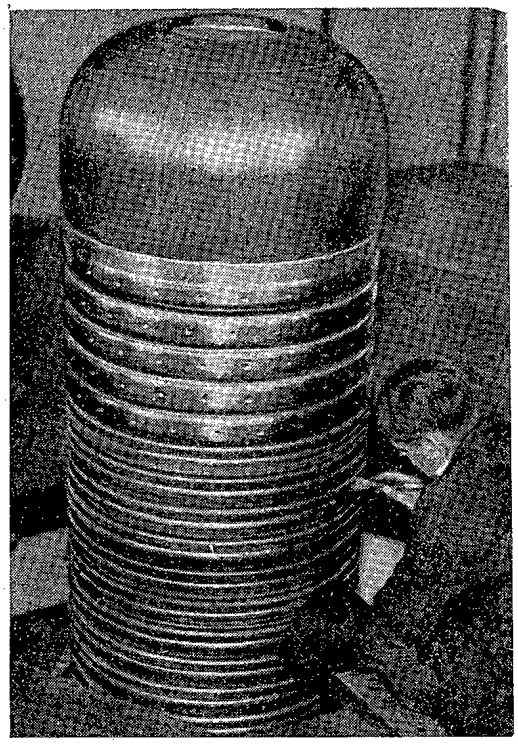

Fig. 5. Central column of transformer.

the sections in the course of conditioning. The layers of the sections are insulated with paper impregnated with epoxy resin. After a special impregnation process, the sections become monolithic with the necessary electrical and mechanical characteristics. Coil 7 has 36 turns. The condenser battery 12 consists of 24 condensers with a total capacity of 480 μF and an operating voltage of 500 V; they are set in a space of the head 4. The transformer dimensions and the number of secondary windings chosen given the system a natural frequency of 50 cps.

Injector and Accelerating Tube. The injector of the experimental apparatus has an indirectly-heated lanthanum-boride cathode 5 mm in diameter and a control electrode 9. For a voltage of 1.5 mV on the whole tube, the voltage relative to the cathode giving complete current cutoff when applied to the control electrode is 2 kV.

The accelerating tube is demountable and consists of eight identical sections interconnected by rubber seals. Each section is made of epoxy rings cemented to Dural electrodes. The total length of the tube is about 1.2 m and the number of insulating rings is 64. The voltage is taken to the electrodes at 18 points by means of elastic contacts 24 connecting the electrodes to the discs 3, the head 4, and the base of the magnetic circuit 16. The voltage for the intermediate rings is conveyed by an ohmic divider 28. At the present time ceramic tubes having a minimum number of vacuum joints are being tested. The tube is provided with 16 short-focus permanent magnetic lenses 29; these give a beam diameter of 3-5 mm for a current of around 100 mA.

Screens 30 made of an 88% Pb alloy are placed at the tube axis. These substantially reduce the radiation arising when electrons fall on the electrodes and so forth. To facilitate evacuation, the electrodes 31 contain apertures displaced relative to each other in neighboring electrodes. The tube is evacuated with an N5S pump using a nitrogen trap.

The injector and tube may be removed through the head 4 without taking the vessel away. The electrodes 31, together with lenses 29 and screens 30, are easily taken out and may be replaced for experimental purposes or when any component goes out of order during use.

The ball bearing 32 and tube sealing 33 ensure smooth fixing and the absence of stress if the insulator in the tube is not coaxial with the magnetic-circuit column.

Containing Vessel, Outlet Window, and Other Systems. The vessel 15 in which the transformer is sited is filled with a mixture of freon and nitrogen at a pressure of up to 15 atm. The gas passes into the vessel through a drying chamber. After overhauling, the whole accelerator is dried under vacuum.

The construction of the system designed for bringing the electron beam out into the atmosphere is determined by the conditions governing the specific technological process in which the accelerated electrons are to be used. In the experimental accelerator, the electrons are let out through a window of titanium foil 50 μ thick and 400 x 40 mm in area, cooled with compressed air.

In order to prevent the radiation arising when the beam is retarded by the object being irradiated from falling into the transformer, a steel shield 34 is placed under the vessel.

Despite the high efficiency of the accelerator, the losses in the windings and magnetic circuit of the transformer, together with those in the injector and its supply system, amount to around 2.5 kW. In order to eliminate heat, there is a water-cooled radiator 35 and a ventilating blower 36, which ensures the necessary gas circulation in the vessel.

Control and Automatic-Control Systems of the Accelerator. The principal control and automatic-control systems of the accelerator are shown in Fig. 6. The voltage on the secondary winding is regulated by varying the transformation coefficient, for which purpose several tappings of the primary winding are provided, together with a switch. The voltage on the secondary winding is measured in steps of 50-100 kV. Smooth regulation of the voltage on the

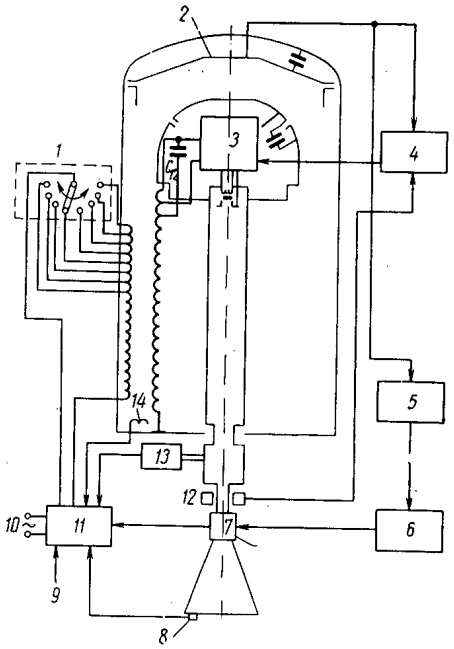

Fig. 6. Block diagram of the control and automation system: 1) Switch; 2) capacitive indicators of tube voltage; 3) injector feed system; 4) power stabilization and control system; 5) sweep stabilization and control system; 6) sweep generator; 7) rotating magnet; 8) foil temperature gage; 9) from pressure gage in boiler; 10) mains; 11) mains cutoff system; 12) Rogowski belt; 13) vacuum gage; 14) breakdown indicator.

tube is effected by varying the voltage drop $\alpha = u_{tube}/u_{IIm}$ as a result of changing the current-pulse width $t_2 - t_1$ and, hence, slightly changing the mean power P. Stabilization of the assigned power is also effected by adjusting the width of the current pulses. A power-control and stabilization circuit is provided for these operations; the sensitive elements of this are a Rogowski belt and the capacitive voltage control on the tube.

The injector supply system generates the voltage on the control electrode u_9 needed to produce the appropriate $i_{tube}(t)$ for maintaining a constant voltage on the tube. If it is necessary to keep u_{tube} constant to 2% or better, a feedback system is set up in the injector supply; this is controlled by capacitive tube-voltage control element situated in the head 4 and provides the u_9. When it is permissible for the electron energy to vary by 5-10%, the control system may be replaced by a source of constant emf, completely cutting off the injector current, capacitive control on the head being connected in opposition to this. Then the injector will be opened for a given time $t_2 - t_1$, depending on the relation between the steady emf and emf arising on the capacitive control. It is also possible to have an arrangement ensuring u_{tube} = const or some other $u_{tube}(t)$ law in accordance with an assigned program.

The injector supply system also generates heating for the cathode. The system itself is fed from some of the turns of the secondary winding. In order to ensure constant supply of the cathode and other circuits situated in the head 4 when the tube voltage is varied between 400 kV and 1.5 mV, an appropriate stabilization system is provided in the injector supply. The various devices for regulating the parameters of the high-voltage components of the supply system(cathode heating, current pulse width, etc.)are controlled, as in ordinary electrostatic generators, by means of insulated filaments. A light-operated feedback scheme for generating u_9 has also been successfully tried. The light source is placed in the grounded part and a photodiode in the head 4. With this system, the moment t_1 at which the control device begins to operate and the current starts flowing through the tube is given at each period of the voltage. In this case, the electrons pass through the tube either as single pulses or with any assigned repetition frequency (up to 50 times per sec).

A time-base generator ensures a linear variation of field in the magnet scanning the electrons along the long side (400 mm) of the outlet window; the scan frequency is 2 kc/sec. The scanning angle is kept constant for different electron energies by a time-base control and stabilization circuit. In the perpendicular direction the beam is scanned by a sinusoidal voltage of industrial frequency.

A switch system is provided in order to switch off the line voltage for external operation of any of the accelerator components.

EXPERIMENTAL RESULTS

The ÉLT-1.5 was tested under various operating conditions. The beam was accelerated both in single pulses and with a repetition frequency of up to 50 cps. The main beam-current measurements were made with a Faraday cylinder situated in air and with a Rogowski belt. The beam energy was determined by means of a capacitive pickup situated in the gap a. The mean power was measured both by a thermal method and from the power required by the transformer, allowing for the steel and copper losses.

The electrons were accelerated in the energy range 400 keV to 1.5 MeV. For an energy of 1.5 MeV the mean power was around 25 mW, the mean current 17 mA, the maximum current in the pulse 100 mA for a pulse width of 5 msec, and the accelerator efficiency approximately 90%. The pulse width was between 0-5 msec. The beam diameter at the outlet from the tube was around 5 mm for a mean power of 25 kW. The beam scanning was carried out in two directions, through angles of ±2.5 and ±25°. The maximum mean power obtained under short-lived conditions was about 30 kW.

CONCLUSION

The construction and operation of the first experimental ÉlT-1.5 accelerator show that the arrangement proposed is feasible and the calculations forming a basis for the construction are valid. The high efficiency and considerable mean power should enable us to use analogous systems for various high-energy radiation processes in metallurgy and other fields.

Direct-action accelerators such as the dynamitron, the insulated-core transformer, and the resonance transformer [2] are closest to the apparatus described as regards parameters. The supply of the dynamitron and insulated-core transformer demands high-frequency converters (the former at hundreds of kc/sec and the latter of about 1 kc/sec). In both systems, the voltage rectification demands a large number of rectifying units, which complicates the reliability aspect. Resonance transformers also operate above industrial frequency.

Systems with hf acceleration (linear accelerators and microtrons), although having greater limiting energies than the systems just mentioned, have relatively lower efficiencies, and plainly cannot compete with the electron transformer in the energy range 1-3 MeV in cases in which beams with a power of many kW are required.

The main difference of the ÉlT-type systems includes the rectification and stabilization of the accelerating voltage by means of the electron beam itself, and also the supply of the system direct from an industrial-frequency network (50 or 60 cps). In addition, these systems make it possible to carry out acceleration with an assigned energy distribution of the electrons, which is required, in particular, when it is desired to obtain a uniform dose over the thickness of the material irradiated.

A failing of the electron-transformer accelerator is the fact that the pulse power in the beam is much greater than the average power. This, however, does not prevent the use of such accelerators, since in high-energy processes the necessary doses are collected over many hundreds of pulses, and this is practically equivalent to the action of a continuous beam. The most serious difficulties may arise in the accelerator tube, which has to pass a pulse current several times exceeding the mean value.

The construction developed for the tube, however, enables the necessary pulse power to be passed. Another failing of the system described is the fact that the back voltage on the tube exceeds the accelerating voltage by up to 10 or 15%. This does not affect the overall electric strength of the system, however, since in the absence of a beam and its associated radiation (although weakened by the special screens), the apparatus (tube and gas gaps) is able to withstand greater voltages.

Further development of the electron transformer should make it possible to raise the energy of the particles obtained in such systems as well as the mean power. In the future, it should clearly be possible to obtain an efficiency close to that of an ordinary transformer (95-98%). At the present time the construction of a 1.5-MeV accelerator designed for serial manufacture is being planned.

In conclusion, we consider it our pleasant duty to thank our colleagues in the Institute of Nuclear Physics of the Siberian Branch of the Academy of Sciences, USSR, who have taken an active part in constructing and setting up the apparatus: engineers G. Krainov, V. Nikolaev, and I. Shalashov, mechanics V. Biryukova, G. Balykov, M. Voronov, M. Gubin, Yu. Efremenkov, A. Kosachev, and M. Stepanov, and technician V. Kirov.

LITERATURE CITED

1. E. A. Abramyan and V. A. Gaponov, A High-Efficiency System for Accelerating Charged Particles [in Russian], Author's certificate No. 906570 as from August 31, 1964.
2. M. Cleland and K. Morganstern, Nucleonics, No. 8, 52 (1960).

EXPERIMENTAL DETERMINATION OF THE RADIATION QUALITY FACTOR NEAR HIGH-ENERGY ACCELERATORS

V. N. Lebedev, M. Zel'chinskii, and M. I. Salatskaya

UDC 577.391

Experimental data characterizing the effective quality factor QF of multicomponent pulse radiation in various parts of a 10-GeV synchrophasotron are presented. The measurements were made by the recombination method. The value of QF varied from 3 to 11. The results of the measurements are compared with values determined for other high-energy accelerators. Values of QF obtained in experiments on particle beams in a 680-MeV synchrocyclotron are also given.

Modern high-energy proton accelerators give rise to strong secondary radiation with a very complex component composition. The energy range of each component stretches from fractions of an electron volt to an energy close to the maximum energy of the accelerated protons. This diversity of radiation, together with the pulsed character of the process, makes it extremely difficlt to determine the degree of radiation hazard. In such a situation it is in practice only possible to study the components giving the greatest contribution to the dose in sites occupied by personnel [1-3]. Moreover, in estimating the contribution of very high-energy nucleons, various simplifying assumptions only satisfied to a first approximation are generally used.

However, even in the case of the absolute validity of these assumptions, an additional error inevitably arises because the relation between the high-energy neutron flux and the dose, as recommended by the rules of [4], cannot be regarded as strict.

Use of the well-known experimental relation between the density of linear stopping power and the quality factor QF* [6, 7] may provide a way out of this. By means of this relation we can calculate the effective QF of any radiation if we know the corresponding spectrum of the linear stopping power (LSP). Knowing the value of the QF, it is easy to estimate the dose equivalent in berads (biological equivalent of radiation). The LSP spectrum in turn may be determined by means of a tissue-equivalent proportional counter [Rossi, 8, 9]. An estimate of the mean LSP can also be obtained by an analysis of the tracks in nuclear emulsions or on photographs from track chambers [10, 11]. Any of these methods, however, is unsuitable for rapid and operational measurements under practical conditions.

The recombination method recently proposed [12, 13] offers the possibility of overcoming some of these difficulties and determining the effective quality factor of unknown radiation simultaneously with absorbed-dose measurements, without requiring an analysis of the LSP spectrum. This method was used for determining the quality factor of mixed pulsed radiation near the high-energy accelerator of the United Institute of Nuclear Research.

Measurements were made with the help of a double tissue-equivalent recombination chamber, described in detail in [14]. The ratio of the ion currents in two chambers (one of which operated in the saturation condition, and the other of which operated under column-recombination conditions) served as a quantity proportional to the quality factor. In the column-recombination condition, the number of recombining ions depends on the linear density of ions in the particle tracks.

The results of the measurements, averaged over the whole volume of the chamber, correspond to an effective tissue depth of 2-5 cm, which is due to the structural peculiarities of the tissue-equivalent chamber. The error

*The term "quality factor" of radiation is proposed by the International Commission on Radiation Units and Measurements (ICRU) [5] for denoting the physically-measurable parameter of radiation characterizing this radiation from the point of view of the expected biological effect, in contrast to the term "relative biological effectiveness" (RBE) which is now recommended for use in radiobiology only.

Translated from Atomnaya Énergiya, Vol. 20, No. 5, pp. 392-396, May, 1966. Original article submitted October 21, 1965.

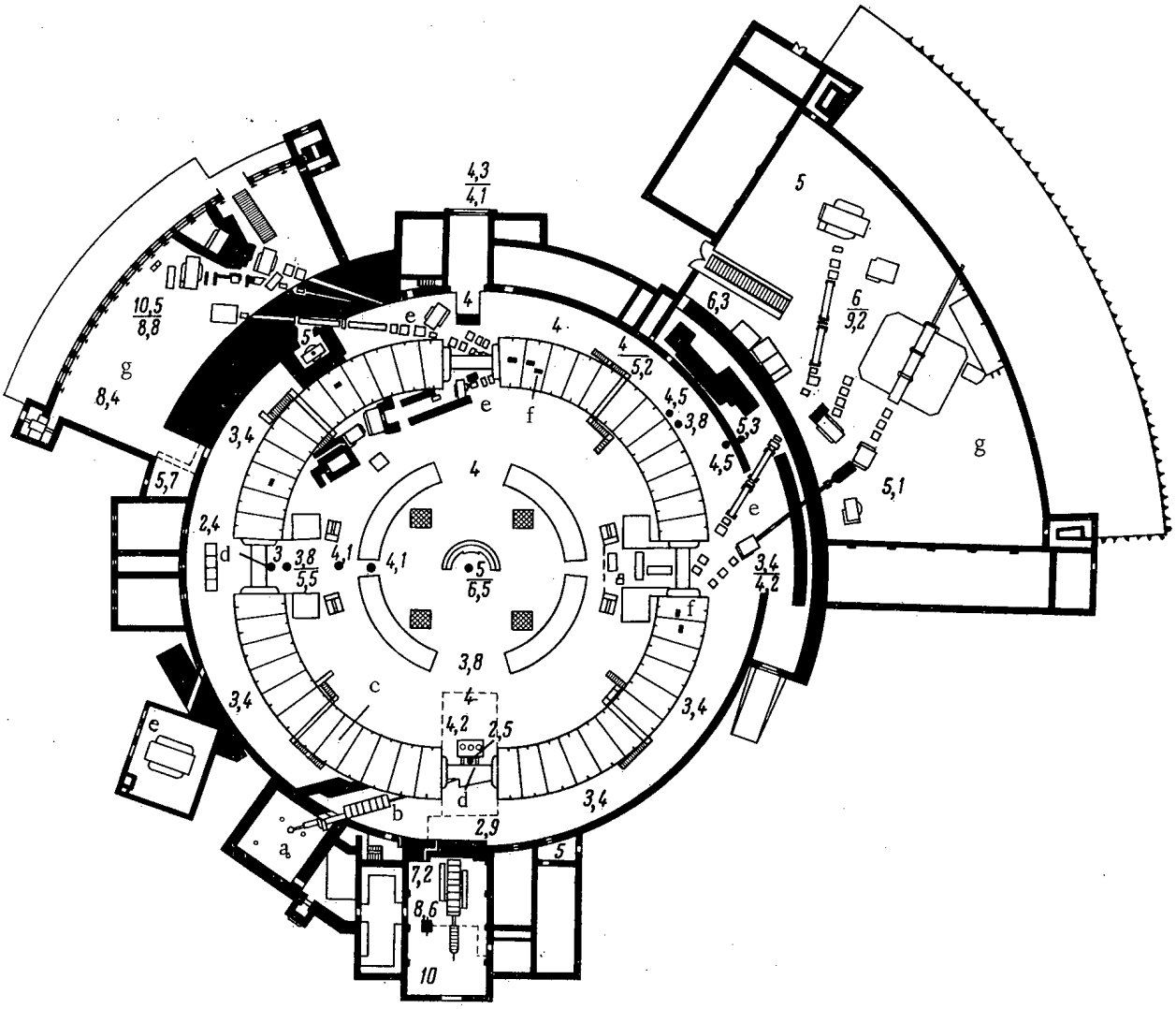

Effective quality factor of mixed radiation: a) 570-keV pre-injector; b) 9-MeV linear accelerator; c) yoke of synchrophasotron electromagnet; d) rectilinear gap; e) high-energy particle channels; f) operating targets; g) experimental room. Under the stroke: values of QF from [3].

arising as a result of the fairly large (30 × 30 cm) dimensions of the chamber (due to inhomogeneity of the radiation field, variations of the spectrum over the volume of the chamber, and so forth) was not taken into account.

The results of measuring the effective quality factor of the radiation at the most characteristic points inside the building of the 10-GeV synchrophasotron are shown in the figure. As expected, the QF reaches a minimum value (≤ 3) at places directly adjacent to the open rectilinear gap of the accelerator. At these points, the main contribution to the dose comes from primary and secondary high-energy particles (relativistic protons and neutrons, mesons, and the electron–photon component) having minimum specific stopping powers. On moving away from the open parts of the vacuum chamber, the quality factor increases sharply, and in the center of the accelerator room reaches a value of 5 (mean energy of fast neutrons at this point equals 0.6 MeV [3]). Opposite to the window in the yoke of the electromagnet (the yoke consists of four quadrants as shown in the figure, each containing 12 oval windows (1 × 1.5 m) and 12 vertical slits 0.2 m broad) the quality factor is 3.8, and opposite the slits it is 4.5, which is due to the different contributions of the high-energy component. The quality factor rises a very little beyond the 60-cm thick wall of silicate brick. This is apparently because the fast-neutron flux, which falls off on passing through the wall, is made up as a result of cascade processes. Beyond the thick shielding in the experimental rooms, the quality factor rises to a maximum value of 6-10. This value of QF agrees closely with the mean neutron energy in these regions (0.4-0.8 MeV) if we remember that in a small experimental room the high-energy component is practically absent.

TABLE 1. Effective Quality Factor of Radiation, Determined for Various Accelerators

Characteristics of regions	Accelerator				
	United Institute of Nuclear Research		3-GeV cosmotron	6.2-GeV bevatron	CERN 28-GeV proton synchroton
	recombination method (see figure)	estimate based on composition of radiation			
In immediate proximity (2-3 m) to the unscreened vacuum chamber of the accelerator	3	–	–	–	4.3–4.1-6.0–5.9* [16]
Outer and inner annular zones along the yoke of the electromagnet (including the center of the room)	3.4-5	4.1-6.5 [3]	5 [10]; 8.1 [11]	1.8±20% [9]	
Beyond the thin shield (up to 60 cm) (site where personnel may be present)	5-6	4.5 [3]		2.8±20% [9]	13–11-8-14* [16]
Beyond the thick shield (in the plane of the equilibrium orbit) (site where personnel are constantly present)	6-10	8.8-9.2 [3]		–	

*At various points.

The measuring error is approximately 30%; it is due to the following factors: primarily to the incomplete tissue-equivalence of the material composing the chamber, the incomplete saturation in the chamber operating in the saturation condition (for strongly ionizing particles), errors arising on measuring the ion current of the chamber, and a certain nonlinearity of the characteristics of the chamber operating in the recombination condition [15, 16]. However, the error in relative measurements (scatter in the readings of the same apparatus) is considerably smaller, and, as might be expected, does not exceed 15%. This fact enables us to distinguish several characteristic regions in the accelerator room as a function of the value of QF (Table 1).

The values given in the figure and in Table 1 agree closely, within the limits of experimental error (except for one point), with the results of estimates based on some quite pessimistic views on the spectrum and composition of the radiation [3].

The value of the effective quality factor of the radiation close to other high-energy accelerators has been estimated by many authors [9-11, 16]. It is very hard, however, to make a comparison of the various results, since the geometry of the shielding differs for different accelerators, and also the disposition of the measuring points with respect to the accelerators is not always very clearly indicated. Nevertheless, we have tried to correlate the data in Table 1. This table shows that the measured results agree fairly well with the estimates, except for the data relating to the bevatron and obtained from an analysis of the LSP spectrum, i.e., the most reliable as regards the method of obtaining information. It is extremely doubtful that these data were erroneous; however, there are no grounds for ascribing a value of QF = 1.8-2.8 to the radiation in regions remote from the accelerator (for example, the control desk), which is very rich in the soft component [17]. We may suppose that this is due to the presence of a large number of relativistic particles at the measuring points, although there is no direct indication of this in [9].

The results of measuring the quality factor of the radiation in collimated particle beams from the 680-MeV synchrophasotron of the United Institute of Nuclear Research are presented in Table 2.

TABLE 2. Comparison of the Effective Quality Factors of Radiation for High-Energy Particles

Type of radiation	Quality factor		
	data of this paper	published data	RBE
Neutrons, $E_{n\ max}$ = 680 MeV	2.7±0.8	–	–
Protons, E_p = 680 MeV	1.8±0.6	1.4* [18]	0.7–† [19-23]
Scattered radiation in experimental rooms beyond thick shield	–	5.3±0.5 [9]; 10–13–3.6-4‡ [16]	–

*For 100-400-MeV protons.

†For 510-730-MeV protons (data relate to live irradiations).

‡At various points.

For a beam of neutrons with a maximum energy of 680 MeV [24], the measurements were made in a water phantom (model) [25]. The maximum of the absorbed dose corresponded to 24 cm of water. The change in the quality factor with depth was insignificant and did not exceed measuring error, right up to 1.2 m. The quality factor was measured in a 680-MeV proton beam without the phantom.

In the third and fourth columns of Table 2 we present, for comparison, some calculated or measured QF values of RBE obtained from live irradiations of animals (mice and dogs).

In conclusion, the authors use this opportunity to thank V. G. Buyanin and E. I. Ob'ezdnov for making the measurements.

LITERATURE CITED

1. R. Wallace, et al., Collection of Articles from the Symposium on Particular Questions of Dosimetry [Russian translation], Gosatomizdat, Moscow (1962), p. 175.
2. B. Moyer, Conference on Shielding of High-Energy Accelerators, New York (1957), p. 38.
3. L. S. Zolin, V. N. Lebedev, and M. I. Salatskaya, Preprint OIYaI No. 2251, Dubna (1965).
4. Health Rules for Working with Radioactive Substances and Sources of Ionizing Radiations, No. 333-60 [in Russian], Gosatomizdat, Moscow (1960).
5. "Izmerit. tekhnika," 10, 54 (1963).
6. Recommendations of the International Commission on Radiation Shielding [Russian translation], IL, Moscow (1958).
7. Health Phys., 9, 357 (1963).
8. H. Rossi and W. Rosenzweig, Radiation Res., 10, 532 (1959).
9. H. Rossi, et al., Health Phys., 8, 331 (1962).
10. K. Brien, et al., In book: "Neutron Dosimetry," 2, Vienna, IAEA (1963), p. 199.
11. J. Handloser, Health Phys., 2, 165 (1959).
12. M. Zel'chinskii, In the collection, "Neutron Dosimetry," 2, Vienna, IAEA (1963), p. 397.
13. A. Sullivan and J. Baarli, Preprint CERN 63-17 (1963).
14. M. Zel'chinskii, V. N. Lebedev, and M. I. Salatskaya, "Pribory i tekhnik éksperimenta," 6, 73 (1964).
15. M. Zel'chinskii, Nukleonika, 7, 175 (1962).
16. J. Baarli, Report CERN DI(HP) (1964).
17. J. Lehman and O. Fekula, Nucleonics, No. 1, 35 (1964).
18. J. Turner, et al., Health Phys., 10, 783 (1964).
19. P. P. Saksonov, et al., Dokl. AN SSSR, 162, 688 (1965).
20. Yu. G. Grigor'ev, et al., In the book: "Biological Effects of Neutron and Proton Irradiations, 1, Vienna, IAEA (1964), p. 223.
21. Collection: "Papers on the Biological Effects of High-Energy Protons" [in Russian], Izd. Instituta gigieny truda i profzabolevanii Akademii meditsinskikh nauk SSSR, Moscow (1962), pp. 10, 65.
22. P. Bonét–Maury, et al., In book: "Biological Effects of Neutron and Proton Irradiation," 1, Vienna, IAEA (1964), p. 261.

23. J. Ashikawa, et al., In book: "Biological Effects of Neutron and Proton Irradiation," 1, Vienna, IAEA (1964), p. 249.
24. V. S. Kiselev, et al., ZhÉ TF, 35, 812 (1958).
25. M. Zel'chinskii, Nukleonika, 10, 77 (1965).

All abbreviations of periodicals in the above bibliography are letter-by-letter transliterations of the abbreviations as given in the original Russian journal. *Some or all of this periodical literature may well be available in English translation.* A complete list of the cover-to-cover English translations appears at the back of this issue.

HELICAL MAGNETIC CONFIGURATIONS WITH MINIMUM $\overline{B}$

N. M. Zueva and L. S. Solov'ev

UDC 533.9

A general consideration of magnetic configurations with helical symmetry and minimum $\overline{B}$ is presented. An approximate analytic expression is obtained for the specific volume $V'(\Phi)$ in the neighborhood of the helical magnetic axis. Exact formulas for the specific volume $V'(\Phi)$ and the mean torsional angle of the lines of force $i = 2\pi\chi'(\Phi)$ are given in terms of single integrals. Graphs of $V'(\Phi)$ and $\chi'(\Phi)$ are plotted from numerical calculations of these integrals up to the separatix of the magnetic surfaces.

An example of a straight periodic field with minimum $\overline{B}$, i.e., a field in which the specific volume $V'(\Phi) = \oint \frac{dl}{B}$ on the axis of the system is maximum, was given in [1]. Furth [2], showed that a field with helical symmetry could also have a minimum B. The magnetic surfaces of such a field constitute a superposition of helical magnetic tubes of constant cross section. We shall study helically-symmetric magnetic configurations in this paper.

General Considerations

An irrotational magnetic field **B** having helical symmetry may be described either by a scalar potential $\mathbf{B} = \nabla\Phi_{max}$ or a flux function ψ. In a cylindrical coordinate system r, Φ, z the helical field depends on two variables, $\mathbf{B} = \mathbf{B}(r, \theta)$, $\theta = \Phi - \alpha z$, where $\alpha = 2\pi/L$, and L is the pitch of the helix. The general expression for the scalar potential of a helical field has the form

$$\Phi_m = B_{z0}z - A\Phi + \sum_{n=1}^{\infty} Z_n(\alpha n r)\sin n\theta, \tag{1}$$

where Z_n are Bessel functions $Z_n(x) = a_n I_n(x) + b_n K_n(x)$. Such a field constitutes a superposition of a homogeneous field B_{z0} parallel to the z axis, the field of a current-carrying filament extending along the z axis, and the field of helical windings set on cylindrical surfaces $r = R_1$ and $r = R_2$, i.e., we consider the case in which $R_1 < r < R_2$.

The flux function ψ is a combination of vector-potential components $\psi = A_z + \alpha r A_\varphi$ and satisfies the equation

$$r\frac{\partial}{\partial r}\cdot\frac{r}{\beta}\cdot\frac{\partial\psi}{\partial r} + \frac{\partial^2\psi}{\partial\theta^2} = \frac{2\alpha r^2}{\beta^2}I, \tag{2}$$

where $\beta \equiv 1 + \alpha^2 r^2$; in the case considered (irrotational field) $I \equiv B_z + \alpha r B_\Phi = \text{const}$. The field components **B** are expressed in terms of ψ:

$$rB_r = \frac{\partial\psi}{\partial\theta}; \quad \alpha r B_z - B_\Phi = \frac{\partial\psi}{\partial r}. \tag{3}$$

For a certain magnetic field $\mathbf{B}(r, \theta)$ the function $\psi(r, \theta)$ may be determined by integration with respect to r for a fixed θ: $\psi = \int_0^r (\alpha r B_z - B_\Phi)\, dr$. The function ψ corresponding to field (1) has the form

$$\psi = B_{z0}\frac{\alpha r^2}{2} + A\ln r - r\sum_{n=1}^{\infty} Z_n'(\alpha n r)\cos n\theta. \tag{4}$$

Translated from Atomnaya Énergiya, Vol. 20, No. 5, pp. 396-401, May, 1966. Original article submitted August 14, 1965.

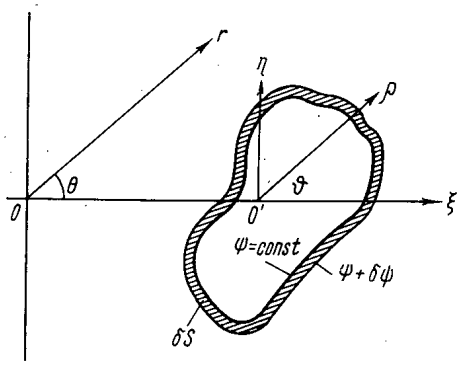

Fig. 1. Intersection of two neighboring magnetic surfaces with the plane z = const.

Thus, we obtain exact expressions for the field and the magnetic surfaces ψ = const in a cylindrical coordinate system. Let us derive approximate analytical expressions for the specific volume and torsion angle of the lines of force in the neighborhood of a helical magnetic tube, and then exact integral expressions suitable for numerical calculation of these quantities.

We note that the tangent of the angle between the helical line and the z axis equals αr, and the field components (parallel to the helical line θ = const, and perpendicular to this and the radius vector r) are respectively $B_{\parallel} = I\sqrt{\beta}$, $B_{\perp} = \partial\psi/\partial r\sqrt{\beta}$. The magnetic axis is the helical line the pitch of which coincides with the pitch L of the field.

Specific Volume of the Magnetic Tube

Let the magnetic surfaces in the section z = const be closed lines $\psi(\rho, \vartheta, z)$ = const surrounding a point $\rho = 0$, displaced through a certain distance r_0 from the z axis. The longitudinal magnetic flux $\delta\Phi$, passing between two neighboring magnetic surfaces equals

$$\delta\Phi = \int B_z\, dS \equiv \bar{B}_z \delta S, \tag{5}$$

where the integration is taken over the area δS of the section z = const (Fig. 1). The volume of the corresponding layer is determined by integration over z:

$$\delta V = \int \delta S\, dz = \delta\Phi \int \frac{dz}{\bar{B}_z}. \tag{6}$$

It follows that the specific volume $V'(\Phi)$ may be put in the form

$$V'(\Phi) = \int \frac{dz}{\bar{B}_z}, \tag{7}$$

where

$$\bar{B}_z = \frac{1}{\delta S} \int B_z\, dS \tag{8}$$

is the mean value of B_z over the area δS.

Since the element of area δS equals $dS = \rho\,\delta\rho\, d\vartheta = \delta\psi \frac{\varrho d\vartheta}{\partial\psi/\partial\varrho}$, then, if we take $B_z = B_0 + B_1$, where B_0 = const is the axial field at the point $\rho = 0$, we get

$$\delta S = \delta\psi \int_0^{2\pi} \frac{\varrho\, d\vartheta}{\partial\psi/\partial\varrho}; \tag{9}$$

$$\bar{B}_z = \frac{\delta\psi}{\delta S} \int_0^{2\pi} B_z \frac{\varrho\, d\vartheta}{\partial\psi/\partial\varrho} = B_0 + \frac{\delta\psi}{\delta S} \int_0^{2\pi} B_1 \frac{\varrho\, d\vartheta}{\partial\psi/\partial\varrho}, \tag{10}$$

and for magnetic surfaces with helical symmetry the specific volume

$$V'(\Phi) = \frac{L}{\bar{B}_z}, \tag{11}$$

where L is the pitch of the helix reckoned along the z axis.

For an approximate calculation of $V'(\Phi)$ let us put B_Z and ψ in the neighborhood of the magnetic axis $\rho = 0$ in the form of series in $\xi = \rho \cos \vartheta$ and $\eta = \rho \sin \vartheta$, and let us confine ourselves to the case in which the magnetic surfaces are symmetric with respect to the ξ axis:

$$B_z = B_0 + b_0\xi + b_1\xi^2 + b_2\eta^2 + \ldots; \tag{12}$$

$$\psi = \psi_1\xi^2 + \psi_2\eta^2 + \psi_3\xi^3 + \psi_4\xi\eta^2 + \ldots \tag{13}$$

in polar coordinates ρ, ϑ these expansions take the form

$$B_z = B_0 + b_0\varrho\cos\vartheta + (b_1\cos^2\vartheta + b_2\sin^2\vartheta)\,\varrho^2 \ldots \equiv B_0 + h_1(\vartheta)\,\varrho + h_2(\vartheta)\,\varrho^2 + \ldots; \tag{14}$$

$$\psi = (\psi_1\cos^2\vartheta + \psi_2\sin^2\vartheta)\,\varrho^2 + (\psi_3\cos^3\vartheta + \psi_4\cos\vartheta\sin^2\vartheta)\,\varrho^3 + \ldots \equiv f_1(\vartheta)\,\varrho^2 + f_2(\vartheta)\,\varrho^3 + \ldots \tag{15}$$

With an accuracy up to ρ^3 we obtain $\varrho \approx \frac{\psi^{1/2}}{f_1^{1/2}} - \frac{f_2\psi}{2f_1^2}$. Hence, we find the following expression for $\overline{B}_Z$ (valid in the neighborhood of the magnetic axis):

$$\bar{B}_z = B_0 + \psi\frac{\delta\psi}{\delta S}\int_0^{2\pi}\left(\frac{h_2}{2f_1^2} - \frac{h_1f_2}{f_1^3}\right)d\vartheta, \tag{16}$$

where

$$\frac{\delta S}{\delta\psi} \approx \frac{1}{2}\int_0^{2\pi}\frac{d\vartheta}{f_1(\vartheta)} = \frac{\pi}{\sqrt{\psi_1\psi_2}}. \tag{17}$$

The value of $V''(\Phi)$ may be determined from the equation $V'(\Phi) \approx \frac{L}{B_0} + V''(\Phi)\frac{\delta\Phi}{\delta\psi}\psi$. Thus,

$$V''(\Phi) = -\frac{L}{B_0^3}\left(\frac{\delta\psi}{\delta S}\right)^2\int_0^{2\pi}\left(\frac{h_2}{2f_1^2} - \frac{h_1f_2}{f_1^3}\right)d\vartheta. \tag{18}$$

On calculating the integrals in this expression we obtain

$$V''(\Phi) = -\frac{h}{B_0^3}\left(\frac{\delta\psi}{\delta S}\right)^2\frac{\pi\psi_2}{4(\psi_1\psi_2)^{5/2}} \times [2\psi_1(b_1\psi_2 - b_2\psi_1) - b_0(3\psi_2\psi_3 + \psi_1\psi_4)]. \tag{19}$$

The location of the magnetic axis, or, in other words, the elliptic-type singular point of the family of lines $\psi = \text{const}$, $z = \text{const}$, is determined by the equations $\frac{\partial\psi}{\partial} = 0$, $\frac{\partial\psi}{d\vartheta} = 0$. The coefficients of the expansions (12), (13) are not arbitrary. In order to determine the relations between these, we use expression (2). The coordinates ξ and η are related to r and θ by the expressions (see Fig. 1)

$$\xi = \varrho\cos\vartheta = r\cos\theta - r_0; \tag{20}$$

$$\eta = \varrho\sin\vartheta = r\sin\theta. \tag{21}$$

Expanding B_Z and ψ in powers of $r - r_0$ and θ in the neighborhood of the magnetic axis O' and using the equation $B_Z = \frac{I}{\beta} + \frac{\alpha r\psi'}{\beta}$ and Eq. (2), we find a relation for the derivatives in the expansions for B_Z and ψ:

$$B_z' = -\frac{\alpha\ddot{\psi}}{r}; \quad B_z'' = \frac{\alpha}{r}\left(\frac{\ddot{\psi}}{r} - \ddot{\psi}'\right); \quad \ddot{B}_z = \frac{\alpha r}{\beta}\ddot{\psi}'; \tag{22}$$

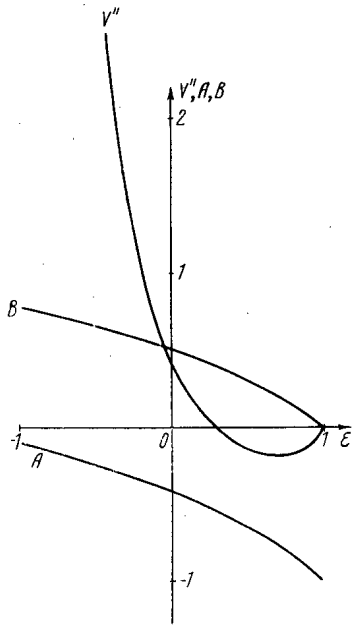

Fig. 2

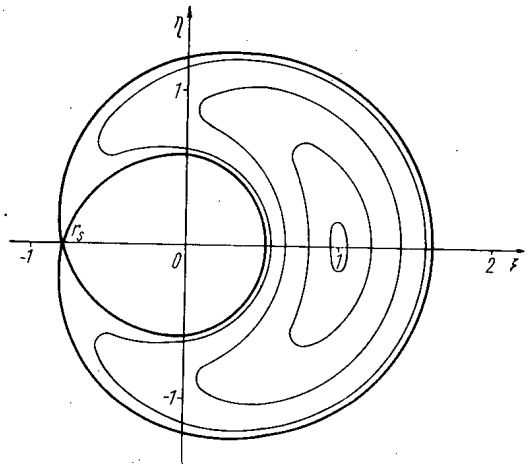

Fig. 3

Fig. 2. Values of V", A, and B as functions of the parameter ε, characterizing the eccentricity of the normal cross sections of the magnetic surfaces in the case of an external current winding.

Fig. 3. Cross sections of magnetic surfaces in the case of an externally-situated helical current winding (40) with $\varepsilon = 0.7$.

$$\psi''' = -\frac{\psi''}{r} + \frac{4-2\beta}{r^3}\ddot{\psi} - \frac{\beta}{r^2}\ddot{\psi}';$$
$$B_0 = \frac{\beta}{2\alpha}\left(\psi'' + \frac{\ddot{\psi}}{r^2}\right) = \frac{B_{\parallel}}{\sqrt{\beta}}. \tag{23}$$

Here $B_{\parallel}$ is the value of the field at the magnetic axis, and the primes and dots indicate derivatives with respect to r and θ, respectively, at the point O', where $\psi' = \dot{\psi} = 0$, $r = r_0$. Thus, the expansions for B_Z and ψ contain altogether three free parameters; for these we may select, for example, $\ddot{\psi}$, ψ'', $\ddot{\psi}'$. Substituting $r = r_0 \approx \xi - \eta^2/2r_0$, $\theta \approx \eta/r_0 - \xi\eta/r_0^2$ into these expressions and omitting the index from r_0 for brevity, we obtain

$$B_z = B_0 - \frac{\alpha\ddot{\psi}}{r}\xi + \frac{\alpha}{2r}\left(\frac{\ddot{\psi}}{r} - \ddot{\psi}'\right)\xi^2 - \frac{\alpha}{2r}\left(\frac{\ddot{\psi}}{r} - \frac{\ddot{\psi}'}{\beta}\right)\eta^2 + \ldots; \tag{24}$$

$$\psi = \frac{\psi''}{2}\xi^2 + \frac{\ddot{\psi}}{2r^2}\eta^2 - \frac{\xi^3}{6}\left(\frac{\psi''}{r} - \frac{4-2\beta}{r^3} + \frac{\beta\ddot{\psi}'}{r^2}\right) + \frac{1}{2}\left(\frac{\psi''}{r} - \frac{2\ddot{\psi}}{r^3} + \frac{\ddot{\psi}'}{r^2}\right)\xi\eta^2 + \ldots \tag{25}$$

By using these expressions we can write the formula for $V''(\Phi)$ in terms of the indendent derivatives $\ddot{\psi}$, ψ'', $\ddot{\psi}'$, taken at the point $\rho = 0$:

$$V''(\Phi) = -\frac{\ddot{\psi}}{2B_0^3(\psi''\ddot{\psi})^{3/2}}\left\{-\frac{4\alpha^2\ddot{\psi}^3}{r^3} - \left[\frac{\ddot{\psi}'}{\beta}\left(\psi'' - \frac{\beta\ddot{\psi}}{r^2}\right) - \frac{2\ddot{\psi}^2}{r^3}\right]\left(\psi'' - \frac{\beta\ddot{\psi}}{r^2}\right)\right\}. \tag{26}$$

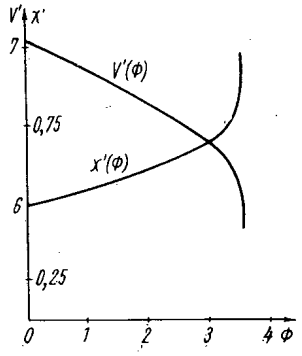

Fig. 4

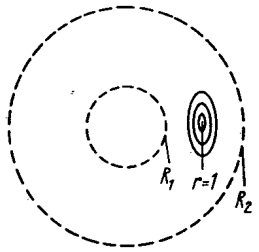

Fig. 5

Fig. 4. Values of V' and χ' as functions of the longitudinal flux Φ in the case of an external current winding (40).

Fig. 5. Disposition of closed magnetic surfaces with axis r = 1 between helical current windings on cylinders r = R_1 and r = R_2.

In the neighborhood of the magnetic axis the helical tubes have elliptic sections; in the plane perpendicular to the magnetic axis the ratio of the elliptical semiaxes equals

$$\frac{b_\perp}{a_\perp} = \left(\frac{r^2\psi''}{\beta\dot{\psi}}\right)^{1/2}. \tag{27}$$

The formula for V" (Φ) may conveniently be expressed in terms of a quantity ε:

$$\varepsilon = \frac{b_\perp^2 - a_\perp^2}{b_\perp^2 + a_\perp^2} = \frac{\psi'' - \beta\dot{\psi}/r^2}{\psi'' + \beta\dot{\psi}/r^2}, \tag{28}$$

and it then takes the form

$$V''(\Phi) = \frac{2\alpha\sqrt{1-\varepsilon^2}}{B_{||}^2\beta^{3/2}(1+\varepsilon)^2} \times \left[\alpha^2 r^2(1-\varepsilon) - \left(\frac{\beta r\dot{\psi}'}{\dot{\psi}} - 1 + \varepsilon\right)\varepsilon\right]. \tag{29}$$

Since the first term in the square brackets is always positive ($|\varepsilon| < 1$), then, in the case in which the normal cross sections of the magnetic tube are circular ($\varepsilon = 0$), the quantity $V''(\Phi) > 0$. For an elliptical normal section ($\varepsilon \neq 0$) the value of V"(Φ) may be negative.

Mean Torsion Angle $i = 2\pi\chi'(\Phi)$

For calculating χ'(Φ) we use the formula $\Phi - \chi = \frac{2\pi}{\alpha}\psi$ [3] relating the longitudinal flux Φ and the azimuthal flux χ to the function ψ in the case of helical symmetry. Then we obtain

$$\chi'(\Phi) = 1 - \frac{2\pi}{\alpha}\psi'(\Phi). \tag{30}$$

If we limit consideration to the zero approximation only in the expansion of χ'(Φ) in powers of Φ, then from expressions (5), (9), we obtain

$$\frac{\delta\Phi}{\delta\psi} \approx B_0\int_0^{2\pi}\frac{\varrho\, d\vartheta}{\partial\psi/\partial\varrho}; \tag{31}$$

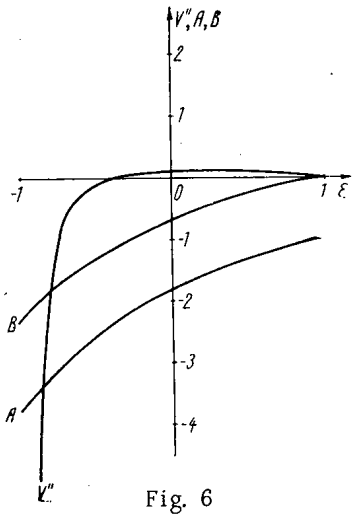

Fig. 6

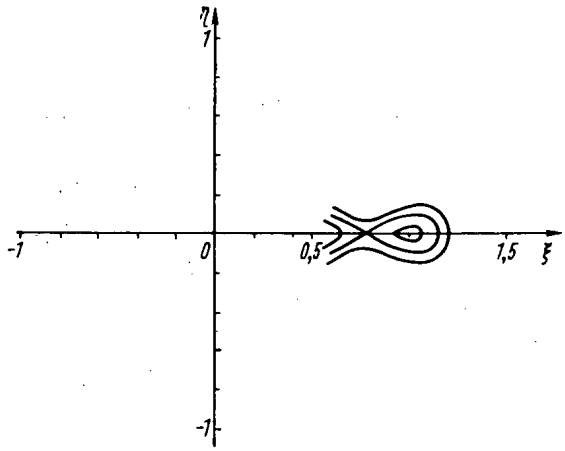

Fig. 7

Fig. 6. Values of V", A, and B as functions of the longitudinal flux ε in the case of an internal current winding (41).

Fig. 7. Cross sections of magnetic surfaces in the case of an internally-situated current winding (41).

then in analogy with the preceding case, we find

$$\chi'(\Phi) = 1 - \sqrt{\frac{1-\varepsilon^2}{\beta}}. \tag{32}$$

Thus, in the neighborhood of the magnetic axis (for $\rho \to 0$) the mean torsion angle of the lines of force $i = 2\pi\chi'(\Phi)$ is completely determined by the eccentricity of the elliptic cross section of the magnetic tube and the inclination of the magnetic helical axis to the z axis of the cylinder on which the magnetic axis is wound.

Exact Expressions for V'(Φ) and i

In a case in which the helical magnetic field contains only the n-th harmonic, i.e., in a cylindrical system of coordinates, the scalar potential has the form

$$\varphi_m = Z - A\varphi + BZ_n(nr)\sin n\theta \quad (\theta = \varphi - z), \tag{33}$$

we can express the integral for V'(Φ) and χ'(Φ) in explicit form. In expression (33) the longitudinal homogeneous field B_{z0} is taken as being equal to unity, and the unit of length is taken as $1/\alpha = L/2\pi$. The potential $A\varphi$ corresponds to the field of a current-carrying filament extending along the z axis: $B_\varphi = -A/r$. The last term in expression (33) describes an n-threaded helical field $Z_n(nr) = a_n I_n(nr) + b_n K_n(nr)$.

The flux function ψ, corresponding to potential (33), has the form

$$\psi = \frac{r^2}{2} + A\ln r - BrZ_n'(nr)\cos n\theta. \tag{34}$$

If we use $S(\psi)$ to denote the area of the magnetic-surface cross section normal to the z axis, we can write the following expressions for $S'(\psi)$ and $\Phi'(\psi)$:

$$S'(\psi) = \int \frac{r\,dr}{\partial\psi/\partial\theta};$$
$$\Phi'(\psi) = \int B_z \frac{r\,dr}{\partial\psi/\partial\theta}. \tag{35}$$

The quantities V'(Φ) and χ'(Φ) are expressed in terms of $S'(\psi)$ and $\Phi'(\psi)$ by means of the formulas

$$V'(\Phi) = 2\pi\frac{S'(\psi)}{\Phi'(\psi)}; \tag{36}$$

$$\chi'(\Phi) = 1 - \frac{2\pi}{\Phi'(\psi)}. \tag{37}$$

The axial field $B_Z = 1 - nBZ_n(nr)\cos n\theta$. Let us introduce the notation $F(r) = r^2/2 - A \ln r$, $f(r) = BrZ'_n(nr)$ and express $\partial\psi/\partial\theta$ in the form of an explicit function of r:

$$\psi = F - f\cos n\theta, \quad \partial\psi/\partial\theta = nf\sin n\theta = n\sqrt{f^2 - (\psi - F)^2}.$$

If we substitute these relations into expressions (35), we obtain the desired formulas for $S'(\psi)$ and $\Phi'(\psi)$:

$$S'(\psi) = \frac{2}{n}\int_{r\,\min}^{r\,\max} \frac{r\,dr}{\sqrt{f^2 - (\psi - F)^2}}; \tag{38}$$

$$\Phi'(\psi) = S'(\psi) + 2\int_{r\,\min}^{r\,\max} \frac{Z_n(nr)(\psi - F)\,dr}{Z'_n(nr)\sqrt{f^2 - (\psi - F)^2}}. \tag{39}$$

In these expressions the integration is taken over r from r_{min} to r_{max} for which the expression under the root vanishes. On calculating these integrals, we obtain exact expressions for $V'(\Phi)$ and $i = 2\pi\chi'(\Phi)$ as functions of ψ.

Results of Numerical Calculations

By way of example, we considered magnetic surfaces formed by the fields:

$$\varphi_m = Z - A\varphi + BI_1(r)\sin\theta; \tag{40}$$

$$\varphi_m = Z - A\varphi + BK_1(r)\sin\theta. \tag{41}$$

The helical field in the first example is created by a single-threaded current winding on a cylinder $r = R_2$ (Figs. 2-4), and in the second example on a cylinder $r = R_1$ (Fig. 5). The radius of the center of the helical magnetic tube r_0 is taken as unity, which corresponds to curvature k and torsion $\varkappa$ of the magnetic axis ($k = \alpha^2 r/\beta = 1/2$, $\varkappa = \alpha/\beta = 1/2$).

Figure 2 shows graphs of $V''(\Phi)$, A, and B as functions of ε. The values of V'' were calculated from formulas (29), where $\frac{\ddot{r}\dot{\psi}'}{\ddot{\psi}} = \frac{n\beta Z_n(n\alpha r)}{\alpha r Z'_n(n\alpha r)}$. The quantities A and B were determined from Eqs. (28) and conditions $\psi'(1, 0) = 0$.

The region of negative $V''(\Phi)$ corresponds to $\varepsilon > 0$. The minimum V'' corresponds to $\varepsilon = 0.7$. For this case, we constructed magnetic surfaces, the intersections of which with the plane $z = 0$ are shown in Fig. 3.

The exact values of $V'(\Phi)$ and $\chi'(\Phi)$ calculated numerically from formulas (35) and (36) up to the separatrix are shown in Fig. 4.

The values of V' and χ' on the magnetic axis ($r = 1$) equal

$$V'(\Phi) = \frac{2\pi}{B_0}; \quad \chi'(\Phi) = 1 - \frac{\sqrt{\ddot{\psi}\psi''}}{B_0} = 1 - \sqrt{\frac{1-\varepsilon^2}{\beta}}, \tag{42}$$

and at the separatrix

$$V'(\Phi) = \frac{2\pi}{B_S}, \quad \chi'(\Phi) = 1, \tag{43}$$

since $\Phi'(\psi) \to \infty$, $S'(\psi) \to \infty$, and the value of $V'(\Phi)$ is determined by the field B_S in an infinitely small region at the edge of the separatrix (see Fig. 3, region around point r_S).

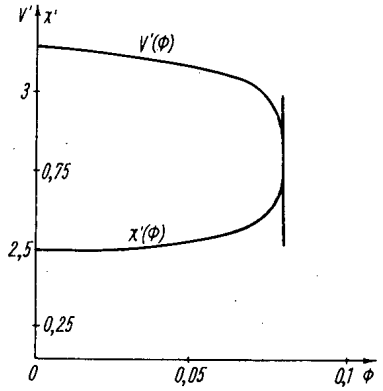

Fig. 8. Values of V' and χ' as functions of Φ in the case of an internal current winding (41).

Figures 6-8 show the corresponding results for the second example (41), the magnetic surfaces being constructed for the case $\varepsilon = -0.7$.

In conclusion, we shall give some analytical expressions (general for the case of helical symmetry) for the specific volumes on the magnetic axis and separatrix. Since the mean value of B_z on the separatrix is determined by the region around the edges of the separatrix only, we have

$$\overline{B}_z = \frac{1}{\delta S}\int B_z\, dS = \frac{1}{n}\sum_{k=1}^{n} B_{Sk}, \tag{44}$$

where the summation is taken over values of B_z on the edges of the separatrix. Remembering the equality $B_z = I/\beta$ at the singular points ($\psi' = 0$), we obtain for $V'(\Phi) = L/B_z$:

$$V'_S = \frac{nL}{\sum_{k=1}^{n} B_{Sk}} = \frac{nL}{I\sum_{k=1}^{n}\frac{1}{\beta_{Sk}}}; \tag{45}$$

$$V'_0 = \frac{L}{B_0} = \frac{L\beta_0}{I}. \tag{46}$$

In the cases considered above, for which there is only one edge to the separatrix ($n = 1$), the ratio of the values of $V'(\Phi)$ on the separatrix and magnetic axis equals

$$\frac{V'_S}{V'_0} = \frac{1+\alpha^2 r_S^2}{1+\alpha^2 r_0^2}. \tag{47}$$

From this we see that the magnetic configuration has a region of minimum $\overline{B}$ (at least near the separatrix), if the distance from the axis of the helical windings to the edge of the separatrix r_S is smaller than the distance to the magnetic axis r_0, i.e., in all cases in which the edge of the separatrix lies on the side of the axis of the helical magnetic configuration. There may be either a minimum or a maximum of B in the neighborhood of the magnetic axis.

Thus, our examination has shown that the possibility of the existence of magnetic configuration of the type described, which a minimum of $\overline{B}$ in the neighborhood of the magnetic axis, is related to the spatial aspects of the magnetic axis and the ellipticity of the normal cross sections of the magnetic surfaces ($\varepsilon \neq 0$).

LITERATURE CITED

1. H. Furth and M. Rosenbluth, Phys. Fluids, 7, 764 (1964).
2. H. Furth, Lectures at the Seminar on Plasma Physics [Russian translation], Trieste (October, 1964).
3. A. I. Morozov and L. S. Solov'ev, Geometry of the Magnetic Field. In the book: "Questions of Plasma Theory" [in Russian], No. 2, Moscow, Gosatomizdat (1963), p. 3.

PARAMAGNETIC EFFECT UNDER THE INFLUENCE OF HIGH-FREQUENCY PRESSURE AND ELECTRON PARAMAGNETIC RESONANCE IN PLASMA

V. M. Glagolev, I. N. Khromkov, and N. S. Cheverev

UDC 533.9

The interaction of uhf fields ($\omega = 2 \cdot 10^{10}$ sec^{-1}) in a space resonator containing dense plasma ($n \approx 10^{13} - 10^{14}$ cm^{-3}) in a steady magnetic field was studied experimentally. Under the influence of hf pressure a paramagnetic current arises in the plasma; the associated effect of an increase in the static magnetic field inside the plasma agrees closely with the calculated relation.

For $\omega_H/\omega = 0.5$ paramagnetic resonance of the electrons takes place; this leads to a sharp rise in plasma pressure p_0, up to $\beta = \frac{8\pi p_0}{H_0^2} \approx 0.2$.

It is well-known that plasma situated in a trap formed by a magnetic field falling (on average) over the radius is unstable with respect to flute perturbations. One means of stabilizing such convective instability is the pressure of an hf field not penetrating into the plasma [1, 2]. Under the influence of hf pressure perpendicular to the direction of the lines of force of the static magnetic field, a steady current develops on the surface of the plasma; this removes the electric field of the flute perturbations and, thus, prevents the drift of plasma to the sides of the trap. This surface current always acts in a direction such that the original magnetic field inside the plasma is increased, i.e., there is a peculiar kind of paramagnetic effect.

Starting from the condition of equilibrium for plasma in hf and static magnetic fields (it is assumed that the electric hf field on the surface of the plasma is zero), for $p_0 < \frac{\tilde{\bar{H}}^2}{8\pi} < \frac{H_0^2}{8\pi}$ the value of the paramagnetic effect is determined by the expression

$$\Delta H = H_i - H_0 \approx \frac{\tilde{\bar{H}}^2}{2H_0}, \tag{1}$$

where $\tilde{\bar{H}}$ is the effective value of the magnetic hf field on the surface of the plasma, H_0, H_i are the static magnetic fields outside and inside the plasma, and p_0 is the plasma pressure.

For practical experimental conditions, when the range of interaction of the hf field with the plasma is limited by some distance h, the formula for the paramagnetic effect on the axis in the middle of the interaction region has the form

$$\Delta H = H_i - H_0 = \frac{\tilde{\bar{H}}^2_{\max}}{4H_0} \cdot \frac{h_{\text{eff}}}{\sqrt{r_0^2 + \left(\frac{h_{\text{eff}}}{2}\right)}}, \tag{2}$$

where r_0 is the radius of the plasma cylinder, h_{eff} is the effective length of the hf-pressure region, allowing for inhomogeneity in the distribution of hf pressure over the length h,

$$h_{\text{eff}} = \frac{1}{\tilde{\bar{H}}^2_{\max}} \int_0^h \tilde{\bar{H}}^2 \, dh;$$

$\tilde{\bar{H}}_{\max}$ being the maximum effective magnetic hf field on the surface of the plasma.

Translated from Atomnaya Énergiya, Vol. 20, No. 5, pp. 401-407, May, 1966. Original article submitted August 3, 1965, revised January 13, 1966.

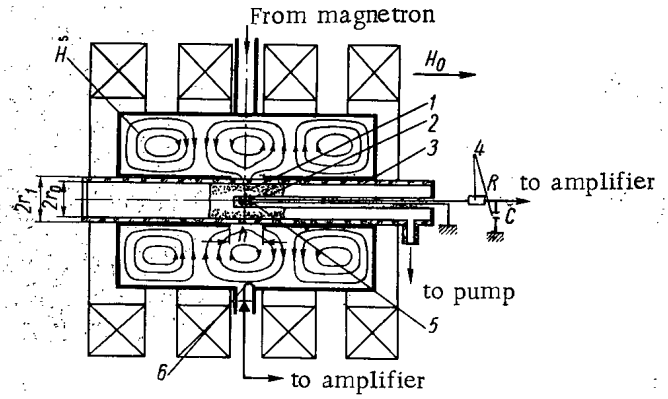

Fig. 1. Arrangement of the apparatus: 1) plasma; 2) stainless-steel screen; 3) quartz tube; 4) integrating circuit; 5) measuring coil; 6) loop for measuring hf fields; r_0 inner radius of quartz tube; r_1 inner radius of central metal tube of resonator; h breadth of annular slit.

The present paper constitutes a continuation and development of [3], which was devoted to a study of the paramagnetic effect in plasma under the influence of the pressure of hf fields.

Description of the Apparatus

The paramagnetic effect in plasma was studied in the apparatus shown schematically in Fig. 1. Electromagnetic oscillations of the H_{013} type with peak magnetic hf fields up to 150 Oe, were set up in the cylindrical vacuum resonator; the lines of force are shown in Fig. 1. The inner cylinder of the resonator had an annular slit into which the hf field penetrated. Electric fields, forming closed circles, were small in the neighborhood of the slit. In the central part of the resonator was a quartz tube with an internal diameter of about 40 mm. The resonator was placed in a static longitudinal magnetic field H_0 which could be regulated between 30 and 1500 Oe. The source of hf energy was a pulse magnetron generating a wavelength of $\lambda_0 \approx 10$ cm ($\omega \approx 2 \cdot 10^{10}$ sec^{-1}). The pulse length of the magnetron was 10-40 μsec. The gas was pumped out of the resonator and quartz tube independently.

In the resonator the residual gas pressure was $\leq 10^{-5}$ mm Hg. For due choice of pressure in the quartz tube, discharge was ignited in the hf fields penetrating into the annular slit. Under the influence of the radial hf pressure, a paramagnetic current developed on the surface of the plasma so formed, so that the static magnetic field inside the plasma rose during the lifetime of the pressure (10-40 μsec). In order to measure the impulsive paramagnetic effect, a small measuring coil 5 mm in diameter and 5 mm long was placed inside the quartz tube in a stainless-steel screen 0.1 mm thick. The screen completely eliminated hf induction to the coil, but had practically no effect on the penetration of the pulsed magnetic field. The signal from the coil was taken to an integrating circuit and amplifier, and, thence to an oscillograph.

In order to determine the absolute magnitude of the hf field in the resonator, a calibrated hf probe (loop) was employed. The law governing the fall-off of the field in a radial direction in the annular gap was established by the measuring method given in [4].

Characteristics of the Plasma

The plasma spread along the lines of force of the static magnetic field in both directions from the annular gap, reaching distances of around 50 cm. The plasma concentration in the gap, estimated from the "cutting off" of electromagnetic waves with λ_0, equal to 4 and 8 mm on transmission of these through the plasma, was $10^{13} < n < 10^{14}$ cm^{-3}, independently of the nature of the gas (hydrogen, nitrogen, argon), in the working pressure range $5 \cdot 10^{-2} - 6 \cdot 10^{-4}$ mm Hg, for static magnetic fields of 30-1500 Oe. The experiments showed that the plasma had no effect on the character of the hf-field distribution within the resonator and annular gap not occupied by plasma. In the plasma itself, the hf field was effectively attenuated on approaching the axis of the system. The measured penetration depth d of the hf field into the plasma roughly corresponded to the characteristic value of the skin layer in plasma ($d \approx \frac{c}{\omega_0}$, where c is the velocity of light, and $\omega_0 = \sqrt{\frac{4\pi ne^2}{m}}$ is the Langmuir frequency of the plasma). This means that, in determining the radial pressure of the hf field on the plasma, we only need to know the component of hf magnetic field on the outer surface of the plasma.

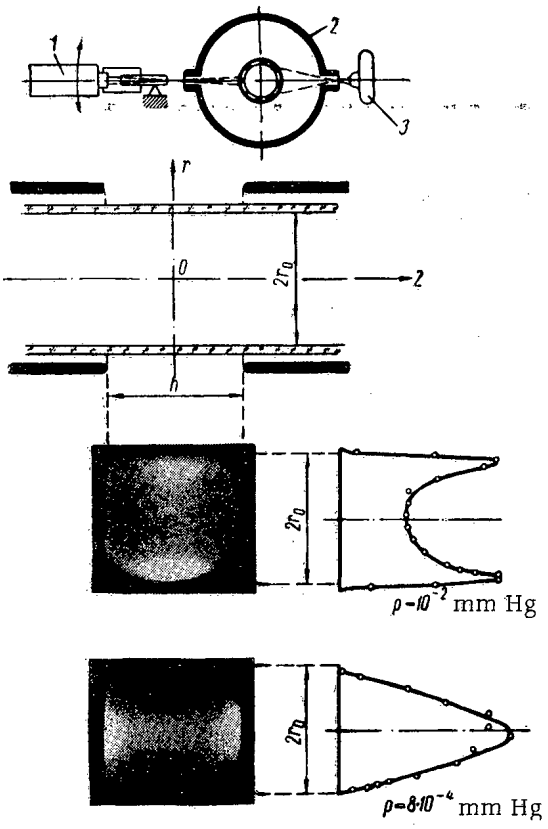

Fig. 2. Photographs of visible light from the plasma and luminosity/radius distribution curves. 1) Photomultiplier with collimator; 2) resonator (view from end); 3) camera.

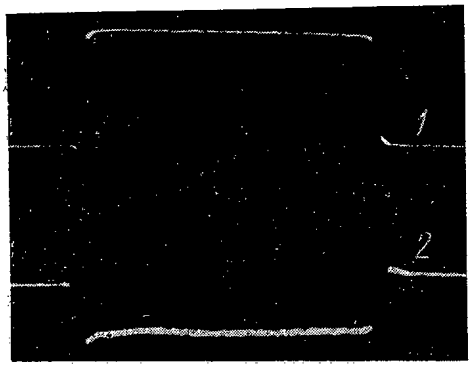

Fig. 3. Oscillograms of the envelopes of 1) the hf resonator pulse and 2) the paramagnetic signal.

It was found in the course of the experiments that the nature of the distribution of the visible light emitted by the plasma over the cross section of the quartz tube depended substantially on the gas pressure. Experiment showed that the light distribution corresponded qualitatively to the distribution of plasma concentration.

At high gas pressure ($\sim 10^{-2}$ mm Hg), the plasma formed a thin ring pressed to the walls of the quartz tube. As gas pressure diminished, the plasma moved away from the walls, and the inner diameter of the plasma ring fell; at a pressure of $\leq 10^{-3}$ mm Hg, a plasma pinch, "detached" from the walls, developed; this had a diameter of some 15 mm. Figure 2 shows two characteristic photographs of the light from the plasma and the corresponding distributions of visible plasma luminosity over the radius of the quartz tube at high and low gas pressures. The photographs and intensity curves were taken from the side in the manner illustrated in Fig. 2.

The "detachment" of the plasma from the walls of the quartz tube was apparently due to the repulsion of charged particles along the magnetic field by the inhomogeneous hf fields in the gap region. At low gas pressure, the ionization time at the quartz-tube walls may exceed the time corresponding to the expulsion of charged particles from the gap region; in such a case plasma is absent from the neighborhood of the walls.

Measurement of Paramagnetic Effect in the Plasma

Figure 3 shows some characteristic oscillograms of the envelopes of the hf resonator pulse (curve 1) and the signal from the measuring coil recording the impulsive change in the static magnetic field in the plasma (curve 2). It was found that, over almost the whole range of static magnetic fields examined, the magnetic field in the plasma increased under the influence of the hf pressure, i.e., there was a paramagnetic effect.

Figures 4 and 5 show typical relationships for the paramagnetic signal ΔH as a function of H^2 on the plasma surface with $\frac{\omega_H}{\omega}$ = const and of $\frac{\omega_H}{\omega}$, i.e., of the magnetic field, since ω = const, for constant values of hf pressure, where ω_H is the electron cyclotron frequency in the static magnetic field.

The relationships shown relate to nitrogen at a pressure of 10^{-2} mm Hg, i.e., to the cases of plasma not "detached" from the walls of the quartz tube. Analogous results were also obtained for low gas pressure ("detached" plasma), independently of the nature of the gas (hydrogen, helium, argon).

In Figs. 4 and 5 the broken lines show the relationships calculated from formula (2). The experimental and computed data agree quite well over a wide range of hf and static magnetic fields. Exceptions include two regions of static magnetic fields. The first relates to low magnetic fields; here static plasma equilibrium may be absent, since the pressure of the hf field is comparable with or greater than that of the static field, so that formula (2) cannot be validly applied in this region. The second discrepancy between theory and experiment occurs at $\omega_H/\omega = 0.5$ (see Fig. 5).

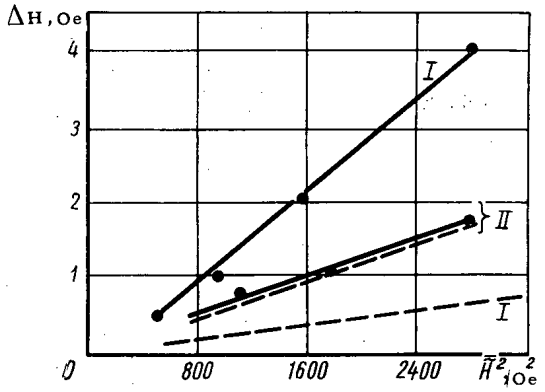

Fig. 4

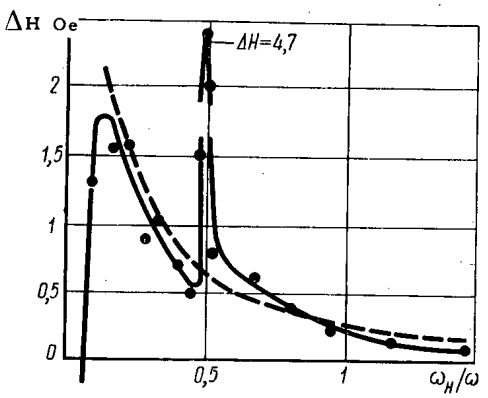

Fig. 5

Fig. 4. Paramagnetic signal as a function of hf pressure. Experimental conditions: r_0 = 1.9 cm, h = 1.9 cm, h_{eff} = 1 cm, p = 10^{-2} mm Hg, ——— experiment; – – – – – calculation; I) ω_H/ω = 0.5; II) ω_H/ω = 0.2.

Fig. 5. Paramagnetic signal as a function of static magnetic field. Conditions of experiment: $\tilde{H}$ = 57 Oe (at plasma surface); r_0 = 1.9 cm, h = 1.9 cm, h_{eff} = 1 cm, p = 10^{-2} mm Hg.

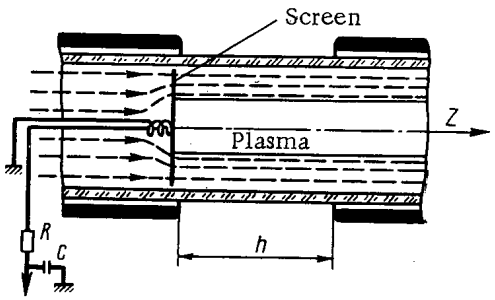

Fig. 6. Experiment for measuring plasma pressure.

Parametric Resonance in Plasma

At ω_H/ω = 0.5 the measured paramagnetic signal for various experimental conditions was five to eight times the calculated value. This was apparently because of the sharp rise in transverse plasma pressure resulting from resonance interaction with the hf field.

In order to determine the plasma pressure, we made the experiment illustrated in Fig. 6; this figure shows the region of the annular gap and the plasma "detached" from the walls of the tube on a large scale. On the one hand, the plasma is limited by a thin (0.1 mm) stainless-steel screen, behind which lies the measuring coil. Under the influence of the hf pressure a paramagnetic current flows on the plasma surface, increasing the static magnetic field inside the plasma. On the other hand, if, as a result of interaction with the hf fields, the transverse energy of the plasma rises, then from the well-known phenomenon of diamagnetism, the static magnetic field inside the plasma should fall. The sign of the signal from the measuring coil will depend on which effect predominates, paramagnetic or diamagnetic. These discussions are only valid for the particular experiment in which the plasma constitutes a continuous cylinder, inside which there are no measuring probes.

The broken lines in Fig. 6 indicate the static magnetic-field lines of force for the case in which the paramagnetic effect is small and the plasma energy, i.e., plasma pressure, is so large that the static magnetic field is completely expelled from the plasma. In this case, for pulsed operating conditions such as ours, the signal from the measuring coil will be determined by the diamagnetism of the plasma, i.e., by its pressure (somewhat under-estimated, since the measuring coil lies in the leakage field).

On carrying out experiments with hydrogen and argon, it was found that, for a static magnetic field with $\frac{\omega_H}{\omega}$ = 0.5, pressure approximately $9 \cdot 10^{-4}$ mm Hg, and hf field on the plasma surface $\tilde{\tilde{H}}$ = 90 Oe, the signal from the measuring coil was diamagnetic and corresponds to 60 Oe, i.e., the static magnetic field in the plasma was reduced by at least 60 Oe.

From the conditions of plasma equilibrium in hf and static magnetic fields

$$\frac{H_i^2}{8\pi} + p_0 = \frac{\bar{\tilde{H}}^2}{8\pi} + \frac{H_\delta^2}{8\pi};$$

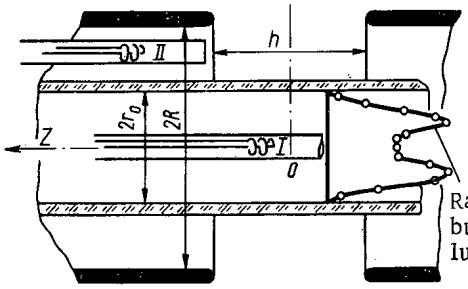

Fig. 7. Arrangement for measuring the paramagnetic signal inside (I) and outside (II) the plasma.

in this case it is not difficult to determine the plasma pressure $\frac{8\pi p_0}{\bar{H}^2} \approx 9$; $\frac{8\pi p_0}{H_0^2} \approx 0.2$, i.e., the plasma pressure is almost an order higher than the hf pressure and comparable with the pressure of the static magnetic field. For magnetic fields with $\frac{\omega H}{\omega} \neq 0.5$, the signal from the measuring coil was on a level with the threshold of sensitivity, i.e., in these cases the energy (pressure) of the plasma was small.

Thus, for $\frac{\omega H}{\omega} = 0.5$ there is a sharp resonance rise in plasma pressure. Since the plasma concentration (including that "detached" from the walls) is $n = 10^{13}$ to 10^{14} cm^{-3}, this means that the resonance rise in plasma energy takes place at $\frac{\omega_0^2}{\omega^2} \approx 10^3$.

The resonance rise in plasma energy is also responsible for the anomalously large paramagnetic signal found with experiments at $\frac{\omega H}{\omega} = 0.5$ (see Figs. 4, 5). In order to explain this we again turn to the measuring arrangement shown in Fig. 1. The total flux of the static magnetic field passing inside the thick-walled (4 mm) metal tube surrounding the quartz tube remains unaltered, independently of the presence or absence of plasma, since under the conditions of our experiment the diffusion time of the magnetic field for passing through the thick metal walls is much larger than the lifetime of the heated plasma (about 40 μsec). Hence, only a redistribution of field can take place: inside the heated plasma the field falls (diamagnetism), and outside the plasma-occupied region (including the location of the measuring coil) (see Fig. 1), it rises. For $\frac{\omega H}{\omega} = 0.5$ the measuring coil records this effect, which is much larger than the paramagnetic effect due to the hf pressure. In the absence of heating, however, i.e., for $\frac{\omega H}{\omega} \neq 0.5$, the paramagnetic effect predominates and it is this which is measured.

If the energy acquired by the plasma in the hf fields is partly transformed into heat as a result of dissipative processes, there should be a flow of heated plasma along the magnetic field beyond the limits of the annular gap. In this case, by moving the measuring coil into a region in which there is no hf field, we can record the impulsive rise in the static magnetic field associated with the diamagnetism of the heated plasma only. Figures 7 and 8 show the apparatus and results of experiments on measuring the distribution of the paramagnetic signal along the axis of the system for $\frac{\omega H}{\omega} = 0.5$. Measurements associated with plasma "detached" from the walls of the quartz tube are presented. The distribution of visible light over the radius of the plasma in the middle of the annular gap is also shown. Measuring coils were placed in two regions not occupied by plasma: inside, on the axis of the system (curve I), and outside, between the quartz tube and the metal wall (curve II); the broken curve (III) gives the computed distribution of the paramagnetic signal due to the radial hf pressure acting in the width of the gap.

By analyzing the results of the experiments, we may draw the following conclusions.

1. For $\frac{\omega H}{\omega} = 0.5$ there is an impulsive rise in the static magnetic field, even outside the range of action of the hf fields. This is due to the transformation of a large part of the plasma energy acquired in the hf field into thermal energy, to the spread of the heated plasma along the magnetic field, and also to the effect of the expulsion of the magnetic field mentioned earlier.

2. A long way from the annular gap, the magnetic fields inside and outside are equal. This means that the plasma is in fact detached from the walls of the quartz tube and the screen of the central measuring coil and is in hydrodynamic equilibrium with the magnetic field.

3. It might have been expected that in the region of the annular gap the difference between the ordinates of curves I and II (see Fig. 8) would have been equal to the ordinates of the computed curve III. This is nevertheless not so. Apparently, in writing down the conditions of equilibrium for this region, we should remember that the magnetic field driven away by the heated plasma may penetrate into the gap and become inhomogeneous instead of

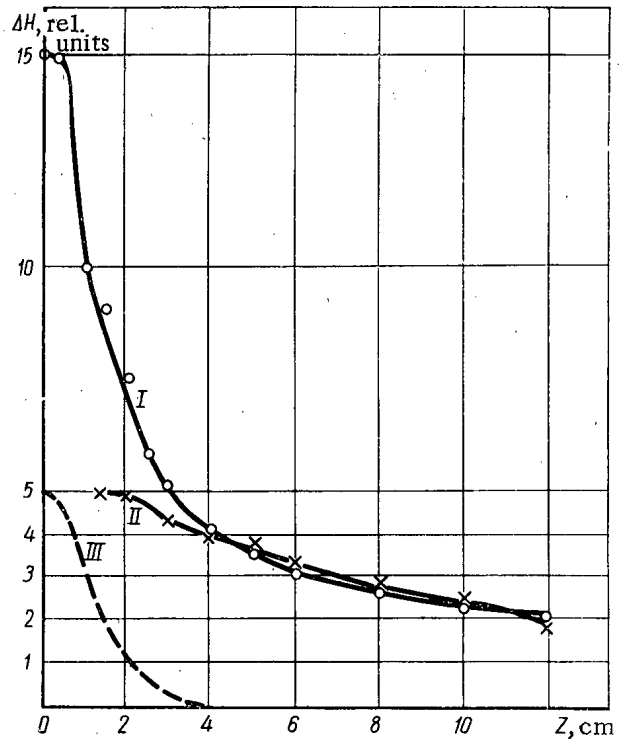

Fig. 8. Distribution of paramagnetic signal along the axis, inside and outside the plasma. Conditions of experiment: h = 2 cm; r_0 = 1.2 cm; R = 2.3 cm.

homogeneous (as is the case a long way from the gap). For an inhomogeneous magnetic field the above relationship between the ordinates of the curves may not even be satisfied in the presence of equilibrium. Probably hydrodynamic equilibrium of the plasma holds even in this region, since, according to the radial light distribution, the plasma pinch is also "detached" from the walls.

Let us consider the reasons underlying the heating of the plasma at $\frac{\omega_H}{\omega} = 0.5$. Since the experiments were made at high frequencies ($\lambda \approx 10$ cm, i.e., $\omega \approx 2 \cdot 10^{10}$ sec^{-1}), we are only concerned with the heating of the electron component of the plasma.

In the region of the annular gap, where interaction between the plasma and the hf field takes place, there is a considerable longitudinal component of the hf magnetic field. This means that, in the region of the gap, electron is acted upon not by the static field $\mathbf{H}_0$, but by $H_0 + H \sin \omega t$. This must lead to a periodic time variation of the Larmor electron-rotation frequency $\omega_H = \frac{e(H_0 + \tilde{H} \sin \omega t)}{mc}$. An oscillatory system in which the frequency changes periodically with time can have several resonances. The principal resonance occurs at $\frac{\omega_H}{\omega} = 0.5$. Such a resonance is usually called parametric. A second resonance occurs at $\frac{\omega_H}{\omega} = 1$; this is the ordinary electron cyclotron resonance. At cyclotron resonance, phase focusing leads to the bunching of the electrons into a single bunch. In the presence of plasma having a substantial concentration, when $\omega_0 > \omega_H$, this rotating bunch creates additional polarization fields, and this leads to the displacement of the natural electron-oscillation frequency. It is well-known that in this case resonance conditions are satisfied for $\omega = \sqrt{\omega_0^2 + \omega_H^2}$ [5]. Under the conditions of our experiments, for which $\omega_0^2 >> \omega_H^2$, resonance should not be observed at $\omega_H = \omega$, as was indeed confirmed.

At parametric resonance, phase focusing leads to the formation of two bunches of electrons. The polarization field created by one bunch will be almost entirely compensated by the field of the other, and resonance should therefore not be displaced. This is apparently why electron paramagnetic resonance is preserved in high-concentration plasma. The electrons of the plasma take on a considerable ordered energy in the hf field, and this is then transformed into heat as a result of dissipative processes.

Thus, we have shown experimentally that a steady paramagnetic current flows in plasma situated in a longitudinal magnetic field under the influence of hf pressure. The increased static magnetic field in the plasma produced by this current (paramagnetic effect) agrees with computed results.

Resonance heating of the electrons in the plasma by the hf field also takes place. This is associated with parametric resonance of the electrons at $\frac{\omega_H}{\omega} = 0.5$ and exists in dense plasma for $\omega_0^2 \gg \omega_H^2$ and $\omega_0^2 \gg \omega^2$.

LITERATURE CITED

1. T. F. Volkov, V. M. Glagolev, and B. B. Kadomstev, Nucl. Fusion, Suppl., Part 3 (1962).
2. T. F. Volkov and B. K. Kadomtsev, "Atomnaya énergiya," 13, 429 (1962).
3. Yu. I. Arsen'ev, et al., Nucl. Fusion, Suppl., Part 2 (1962), p. 687.
4. S. Kitches and A. Schelbery, J. Appl. Phys., 26, No. 5 (1955).
5. V. D. Shafranov, Questions of Plasma Theory [in Russian], 3, Gosatomizdat, Moscow (1963), p. 3.

OPTICAL EXCITATION AND IONIZATION OF FAST HYDROGEN ATOMS

D. P. Grechukhin, É. I. Karpushkina, and Yu. I. Sokolov

UDC 533.9:539.186:539.188

The possibilities of increasing the efficiency of fast hydrogen atom injection into a magnetic trap by the following methods are considered.

1. By increasing the population of higher levels ($n \approx 10$) in a fast hydrogen atom beam through irradiation by quanta in resonance with a selected $n_1 l_1 \rightarrow n_2 l_2$ transition, for example 2s–10 p. The dependence of the $n_2 l_2$-level population on radiation density and atom time-of-flight in the light field was found. On the basis of the data obtained, an estimate was made of the required power of the light source.

2. By photoionization of hydrogen atoms directly in the active region of the trap. On the basis of a calculated radiation wavelength dependence for the value of the hydrogen atom photoionization cross section, the intensity of the light flux needed for efficient ionization of the atoms was estimated.

A consideration of the process of filling a magnetic trap by injecting a beam of highly excited neutral atoms shows that the methods presently being used for producing fast, highly-excited hydrogen atoms by the dissociation of protons in a gas target is unprofitable from the practical point of view because all possible hydrogen atom states become populated in that case, the population dropping sharply with increase in principal quantum number [1-7]. Because of this, only a small fraction ($\sim 10^{-4}$) of the initial ion current is captured in the trap [8, 9].

It is possible to achieve an increase in the population of any given level in a beam of neutral hydrogen atoms by exciting, in one way or another, the atoms which are in one of the lowest, and, therefore, most densely populated, states. Such selective excitation can be accomplished, for example, by irradiating H_1^0 atoms with quanta in resonance with the transition from a lower $n_1 l_1$ to a higher $n_2 l_2$ state.

Suppose that the target in which molecular dissociation or proton charge-exchange occurs has a sufficiently sharp boundary and that the beam of H^0 atoms escaping from it then falls into an irradiation chamber having a residual gas density sufficiently small so that one can neglect collisions leading to the following hydrogen atom transitions: 1s → 2s, 2s → 1s, 1s → np, 2s → np, np → 1s, ns → 2p, and also to the ionization of hydrogen atoms in the 1s and 2s states.

Consider the process from the initial metastable 2s state as a general case of one-photon pumping to an np level in the hydrogen atom.

The spectral density of the radiation per unit volume in the region of the beam will be measured in units $u^0_{i,k} = \frac{8\pi h \nu_{i,k}^3}{c^3}$, where $\nu_{i,k}$ is the frequency corresponding to the i → k transition. Thus, $u_{i,k} = u^0_{i,k} I$, where I is a dimensionless quantity characterizing the energy density of the radiation.

From a solution of the system of transport equations including the 2s–2p-transition through the action of an electric field in the irradiation chamber, it follows for the process under consideration that the fraction of atoms in the initial state which are transferred into level n during a time t can be represented in the following form:

$$p_{np}(t) = \frac{f_{2,n}}{\sqrt{\left(\frac{B_1}{2}\right)^2 - B_0}} e^{-\frac{B_1 t}{2}} sh \sqrt{\left(\frac{B_1}{2}\right)^2 - B_0 t}, \quad (1)$$

Translated from Atomnaya Énergiya, Vol. 20, No. 5, pp. 407-412, May, 1966. Original article submitted September 16, 1965.

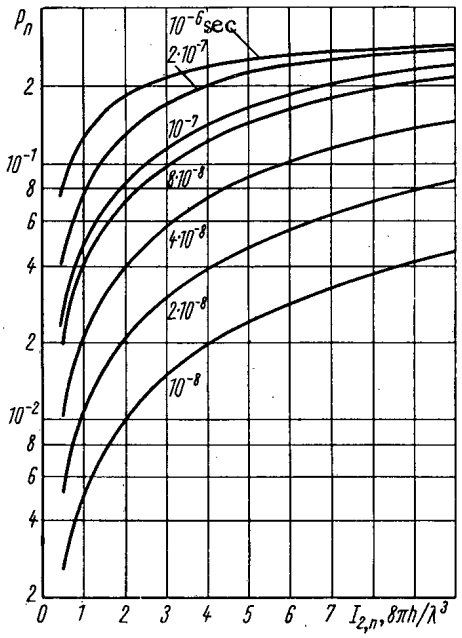

Fig. 1. Dependence of p_n on $I_{2,n}$ for the 1s–2p–10d transition ($I_{1.2}$) = 0.2).

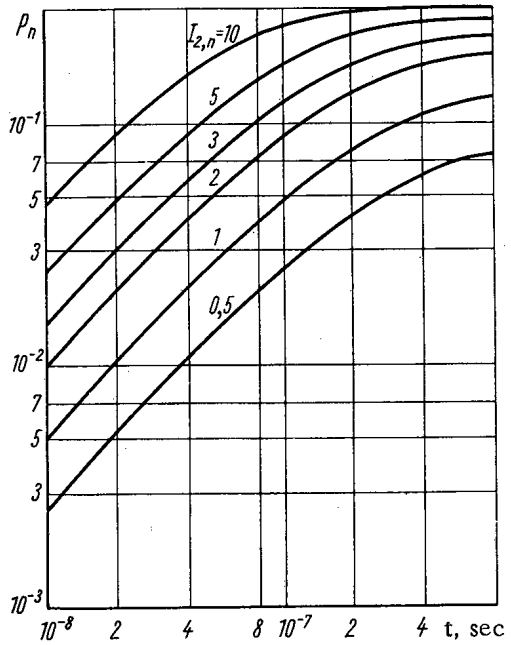

Fig. 2. Dependence of p_n on t, time of flight in the radiation field, for the transition 1s–2p–10d ($I_{1.2}$ = 0.2).

where

$$B_0=\varphi_{2,1}\zeta_{n,\alpha}+\varphi_{2,1}f_{n,2}+\varphi_{2,1}\varphi_{n,2}+\varphi_{2,1}\varphi_{n,1}+f_{2,n}\zeta_{n,\alpha}+f_{2,n}\varphi_{n,1};\quad B_1=\varphi_{2,1}+f_{2,n}+\zeta_{n,\alpha}+f_{n,2}+\varphi_{n,2}+\varphi_{n,1};\quad f_{2,n}=B_{2s,np}u_{2,n};\quad f_{n,2}=B_{np,2s}u_{2,n};\quad \varphi_{n,2}=A_{np,2s};\quad \varphi_{n,1}=A_{np,1s};$$
$$\varphi_{2,1}=6{,}25\cdot10^8\,(F/475)^2\ \text{cm}^{-1}.$$

Here, $A_{i,k}$ and $B_{i,k}$ are the Einstein coefficients for spontaneous and induced radiation transitions, respectively; F is the electric field in the irradiation chamber; $\zeta_{n,\alpha}$ is the ionization probability for an excited state, equalling $\sum_i vn_i\sigma_i+\int j(\omega)\,\sigma(\omega)\,d\omega$, where v is the velocity of the $H_1^0(n, l)$ atom with respect to a gas molecule; n_i is the density of particles of type i (ions, electrons, molecules with dipole and quadrupole moments) in the residual gas of the irradiation chamber; σ_i is the ionization cross section of the $H_1^0(n, l)$ atom for type i particles (for $n \gg 1$); $j(\omega)$ is the flux of quanta per unit frequency range; $\sigma(\omega)$ is the corresponding differential photoionization cross section.

If at the time of escape from the neutralizing target (t = 0), the number of $H_1^0(2s)$ atoms in the beam is $n_0p_{2s}(0)$, the number of atoms transferred to the np level after a time t because of irradiation will be $n_0p_{2s}(0)p_{np}(t)$.

Calculation of the population $p_{np}(t)$ for the case of one-photon pumping from the 1s state is carried out in a similar manner. However, since the 1s state is stable, the corresponding transport equations will not contain the term involving the probability of a transition under the action of an electric field.

For two-photon pumping from the 1s state, the atoms must be irradiated simultaneously by quanta with frequencies $\nu_{1.2}$ and $\nu_{2,n}$ in resonance with the 1s → 2p and 2p → n (s, d) transitions.

In this case, the fraction of atoms in the initial state which is transferred to level n is determined in the following manner:

$$p_n(t)=\frac{\alpha_{1,2}\alpha_{2,n}}{\gamma\Delta}\left[\Delta-\frac{1}{2}(\varkappa+\Delta)e^{-\frac{1}{2}(\varkappa-\Delta)t}+\frac{1}{2}(\varkappa-\Delta)e^{-\frac{1}{2}(\varkappa+\Delta)t}\right], \tag{2}$$

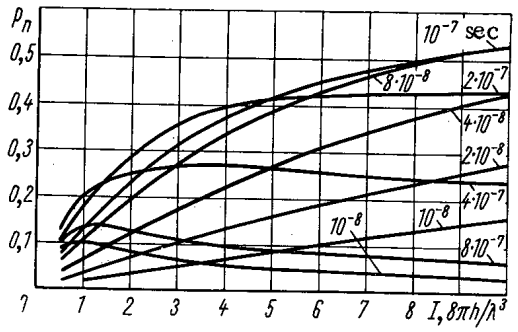

Fig. 3. Dependence of p_n on I for 2s–10p transition.

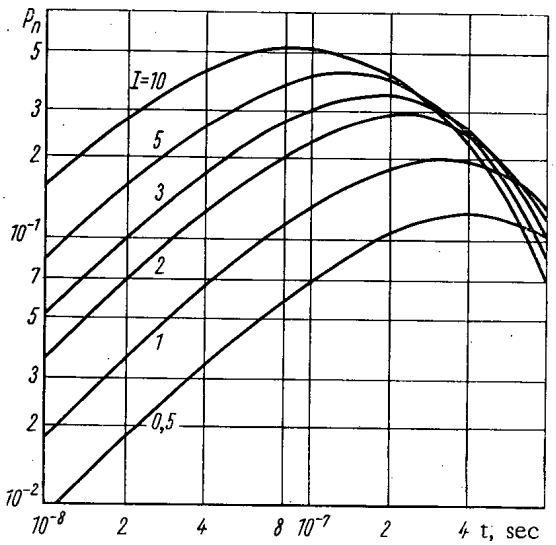

Fig. 4. Dependence of p_n on time of flight in radiation field for 2s–10p transition.

where

$$\varkappa = (\beta_{2,1} + \alpha_{1,2} + \alpha_{2,n} + \beta_{n,2} + C_{n,1}); \quad \gamma = (\alpha_{1,2}\alpha_{2,n} + \alpha_{1,2}\beta_{n,2} + \alpha_{1,2}C_{n,1} + \beta_{2,1}\beta_{n,2} + \beta_{2,1}C_{n,1} + \alpha_{2,n}C_{n,1}); \quad \Delta = +\sqrt{\varkappa^2 + \gamma^2}; \quad \alpha_{1,2} = u_{1,2}B_{1,2}; \quad \alpha_{2,n} = u_{2,n}B_{2,n}; \quad \beta_{2,1} = u_{1,2}B_{2,1}; \quad \beta_{n,2} = u_{2,n}B_{n,2}; \quad C_{n,1} = \sum_{k<n} A_{nk}.$$

It follows from expression (2) that, in the limit, when $1/2\,(\varkappa - t) \to \infty$,

$$p_n(t) \longrightarrow \frac{\alpha_{1,2}\alpha_{2,n}}{\gamma} = p_n(\infty),$$

which corresponds to saturation.

The dependence of population p_n on resonance radiation density I and on atom flight time t in the light field is shown in Figs. 1-4 for the 2s–np and 1s–2p–n(s, d) processes. In determining the dependence, consideration was given to photoionization from the n(s), n(p), and n(d) levels through the action of monochromatic quanta in resonance with the transitions mentioned. The photoionization effect is negligibly small and is apparent as a reduction in the value of p_n with increasing I for large atom flight times in the light field.

In considering the 2s–np process, the electric field strength inside the beam was assumed to be 3 V/cm. This value is evidently reasonable for beam currents of ~50 mA. It should be pointed out that the nature of the $p_n(I)$ curves does not change significantly for changes in field strength from 0 to 10 V/cm. The values for p_n were based on the assumption that the irradiation chamber pressure was 10^{-6} mm Hg. The proton energy was assumed to be 20 keV.

From the calculations and from the curves shown in Fig. 1-4, efficient pumping to an n level (for $n \approx 10$) requires the following radiation density:

1) $I_{1,n}$ must not be less than 0.1 for one-photon pumping from the 1s state, i.e., for the excitation of 1s–np transitions;

2) the values of $I_{1,2}$ and $I_{2,n}$ must be not less than 0.2 and 1, respectively, for two-photon pumping from the 1s state, i.e., for the excitation of 1s–2p–n(s, d) transitions;

3) the value of $I_{2,n}$ must be not less than 1 for one-photon pumping from the 2s state, i.e., for excitation of 2s–np transitions.

Take the 2s–10p transition ($\lambda = 3.78 \cdot 10^{-5}$ cm) as an example. In this case, the problem of efficient excitation of the transition specified in a beam of hydrogen atoms reduces to the following: it is necessary to produce along the beam trajectory a light field with density $I \approx 2$ and frequency $\nu_{2s,10p} = 8 \cdot 10^{14}$ sec^{-1} in the spectral range $\Delta\nu = H_s$, where H_s is the natural width of the line which corresponds to the 2s–10p transition, and is $2.6 \cdot 10^7$ sec^{-1}. The requirement specified is equivalent to one that demands there pass through an area of 1 cm^2 located on the beam trajectory a light flux with an intensity

$$P = \frac{8\pi h}{\lambda^3} cIH_s = 4{,}7 \cdot 10^6 \text{ erg/sec} \cdot \text{cm}^2.$$

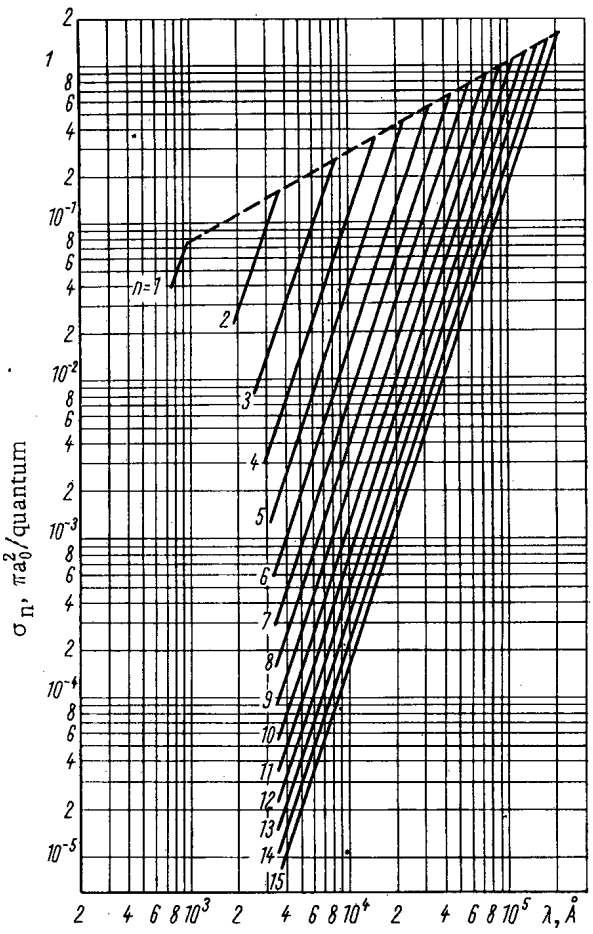

Fig. 5. Dependence of the average value σ_{pn} of the hydrogen atom photoionization cross section for levels with principal quantum number n on wavelength λ ($\bar{\sigma}_n = \frac{1}{n^2}\sum_{l=0}^{l=n-1} \sigma_{nl}(\lambda)(2l+1)$, a_0 is the Bohr radius).

From the data presented, it follows that the specific radiation intensity required for efficient transition of H_1^0 atoms to higher levels is not too great. However, in estimating the actual intensity of a lamp which will provide the required density I on the beam trajectory, change in radiation frequency because of the Doppler shift acquires vital importance. The effect of the latter on the efficiency of an illuminating system is different depending upon whether the radiation at each point of the lamp is propagated in all directions or whether the source gives a directed light flux.

Consider the following illuminating systems:

1) illumination by a collimated bundle of rays (laser case); 2) illumination by an extended isotropic source located along the beam trajectory.

1. Let a laser be used for illumination, operating in the pulsed or continuous mode of operation as demanded by the required injection time. If the frequency ν_0 of the line emitted by the laser does not coincide with the frequency $\nu_{i,k}$ of the hydrogen atom, the frequency difference can be compensated within known limits by means of the Doppler shift $\Delta\nu = \nu_0 \frac{v}{c}\cos\alpha$, where α is the angle between the beam trajectory and the direction of the light flux; v is the velocity of the beam atoms.

In estimating the efficiency of the process of hydrogen atom excitation by laser beam illumination, it is necessary to consider the relationship between the width $\Delta\nu_0$ of the line emitted by the laser and the "collector width," i.e., the spread of Doppler shifts

$$\Gamma = \Gamma_E + \Gamma_\alpha,$$

where $\Gamma_E = \frac{\nu_{i,k} v\cos\alpha}{2c}\cdot\frac{\Delta E}{E}$ is the spread resulting from nonuniformity in the energy of beam atoms; $\Gamma_\alpha = \nu_{i,k}\frac{v}{c}\sin\alpha\Delta\alpha$ is the spread resulting from nonparallelism of their trajectories and from divergence of the laser beam. Here, $\nu_{i,k} = \nu_0(1+\frac{v}{c}\cos\alpha)$ is the line frequency in the moving atom system at the point of intersection of the beam trajectory and the light rays; ΔE is the energy spread of the beam atoms; Δα is the total angular divergence of the atomic beam and laser beam.

If we assume $\Delta E/E = 10^{-2}$, Γ_E turns out to be $\sim 10^{10}$ sec^{-1}. In order that the value of Γ_α be of the same order of magnitude, Δα must not be greater than $\sim 10^{-3}$ radians which places extremely rigid requirements on atomic beam collimation.

The conditions specified considerably increase the required intensity of laser radiation. For a width Γ of the order of the natural width $H_{2s,\,10p} = 2.6\cdot 10^7$ sec^{-1}, the radiation intensity of a laser which emits a spectral line of the same width must be ~ 0.5 W/cm^2 (for I = 2). For greater collector widths, this value must be increased in proportion to the ratio $\Gamma/H_{2s,\,10p}$, which for a practially acceptable value $\Gamma \approx 10^{10}$ sec^{-1} comes to as much as ~ 500 W/cm^2.

2. For an isotropic source located parallel to the trajectory of the beam at a distance r, we find the total intensity of a radiator with a length l which is determined by the required atom flight time in the light field.

If the source emits a single spectral line of width H_s, the light flux in the required frequency range through an area s = 1 located on the beam trajectory will be produced only by the radiation from a segment $\Delta x = r\frac{c}{v}\frac{H_s}{\nu_{i,k}}$.

For r = 10 cm, v = $3 \cdot 10^8$ cm/sec, $\nu_{i,k} = 8 \cdot 10^{14}$ sec^{-1}, and $H_s = 2.6 \cdot 10^7$ sec^{-1}, Δx is $3.3 \cdot 10^{-5}$ cm. Under the specified conditions, the flux intensity P is determined in the following manner:

$$P = \frac{8\pi h}{\lambda^3} cIH_s = \frac{P_{\Delta x}}{r^2},$$

where $P_{\Delta x}$ is the radiation intensity of the segment Δx expressed in erg/sec-sr.

Illumination of the beam by an extended isotropic source emitting a single, narrow line ($\sim H_s$) is similar to illumination by a chain of "point" sources, each of which has a length Δx and radiates $P_{\Delta x}$ (erg/sec-sr). The total power of a lamp with length l will be $W = 4\pi P_{\Delta x} l/\Delta x$. For $P_{\Delta x} = r^2 P = 5 \cdot 10^8$ erg/sec-sr and l = 50 cm, $W \approx 10^9$ W.

If an extended isotropic source emits a spectral band of width H, the solid angle $\Delta\omega$, within which is propagated radiation, emitted by an elementary area $d\sigma$, having the frequency $\nu_{i,k}$ in the system of the moving atom, turns out to be proportional to the width H. Optimal conditions for illumination of the beam occur when $H = 2\nu_{i,k} v \cos\frac{\alpha}{c}$, i.e., twice the value of the maximum Doppler shift calculated for frequency $\nu_{i,k}$ and velocity v; α is the smallest angle between the lines passing through the outermost points of the radiator and the trajectory of the atoms.

In the case under consideration, the expression for the total power of the lamp takes the following form:

$$W = 4\pi u_{i,k} r v \nu_{i,k} l.$$

For I = 2, r = 10 cm, v = $3 \cdot 10^8$ cm/sec, $\nu_{i,k} = 8 \cdot 10^{14}$ sec^{-1}, and l = 50 cm, the total power W is $\sim 10^9$ W.

The data that has been obtained makes it possible to reach the following conclusion. Intense proton pumping to higher levels of hydrogen atoms by means of an isotropic source of any kind appears to be practically unrealizable because of the influence of the Doppler effect, which leads to a sharp reduction in the efficiency of the illuminating equipment because of the resonance nature of the process. Only those systems are of interest in which narrow, well-collimated beams of atoms are illuminated by a laser beam.

It was mentioned above that an increase in the efficiency for capture of highly-excited hydrogen atoms can be achieved, in principle, by their photoionization directly in the magnetic field of the trap. The dependence of photoionization cross section on radiation wavelength is shown in Fig. 5. The figure indicates that the most intense ionization of hydrogen atoms at the level n = 10 occurs with illumination of the beam by infrared radiation having a wavelength of $\sim 9\ \mu$. The associated evaluation indicates that the required radiation intensity must be about 10^4 W/cm^2 for a flight time of the light field of $\sim 10^{-7}$ sec.

It should be pointed out that the values given for the power can be reduced by approximately two orders of magnitude because of multiple reflection of the light, since the reflection coefficient in this wavelength region reaches 99% for some metals. In this way, the value of the radiation density approaches a quantity which can be achieved with a gas laser, a laser operating with a $N_2 + CO_2$ mixture ($\lambda = 10.6\ \mu$), for example.

The authors are grateful to I. N. Golovin for discussions and for consideration of this work, and to Z. V. Tokareva for numerical computations and for drawing the curves.

LITERATURE CITED

1. I. Jackson and H. Schiff, Phys. Rev., 89, 359 (1953).
2. C. Barnett, W. Gauster, and J. Ray, Atomic and Molecular Collision Cross Sections, ORNL-3113.
3. D. Sweetman and A. Riviere, Report 1B10 presented by Great Britain at the Sixth International Conference on Ionization Phenomena in Gases, Paris (1963).
4. A. Futch and C. Damm, Nucl. Fusion, 3, 124 (1963).
5. S. V. Bobashev, E. P. Andreev, and V. A. Ankudinov, ZhÉTF, 45, 1759 (1963).
6. S. Butler and R. May, Phys. Rev., 137, (No. 1a), 10 (1965).
7. J. Hiskes, Phys. Rev., 137, (No. 2a), 361 (1965).
8. L. I. Artemenkov, et al., Report 21/238 presented by the USSR at the Second International Conference on Plasma Physics, Culham (1965).
9. L. Kuo, et al., Phys. Fluids, 7, 988 (1964).

THE EFFECT OF CERTAIN CYCLE PARAMETERS ON THE EFFICIENCY OF A NUCLEAR GAS TURBINE UNIT

E. F. Ratnikov and M. V. Shustov

UDC 621.039.553.3

The effect is analyzed of the increase of the effective pressure ratio, the regeneration factors, the initial gas pressure, temperature of the fuel element cladding, hydraulic resistance of the gas circuit on the internal efficiency of a nuclear gas turbine unit, taking into account the characteristics of the active zone of the reactor. The results are given of the effect on the efficiency of a nuclear gas turbine unit (NGTU) of the intermediate heating and cooling of the gas. A possible circuit for a NTGU is discussed, with one intermediate heating and three-stage cooling of the gas.

In connection with the development of high temperature gas cooled reactors, interest has been aroused for some time past in the nuclear gas turbine unit. Even now, high temperature reactors are operating and are under construction in a number of countries (Great Britain, USA, and the Federal German Republic), in which the gas is heated up to a relatively high temperature (750-850°C) [1-3]. In plans for the development of nuclear energy generation, the construction of relatively large-scale high temperature reactors with gas cooling is specified. The feasibilities of heating the gas to a temperature which is considerably in excess of 1000°C is being studied in experimental units at the present time (for example, in the UNTREX experimental unit in the USA, the gas temperature at the outlet from the reactor is 1320°C [4]). The limits of practical application of high temperature units with gas cooling are being considerably extended as a result of the positive solution of the cooling of fast reactors with helium.

Recently, plans for fixed and marine NGTU have been worked out. The planned units are usually single loop with two-stage gas compression, preferably with helium cooling and a gas temperature prior to the turbine of 750-800°C.

The results are given in this paper of an investigation of the effect of the individual parameters (temperature and pressure of the gas prior to the turbine, effective pressure ratio, regeneration factors, etc.) of a NGTU and also NGTU designs (intermediate gas cooling and heating) on the internal efficiency of the unit, taking into account the operation of the reactor.

Figure 1 shows the simplest layout of a NGTU, and Fig. 2 shows the T–S diagram of the working cycle. The internal efficiency of this unit, taking into account the effect of certain characteristics of the reactor core, can be described by the following expression

$$\eta_i = \frac{\left[\left(1-\frac{\Delta p^m}{\sigma^m}\right)\eta_{GT} - \frac{\tau}{\eta_C}(\sigma^m - 1)\right] K_t}{\delta - \mu\left[1-\left(1-\frac{\Delta p^m}{\sigma^m}\right)\eta_{GT}\right] - (1-\mu)\tau\left(1+\frac{\sigma^m-1}{\eta_C}\right)}, \quad (1)$$

where

$$\Delta p = \frac{p_1 + \Delta p_p + \sigma \Delta p_{r \cdot c}}{p_1}; \quad (2)$$

$$K_t = \frac{k_r k_{\Delta t}}{k_G}\left[0.5 + \sqrt{\frac{0{,}25}{\sin^2\frac{\pi}{2}\cdot\frac{H}{H_{equ}}} + \left(\frac{k_h k_G \bar{c}_p G_C}{k_{\Delta t}\alpha_c F_s}\right)^2}\right]; \quad (3)$$

Translated from Atomnaya Énergiya, Vol. 20, No. 5, pp. 412-415, May, 1966. Original article submitted October 30, 1965.

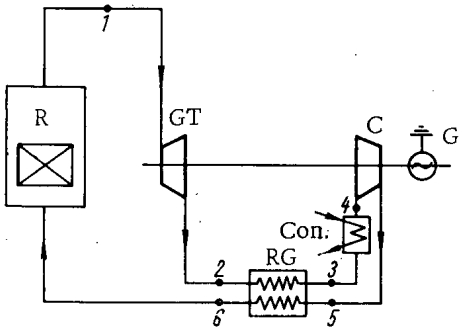

Fig. 1. Schematic diagram of a gas turbine unit: R) reactor; GT) gas turbine; C) compressor; RG) regeneration; Con) condenser; G) generator.

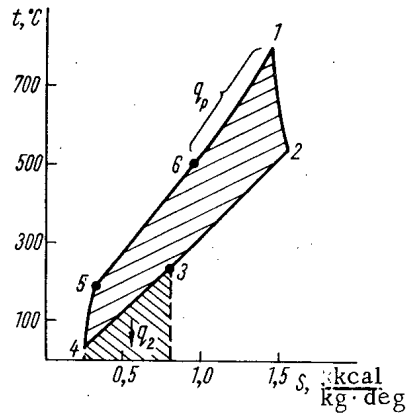

Fig. 2. T–S diagram of the working cycle of a gas turbine unit (t_1 = 800°C; σ = 2.5; μ = 0.9).

$$\sigma = \frac{p_5}{p_4}\ ; \tag{4}$$

$$\tau = \frac{T_4}{T_1}\ ; \tag{5}$$

$$\delta = \frac{T_W^{max}}{T_1}\ ; \tag{6}$$

$$\mu = \frac{T_6 - T_5}{T_2 - T_5}\ . \tag{7}$$

In Eqs. (1)-(7), the following arbitrary symbols are used: σ, effective pressure increase ratio in the cycle; μ, the heat regeneration factor of the gas; p_1, the initial gas pressure in the cycle; Δp_r, the hydraulic resistance of the reactor (with pipelines); $\Delta p_{r.c.}$, the hydraulic resistance of the regenerator and condensers (with pipelines); k_r, k_h, the nonuniformity factors along the radius and height of the reactor respectively; k_G, the nonuniformity factor of the gas supply through the channels; $k_{\Delta t}$, a factor which takes into account the temperature variations of the channel wall from the calculated value; H, the height of the reactor channel; H_{equ}, the equivalent height of the reactor channel; c_p, the mean specific heat of the gas; G_C, the total coolant supply; α_c, the heat transfer factor to the coolant; F_S, the total surface area of the fuel element cladding; T_W^{max}, the maximum wall temperature of the fuel element cladding; η_{GT}, the gas turbine efficiency; η_C, the compressor efficiency; T_1, T_2, T_4, T_5, T_6, P_4, P_5, the absolute temperatures and pressures corresponding to the points in Fig. 1;

$$m = \frac{k-1}{k}\ , \text{ where } k = \frac{c_p}{c_v}\ .$$

It follows from Eqs. (1)-(7) that the internal efficiency of the gas turbine cycle depends on a very large number of variables, some of which define the gas turbine section (σ, τ, μ, $\Delta p_{r.c}$, η_{GT}, η_C, etc.), and others define the reactor section of the unit (δ, G_C, α_C, F_S, etc.).

Figure 3 shows the change of internal efficiency of the cycle η_i on the effective pressure increase ratio σ and the regeneration factor μ for t_1 = 800, 1000 and 1300°C and, correspondingly, t_W^{max} = 900, 1100 and 1400°C (helium gas). It is assumed for the calculations that η_{GT} = 0.87; η_C = 0.85; hydraulic resistance of the loop ($\Delta p_r + \Delta p_{r.c}$) = 2.5 kg/cm^2; gas pressure p_1 prior to the turbine is 60 atm; the gas temperature after the condenser

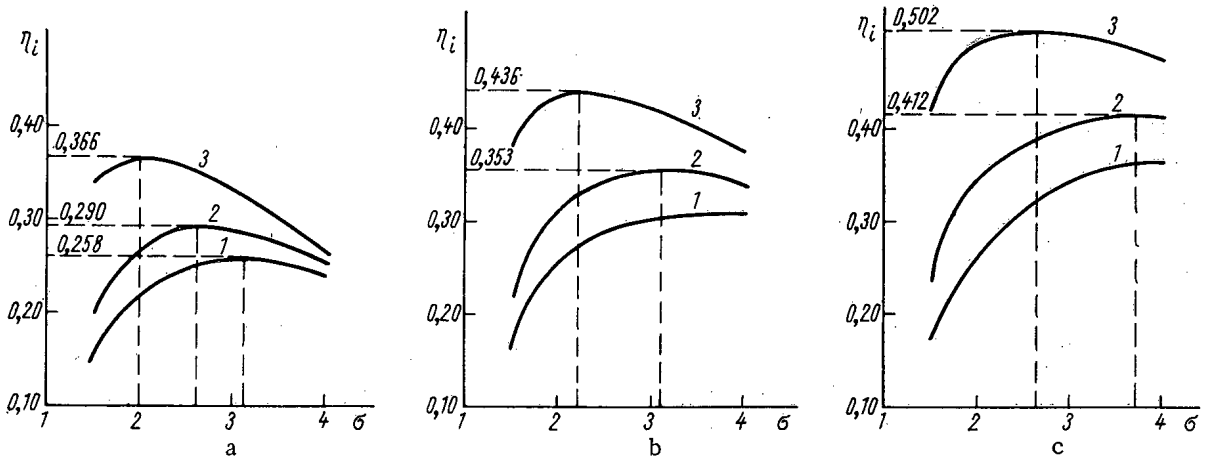

Fig. 3. Relationship $\eta_i = f(\sigma, \mu)$ at different values of t_1: a) t_1 = 800°C; b) 1000°C; c) 1300°C; 1) μ = 0.5; 2) −0.7; 3) −0.9.

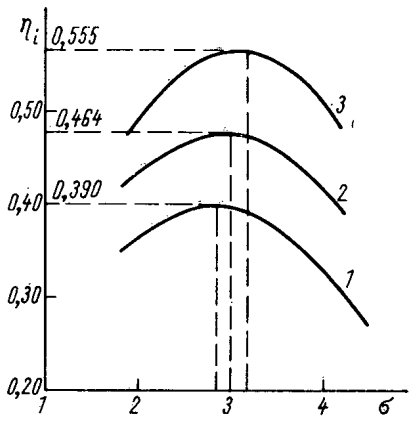

Fig. 4. Relationship $\eta = f(\sigma)$ for intermediate gas cooling (μ = 0.9): 1) t_1 = 800°C; 2) 1000°C; 3) 1300°C.

is 35°C*. It follows from Fig. 3 that the relationship $\eta_i = f(\sigma)$ is curvilinear, with a maximum η_i at a completely defined effective pressure ratio σ.

The numerical values of η_i^{max} and $\sigma_{opt.}$ depend, to a considerable degree, on the values assumed for μ and t_1. An increase of the regeneration factor μ increases the efficiency of the unit and reduces the optimum value of the effective pressure ratio. An increase of the temperature of the gas prior to the turbine leads to an increase of the efficiency and of the effective pressure ratio. For example, for μ = 0.9:

t_1, °C	η_i^{max}, %	σ_{opt}
800	36.66	2.0
1000	43.6	2.2
1300	50.2	2.6

The change of temperature of the fuel element cladding t_W^{max} has relatively little effect on the efficiency of the NGTU. This can be seen from the following data (for t_1 = 800°C, σ = 2.0 and μ = 0.9):

t_W^{max}, °C	t_W^{max}, °C	η_i, %
860	60	36.68
900	100	36.66
1060	160	36.60

An increase of temperature of t_W^{max}, i.e., an increase of the difference $(t_W^{max} - t_1)$ reduces the efficiency of the unit somewhat, because of the irreversible heat losses at the heat exchanger. A change of the initial gas pressure p_1 has a more significant effect on the magnitude of η_i. For example, with t_1 = 800°C, σ = 2.0, μ = 0.9 and $(\Delta p_r + \Delta p_{r.c.})$ = 2.5 kg/cm²:

p_1, atm	η_i, %
60	36.66
80	37.70
100	38.80

*All calculations are carried out with unchanged reactor powers (N_c = 100 MW) and geometrical parameters F_s H, H_{equ}.

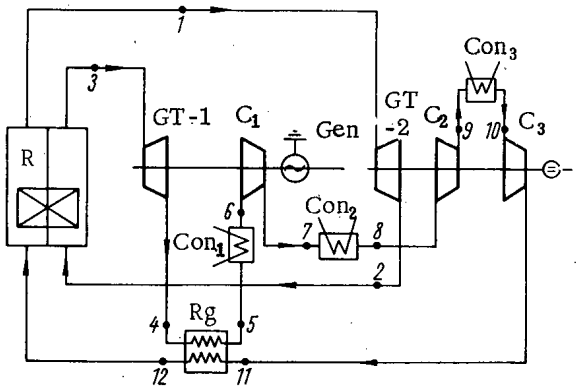

Fig. 5

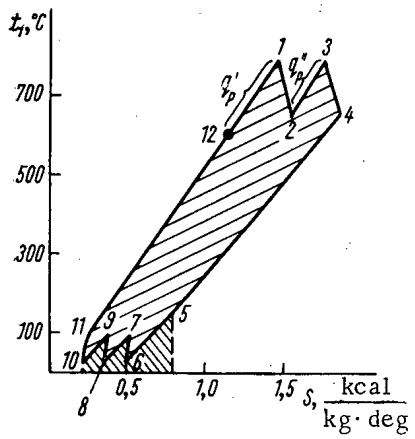

Fig. 6

Fig. 5. Schematic diagram of a NGTU with intermediate gas heating and cooling.

Fig. 6. T–S diagram of the operating cycle of a NGTU with intermediate gas heating and cooling (points 1-12 correspond to the points shown in Fig. 5).

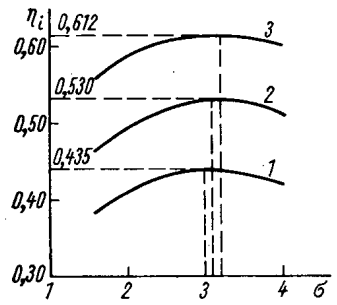

Fig. 7. Relationship $\eta = f(\sigma)$ with intermediate gas cooling and heating ($\mu = 0.95$): 1) $t_1 = 800°C$; 2) 1000°C; 3) 1300°C.

With every increase of the initial gas pressure by approximately 20 atm, the absolute value of the internal efficiency of the NGTU increases by 1.1%. However, since the installation becomes more complex with increase of pressure, the advantage of increasing the efficiency by the use of higher pressure requires economical justification. The hydraulic resistance of the reactor and gas turbine sections of the unit (Δp_r and $\Delta p_{r.c.}$ respectively) also has a significant effect on the efficiency; this can be seen from the following data (for $t_1 = 800°C$, $\sigma = 2$, $\mu = 0.9$ and $p_1 = 60$ atm):

$\Delta p_r + \Delta p_{r.c.}$, kg/cm^2	η_i, %
1.5	38.3
2.5	36.66
4.0	33.63

The use of intermediate gas cooling and compression has a considerable effect on the parameters of a NGTU. Figure 4 shows the relationship $\eta_i = f(\sigma)$ for a NGTU circuit with intermediate gas cooling and two-stage compression (for $\mu = 0.9$ and conditions assumed to be as before). It follows from Fig. 4, that the internal efficiency and the effective pressure ratio are increased. The absolute increase of η_i is 2.5-5% (a more significant increase is observed at high values of t_1). The effective pressure ratio increases with change of t_1. In this case, the limits of the change of σ_{opt} as a function of t_1 are contracted considerably (for a change of t_1 from 800 to 1300°C, σ varies within 10% limits).

In order to investigate the effects of intermediate gas cooling and heating on the efficiency of a NGTU, the installation layout shown in Fig. 5 was used. The operating cycle of the unit is plotted in Fig. 6 through the points shown in Fig. 5.

The special feature of this NGTU layout (see Fig. 5) consists in that the working substance (a gas) passes twice through the reactor core. The gas, which is heated in the reactor, enters the gas turbine GT-2 on the shaft of which are located the compressors C_1 and C_2 and it is then returned to the reactor. Here, the gas is heated up to the initial temperature t_1 and enters the gas turbine GT-1 on the shaft of which are located the low pressure compressor C_1 and the current generator Gen. After the turbine GT-1, the gas passes through the regenerator RG, the first condenser Con_1 and the compressor C_1. The gas is then cooled twice and compressed in the compressors C_2 and C_3. After compressor C_3, the gas passes through the regenerator and enters the reactor.

In this design of NGTU the gas is fed to each section of the core at temperatures which differ by only relatively small amount (50-100°C) but at different pressures. The internal efficiency of a NGTU with a single intermediate heating and three-stage cooling of the gas attains extremely high values (Fig. 7). The calculations are

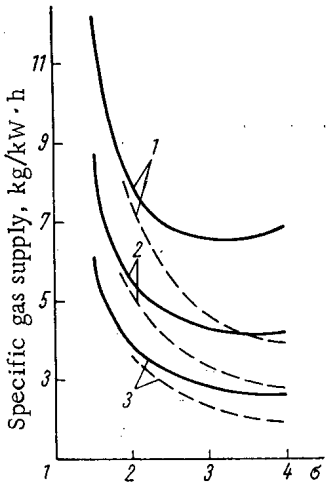

Fig. 8. Change of specific gas supply: ——— according to the design of Fig. 1; – – – – according to the design of Fig. 5; 1) t_1 = 800°C; 2) 1000°C; 3) 1300°C.

carried out for the following conditions: $(\Delta p_T + \Delta p_{T.C.}) = 3$ kg/cm^2, $\mu = 0.95$, $p_1 = 60$ atm, $(t_W^{max} - t_1) = 100$°C, $\eta_{G.T.} = 0.87$, $\eta_C = 0.85$.

It can be seen from Fig. 7, that the internal efficiency of the gas turbine unit lies within the limits 44-61% (for t_1 = 800-1300°C), and the optimum effective pressure ratio lies within the limits 3 to 3.2.

If we assume that in the next few years a gas temperature of the order of 1000°C will be attained for the reactor and gas turbine, the construction of a NGTU based on the design in Fig. 5 will make it possible to obtain an efficiency (net) of ~ 50 %.

Figure 8 shows the change of specific gas supply for the designs shown in Figs. 1 and 5. As a rule, the minimum value of the specific gas supply is found at higher effective pressure ratios. For the design in Fig. 1:

t_1, °C	σ	g_{min}, kg/kW·h
800	3.15	6.6
1000	3.5	4.2
1300	3.8	2.6

For the design in Fig. 5, the specific gas supply is significantly lower and the minimum values of g_{min} are attained at higher values of σ. For example, with t_1 = 800°C and σ = 3, the specific gas supply is less by a factor of almost 1.5, and the minimum value of g_{min} is ~4 kg/kW·h (for $\sigma \approx 4$).

LITERATURE CITED

1. Engineer, No. 5623, 5624 (1963).
2. Energia nucl., 4, No. 6 (1962).
3. VDI Nachr., No. 3, 19 (1965).
4. Atomics, No. 6, 17 (1964).

All abbreviations of periodicals in the above bibliography are letter-by-letter transliterations of the abbreviations as given in the original Russian journal. *Some or all of this periodical literature may well be available in English translation.* A complete list of the cover-to-cover English translations appears at the back of the first issue of this year.

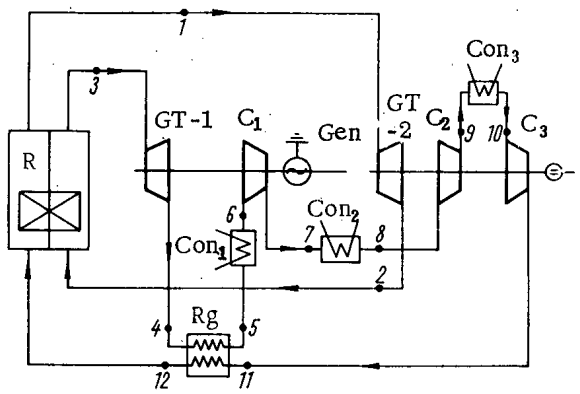

Fig. 5

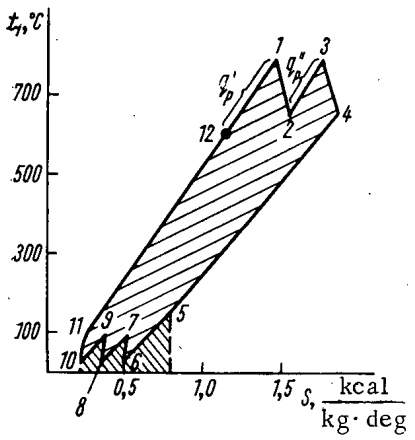

Fig. 6

Fig. 5. Schematic diagram of a NGTU with intermediate gas heating and cooling.

Fig. 6. T—S diagram of the operating cycle of a NGTU with intermediate gas heating and cooling (points 1-12 correspond to the points shown in Fig. 5).

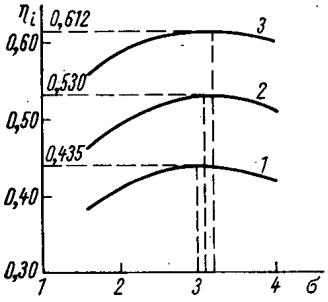

Fig. 7. Relationship $\eta = f(\sigma)$ with intermediate gas cooling and heating ($\mu = 0.95$): 1) $t_1 = 800°C$; 2) 1000°C; 3) 1300°C.

With every increase of the initial gas pressure by approximately 20 atm, the absolute value of the internal efficiency of the NGTU increases by 1.1%. However, since the installation becomes more complex with increase of pressure, the advantage of increasing the efficiency by the use of higher pressure requires economical justification. The hydraulic resistance of the reactor and gas turbine sections of the unit (Δp_r and $\Delta p_{r.c.}$ respectively) also has a significant effect on the efficiency; this can be seen from the following data (for $t_1 = 800°C$, $\sigma = 2$, $\mu = 0.9$ and $p_1 = 60$ atm):

$\Delta p_r + \Delta p_{r.c.}$, kg/cm^2	η_i, %
1.5	38.3
2.5	36.66
4.0	33.63

The use of intermediate gas cooling and compression has a considerable effect on the parameters of a NGTU. Figure 4 shows the relationship $\eta_i = f(\sigma)$ for a NGTU circuit with intermediate gas cooling and two-stage compression (for $\mu = 0.9$ and conditions assumed to be as before). It follows from Fig. 4, that the internal efficiency and the effective pressure ratio are increased. The absolute increase of η_i is 2.5-5% (a more significant increase is observed at high values of t_1). The effective pressure ratio increases with change of t_1. In this case, the limits of the change of σ_{opt} as a function of t_1 are contracted considerably (for a change of t_1 from 800 to 1300°C, σ varies within 10% limits).

In order to investigate the effects of intermediate gas cooling and heating on the efficiency of a NGTU, the installation layout shown in Fig. 5 was used. The operating cycle of the unit is plotted in Fig. 6 through the points shown in Fig. 5.

The special feature of this NGTU layout (see Fig. 5) consists in that the working substance (a gas) passes twice through the reactor core. The gas, which is heated in the reactor, enters the gas turbine GT-2 on the shaft of which are located the compressors C_1 and C_2 and it is then returned to the reactor. Here, the gas is heated up to the initial temperature t_1 and enters the gas turbine GT-1 on the shaft of which are located the low pressure compressor C_1 and the current generator Gen. After the turbine GT-1, the gas passes through the regenerator RG, the first condenser Con_1 and the compressor C_1. The gas is then cooled twice and compressed in the compressors C_2 and C_3. After compressor C_3, the gas passes through the regenerator and enters the reactor.

In this design of NGTU the gas is fed to each section of the core at temperatures which differ by only relatively small amount (50-100°C) but at different pressures. The internal efficiency of a NGTU with a single intermediate heating and three-stage cooling of the gas attains extremely high values (Fig. 7). The calculations are

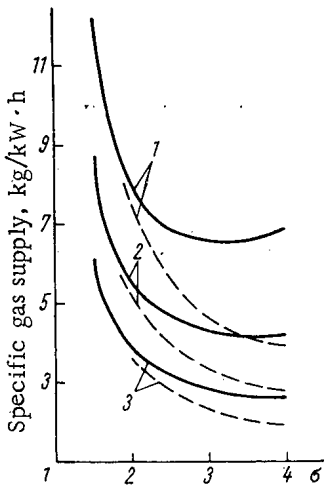

Fig. 8. Change of specific gas supply: ——— according to the design of Fig. 1; – – – – according to the design of Fig. 5; 1) t_1 = 800°C; 2) 1000°C; 3) 1300°C.

carried out for the following conditions: $(\Delta p_r + \Delta p_{r.c.}) = 3$ kg/cm^2, $\mu = 0.95$, $p_1 = 60$ atm, $(t_W^{max} - t_1) = 100$°C, $\eta_{G.T.} = 0.87$, $\eta_C = 0.85$.

It can be seen from Fig. 7, that the internal efficiency of the gas turbine unit lies within the limits 44-61% (for t_1 = 800-1300°C), and the optimum effective pressure ratio lies within the limits 3 to 3.2.

If we assume that in the next few years a gas temperature of the order of 1000°C will be attained for the reactor and gas turbine, the construction of a NGTU based on the design in Fig. 5 will make it possible to obtain an efficiency (net) of ~ 50 %.

Figure 8 shows the change of specific gas supply for the designs shown in Figs. 1 and 5. As a rule, the minimum value of the specific gas supply is found at higher effective pressure ratios. For the design in Fig. 1:

t_1, °C	σ	g_{min}, kg/kW·h
800	3.15	6.6
1000	3.5	4.2
1300	3.8	2.6

For the design in Fig. 5, the specific gas supply is significantly lower and the minimum values of g_{min} are attained at higher values of σ. For example, with t_1 = 800°C and σ = 3, the specific gas supply is less by a factor of almost 1.5, and the minimum value of g_{min} is ~4 kg/kW·h (for $\sigma \approx 4$).

LITERATURE CITED

1. Engineer, No. 5623, 5624 (1963).
2. Energia nucl., 4, No. 6 (1962).
3. VDI Nachr., No. 3, 19 (1965).
4. Atomics, No. 6, 17 (1964).

All abbreviations of periodicals in the above bibliography are letter-by-letter transliterations of the abbreviations as given in the original Russian journal. *Some or all of this periodical literature may well be available in English translation.* A complete list of the cover-to-cover English translations appears at the back of the first issue of this year.

DISTRIBUTION OF FAST FISSION NEUTRONS ALONG STRAIGHT, CYLINDRICAL DUCTS IN WATER

V. P. Mashkovich, A. N. Nikolaev,
V. K. Sakharov, B. I. Sinitsyn, and S. G. Tsypin

UDC 539.125.52

A study was made of the transmission of neutrons from the BR-5 reactor inside straight, cylindrical ducts, 144 and 90 mm in diameter, located in water. Sulfur and aluminum threshold detectors were used to detect the neutrons.

Data was obtained for the attenuation along the axis of straight, cylindrical ducts of the fast neutron flux from disc, and plane, infinite monodirectional sources of fission neutrons; the effect of displacement on the attenuation of neutron radiation in the ducts was studied. The information obtained can be used to calculate the transmission of neutron radiation along stepped ducts.

In planning shielding for equipment which contains radiation sources, it is often necessary to consider the transmission of radiation through slits and ducts which penetrate the shield.

Previous experimental and theoretical studies made of the transmission of neutrons through slits and ducts in shielding, for example, [1-5], have been devoted to a study of the effects of ducts and slits on the transmission in shields of neutron radiation from isotropic and cosine-law sources. The present work is a study of the effect of straight, cylindrical ducts in water on the transmission of fast fission neutrons from monodirectional sources.

The experiments were performed on the B-2 facility [6] of the BR-5 reactor [7]. The reactor core was the neutron source. Neutrons from the core, which is surrounded by a nickel reflector, penetrated the reactor shield through a channel ~220 cm long and ~30 cm in diameter. The total angular divergence of the neutron beam at the exit of the reactor channel was ~5°. The fast neutron spectrum at the exit of the reactor channel for neutron energies $E_N > 3$ MeV was practically the same as the fission spectrum [8].

The experimental apparatus, a sketch of which is shown in Fig. 1, was a water-filled steel tank 137 × 139 × 217 cm in size. The neutron beam from the reactor entered the tank through the center of the 137 × 139 cm wall. Straight, cylindrical ducts 9.0 and 14.4 cm in diameter were simulated by straight, hollow, polyethylene pipes 200 cm long, with walls 1 cm thick, and having the above-mentioned internal diameters. By means of a special mounting system, these pipes were located in the water tank at various distances D from the axis of the neutron beam so that the axis of the pipe was always strictly parallel to the beam axis. As fast neutron detectors, $S^{32}(n, p)P^{32}$ and $Al^{27}(n,\alpha)Na^{24}$ threshold detectors were used with effective threshold energies of ~3 MeV and 7 MeV, respectively. The detectors were in the form of discs 35 mm in diameter made up of type AV-000 aluminum (4 mm thick) and chemically pure sulfur (6 mm thick). The fast neutron distribution was determined by a previously described method [8] from the β activity induced in the detectors.

By means of special detector holders, the neutron detectors were placed at different distances z along the axis of the hollow, cylindrical duct. Since several detectors were set up along the duct at the same time during the measurements, corrections were made in the experimental data for absorption in the detectors.

The fast neutron flux distribution, including the correction mentioned, obtained from sulfur and aluminum detector measurements at D = 0, agreed with experimental limits of error. It is shown in Fig. 2 (curve 1). It is of interest to include the angular divergence of the beam in the data shown and to obtain the fast neutron distribution from a disc, monodirectional source. Inclusion of the angular divergence is made by multiplying the data shown in curve 1 by a correction coefficient k which is determined from the relation $k = (H + z)^2/H^2$, where H = 270 cm is the distance from the center of the reactor core to the front face of the duct; z is the distance along the duct. The correction was made with the assumptions that the reactor core, for this experimental geometry, can be taken as a

Translated from Atomnaya Énergiya, Vol. 20, No. 5, pp. 416-418, May, 1966. Original article submitted August 3, 1965; revised November 29, 1965.

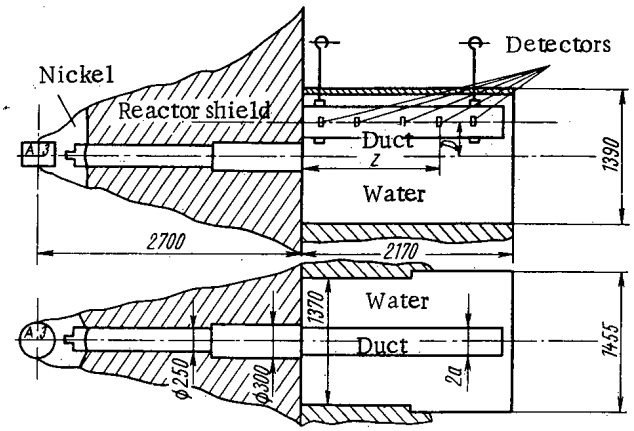

Fig. 1. Schematic diagram of experimental apparatus (dimensions given in mm).

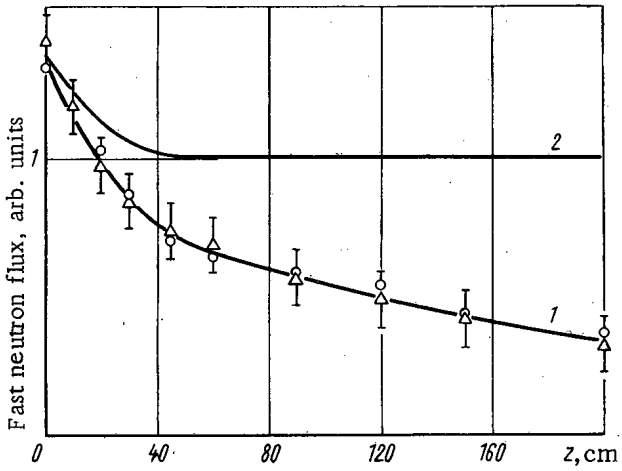

Fig. 2. Attenuation along straight, cylindrical ducts 9(Δ) and 14.4 (O) cm in diameter of the fast neutron flux from ~ 30 cm disc source by sulfur detector measurements at D = 0: 1) attenuation of neutron flux from a disc source with 5° angular divergence; 2) attenuation of neutron flux from a disc, monodirectional source with no angular divergence.

point source of neutrons located at the center of the core and that the angular divergence of the source affects only the flux of unscattered neutrons.

The neutron distribution including the correction for beam divergence is shown in Fig. 2 (curve 2).

The polyethylene pipes were located in the tank of water at various distances D with respect to the axis of the reactor channel. In this way, the effect of the magnitude of the displacement of the duct on fast neutron transmission was studied. Shown in Figs. 3 and 4 is the experimental data, obtained with sulfur detectors, for the transmission of fast neutrons along the duct with various values of the displacement D and various values of the distance z along ducts of two diameters. The data obtained with aluminum detectors gave a similar relationship for the dependence of fast neutron attenuation in the duct on the amount of displacement D.

The results presented in Figs. 3 and 4, confirm that the introduction of displacements in straight, cylindrical ducts can be an effective means for attenuation of radiation along a duct. To obtain the maximum effect from the introduction of a displacement, it is sufficient that its magnitude be somewhat greater than R. For large values of the displacement ($D \geqslant 2R$), the curve for fast neutron distribution along the duct as a function of the amount of displacement agrees, within experimental error, with the fast neutron distribution in pure water without ducts present.

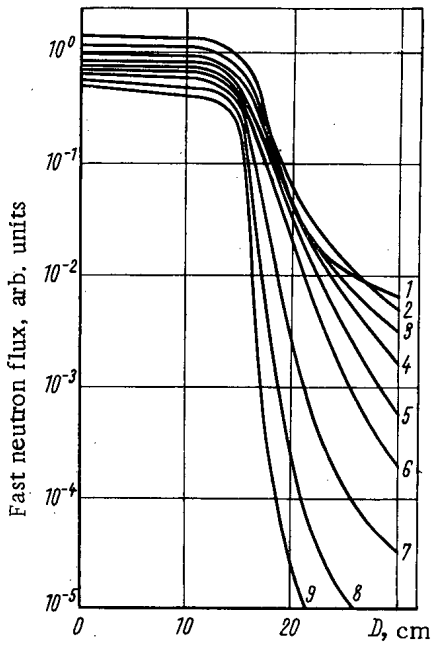

Fig. 3

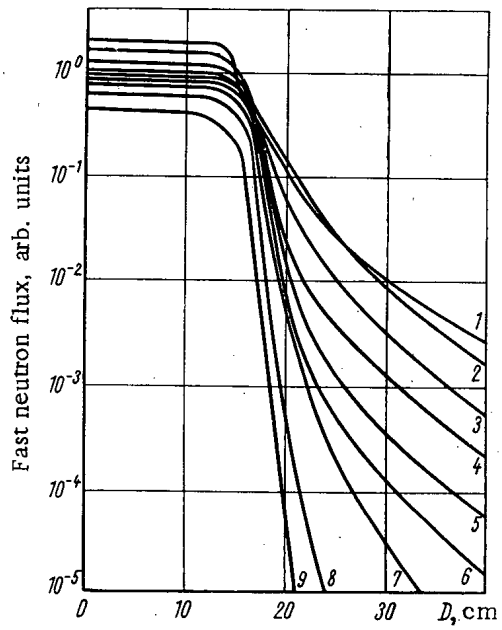

Fig. 4

Fig. 3. Attenuation of fast neutron flux, measured with sulfur detectors, as a function of the amount of displacement D for various distances z along a duct 9 cm in diameter: 1) z = 0 cm; 2) 10 cm; 3) 20 cm; 4) 30 cm; 5) 45 cm; 6) 60 cm; 7) 90 cm; 8) 120 cm; 9) 150 cm.

Fig. 4. Attenuation of fast neutron flux, measured with sulfur detectors, as a function of the amount of displacement D for various distances z along a duct 14.4 cm in diameter: 1) z = 0 cm; 2) 10 cm; 3) 30 cm; 4) 45 cm; 5) 60 cm; 6) 90 cm; 7) 120 cm; 8) 150 cm; 9) 200 cm.

The data shown in Figs. 3 and 4 represent the fast neutron flux distribution along straight, cylindrical ducts from a disc monodirectional source with an angular divergence of ~ 5° whose axis is displaced by a distance D from the duct axis. This data can be used to obtain the fast neutron distribution along ducts from an infinite, plane, monodirectional source with the same angular divergence. The conversion from a disc source to an infinite, plane source is accomplished by means of the formula

$$\Phi_\infty(z) = C \int_0^\infty \Phi_{\text{disc}}(z, D)\, D\, dD,$$

where $\Phi_\infty(z)$ is the neutron flux at a distance z on the axis of a straight, cylindrical duct from an infinite, plane source; $\Phi_{\text{disc}}(z, D)$ is the neutron flux at a distance z along the axis of a duct located at a distance D from the axis of the disc source beam; C is a constant.

Results of the conversion using the formula given above are shown in Fig. 5 (curve 1) for ducts 9.0 and 14.4 cm in diameter using sulfur detector measurements. Measurements with aluminum and sulfur detectors agreed within experimental error. The same distribution is shown in Fig. 5 (curve 2) including the appropriate correction for the geometrical divergence of the beam.

The distribution along straight, cylindrical ducts of fast neutrons from monodirectional sources obtained in this way indicates that no change in the flux is observed, within an accuracy of 15%, for monodirectional sources starting at approximately $z/a > 8$, in contrast to similar distributions from isotropic sources where a sharp decrease in flux occurs over the entire length of the duct. This is evidence that the main contribution at these distances to the total fast neutron flux is made by the "direct" neutron flux Φ_d entering through the front face of the duct. One should also note that at smaller distances from the source, the contribution from the "leakage" neutron flux Φ_l, which enters the duct through its walls, does not exceed 30-40% of Φ_d. In contrast to the isotropic case where this component of the flux can be several times greater than Φ_d [3-5] at distances $z/a < 30$.

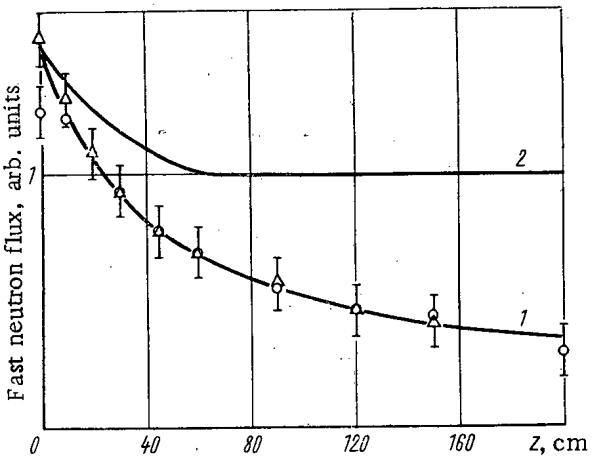

Fig. 5. Attenuation along straight, cylindrical ducts 9 (△) and 14.4 (○) cm in diameter of the fast neutron flux from an infinite, plane source: 1) attenuation of neutron flux from an infinite, plane source with angular divergence ~ 5°; 2) attenuation of neutron flux from infinite, plane, monodirectional source.

In conclusion, the authors are grateful to A. A. Goncharenko, P. I. Kotikov, V. M. Sakharov, and Yu. V. Kharizomenov for assistance in performing the experiments and in analyzing the data.

LITERATURE CITED

1. A. Simon and C. Clifford, Nucl. Sci. and Engng., 1, 103 (1956).
2. R. Schamberger, et al., The Transmission of Neutrons and Gamma-Rays through Air Slot, US AEC Report BNL-2019-2029 (1954).
3. F. Shore and R. Schamberger, The Transmission of Neutrons through Duct in Water, US AEC Report BNL-390 (1956).
4. Reactor Handbook, 3, Chap. 12, Ed. Blizard, New York (1962).
5. E. A. Kramer-Ageev, et al., Atomnaya Énergiya, 19, 46 (1965).
6. S. G. Tsypin, Problems of Reactor Shielding Physics, D. I. Broder, et al., eds., Atomizdat, Moscow (1963), p. 243.
7. A. I. Leipunskii, et al., Atomnaya Énergiya, 7, 193 (1959).
8. V. P. Mashkovich, et al., Problems of Reactor Shielding Physics, D. I. Broder, et al., eds., Atomizdat, Moscow (1963), p. 182.

All abbreviations of periodicals in the above bibliography are letter-by-letter transliterations of the abbreviations as given in the original Russian journal. *Some or all of this periodical literature may well be available in English translation.* A complete list of the cover-to-cover English translations appears at the back of this issue.

THEORY OF AZEOTROPIC RECTIFICATION WITH STEAM, EXEMPLIFIED BY THE SYSTEM TRIBUTYL PHOSPHATE – CARBON TETRACHLORIDE

B. Ya. Zil'berman, V. N. Komarov, and M. F. Pushlenkov

UDC 66.048.6:661.723.2 + 66.062.6

A theoretical analysis of rectification of the ternary system TBP–CCl_4–H_2O is based on an extension of the principle of constant molar overflow to a system of separating phases for which "fictitious" component concentrations are introduced, based on the total for both liquid phases.

The equation obtained for the operating graph is formally analogous to that for rectification of a homogeneous two-component system; the difference is that it contains "fictitious" component concentrations in the condensed phase. The authors give a sample calculation of the mass and heat balance of the column.

Much attention is presently being paid to the regeneration of extractants. In the treatment of irradiated fuel use has been made of tributyl phosphate (TBP) diluted with carbon tetrachloride [1, 2]. Reference [1] describes the use of azeotropic steam rectification for the separation of this extractant into its components. The present paper aims to calculate the equilibrium of a column designed for this purpose.

The literature does not contain an analysis of the continuous rectification of a mixture composed of separating phases (a hetero-azeotropic system) for all practically important compositions. There is in fact only one paper [3], which gives a relatively simple graphical analysis for rectification of the separating two-component system hexone–water.

In the present paper we consider a simplified analytical method for analyzing the rectification of a three-component system (TBP–CCl_4–H_2O), in which the third component is specially added to reduce the boiling point.

The first requirement is a knowledge of the volatility of each component in the presence of the others. The literature [4] contains detailed information for pure CCl_4 and H_2O, but for TBP there are data only for isolated points [5, 6]. The present authors have studied liquid–vapor equilibrium in this system TBP–CCl_4–H_2O, in the separation region at atmospheric pressure. The apparatus used was described in [7]. We also made parallel measurements of the mixture's boiling point. The results are shown in Fig. 1, which for comparison also gives values calculated from Dalton's law. It will be seen that, within the accuracy required in such cases (±10%), the nonideality of the system can be neglected. At 70-100°C the vapor pressure of TBP is less than 0.25 mm Hg, and the same value is found in the ternary system. In what follows, we shall, therefore, ignore the vapor pressure of TBP.

It is assumed that the condition of constant molar overflow is valid for a separating system. This means that the total number of moles in both phases is constant. In calculating the material balance we thus use "fictitious" component concentrations [x_i] referring to the sum of the moles in both phases. We then calculate the true concentrations x_i of the components in the liquid phases and determine the composition of the vapor phase on the plate by means of Henry's and Dalton's laws.

There are two liquid phases in equilibrium with one another and with the vapor phase, and, therefore, the volatility of each component can be calculated from the composition of either of the liquid phases. In our case, it is more convenient to calculate the proportion of CCl_4 in the vapor from the composition of the organic phase. The organic substances have low solubilities in water, the volatility of the water is determined by its saturated vapor pressure at any given temperature. The solubility of water in the organic phase is also low. The mutual solubilities of the phases cannot be calculated to within the required degree of accuracy by comparing the equations of material balance.

Translated from Atomnaya Énergiya, Vol. 20, No. 8, pp. 419-421, May, 1966. Original article submitted July 23, 1965.

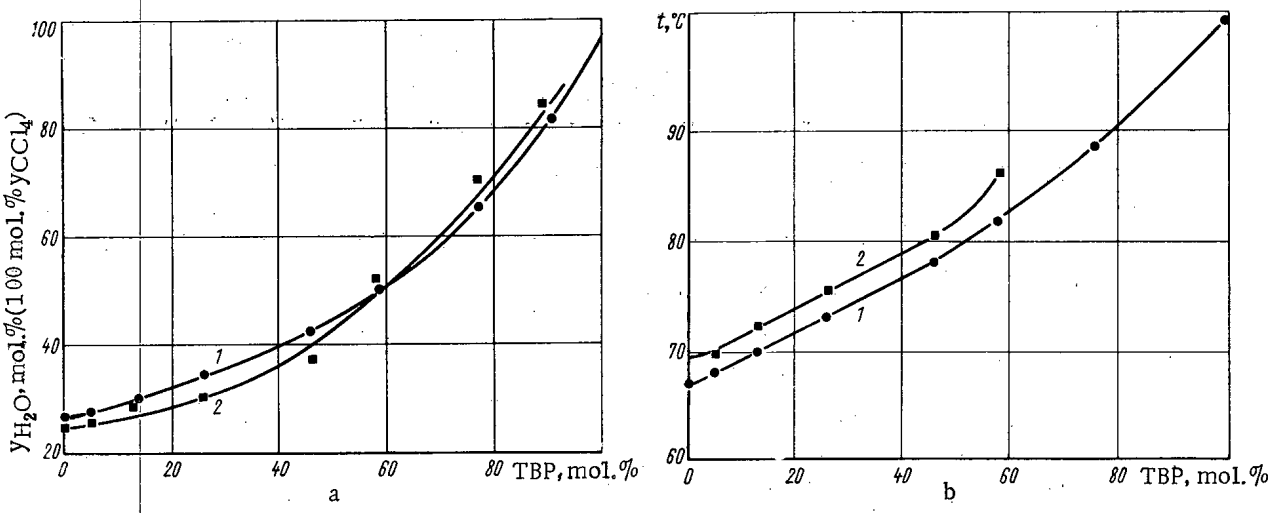

Fig. 1. Vapor composition (a) and boiling point (b), plotted versus composition of organic phase in the presence of water phase at 770 mm Hg. 1) Calculated from ideal equation of state; 2) experimental data.

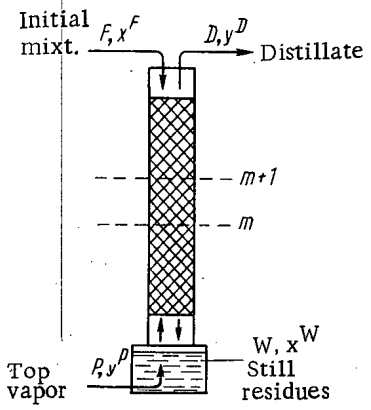

Fig. 2. Model for analysis of azeotropic rectification: x, true composition of liquid phase (molar fractions); [x], "fictitious" composition of liquid phase; y, composition of vapor phase; m, number of theoretical plates; F, number of moles of feed of composition x^F; P, number of moles of live steam of composition y^P; W, number of moles of still residues of composition $[x^W]$; D, Number of moles of distillate of composition y^D.

The column was analyzed by successive approximations. The model used for the calculation is shown in Fig. 2. By the principle of constant molar overflow, the amount of top vapor is equal to the number of moles of evaporated distillate (the hetero-azeotrope of CCl_4–H_2O).

With the usual notation (cf. Fig. 2), let us write down the equation of mass balance for the column:

$$F + P = D + W;$$
$$Fx^F + Py^P = Dy^D + W\,[x^W].$$

By what has been said, we have P = D, so that F = W. Calculating per mole of distillate of azeotropic composition, P = D = 1, i.e.,

$$Fx^F + y^P = y^D + F\,[x^W].$$

Hence,

$$F = \frac{y^P - y^D}{[x^W] - x^F}.$$

For each plate

$$F\,[x^{m+1}] + Py^P = W\,[x^W] + Py^m;$$

and for P = 1 and W = F we get

$$[x^{m+1}] = \frac{y^m}{F} + \frac{F\,[x^W] - y^P}{F}.$$

Let the composition of the feed liquid be $x^F_{CCl_4} = 0.9$, $x^F_{TBP} = 0.1$, $x^F_{H_2O} \approx 0$. Then the equilibrium composition of the hetero-azeotrope (distillate) will be $y^D_{CCl_4} = 0.712$, $y^D_{H_2O} = 0.288$, $y^D_{TBP} = 4 \cdot 10^{-5}$. From the condition of constant molar overflow, we find that, for complete separation of TBP and CCl_4, the latter must be replaced by water in the still residues. Thus, the "fictitious" composition of the still residues is $[x^W_{CCl_4}] \approx 0$, $[x^W_{TBP}] = 0.1$, $[x^W_{H_2O}] = 0.9$. Then, in our case, calculating with respect to CCl_4, we get $F = \frac{0 - 0.712}{0 - 0.9} = 0.79$, inasmuch as $[x^W_{CCl_4}] \approx y^P_{CCl_4} = 0$.

Mass and Heat Balances of Azeotropic Rectification Column

Plate No.	Phase compositions: liquid [x] CCl_4	H_2O	TBP	vapor y CCl_4	H_2O	B. P. at 760 mm Hg, °C	t_B° − 70°C	Heat intake, joule/mole: liquid	vapor	sum	Heat output, joule/mole: liquid	vapor	sum	Diff. joule/mol
Still residues	10^{-5}	0,90	0,1	$2\cdot10^{-4}$	1,0	100	30	4000	40 600 *	44 600	1600	43 000	44 600	0
1	$2{,}5\cdot10^{-4}$	0,90	0,1	$5\cdot10^{-3}$	1,0	100	30	3600	43 000	46 600	4000	43 000	47 000	−400
2	$6\cdot10^{-3}$	0,89	0,1	0,10	0,90	97	27	1160	43 000	44 160	3600	38 400	42 000	+2160
3	0,13	0,77	0,1	0,57	0,43	78	8	0	38 400	38 400	1160	35 200	36 360	+2040
4	0,72	0,18	0,1	0,70	0,30	70	0	0	35 200	35 200	0	33 100	33 100	+2100
5	0,88	0,02	0,1	0,71	0,29	70	0	0	33 100	33 100	0	32 900	32 900	+200
Feed	0,90	0	0,1	—	—	70	0	0	—	—	—	—	—	0
										Total . . .				+6100

*Heat intake from top steam.

The equation of the working curve takes the form

$$[x^{m+1}_{CCl_4}] = \frac{y^m_{CCl_4}}{0,79} + [x^W_{CCl_4}],$$

where $[x^W_{CCl_4}] << 0.01$.

Let us write down the contents of CCl_4 and TBP: $x^W_{CCl_4} = 10^{-4}$, i.e., from the balance, $[x^W_{CCl_4}] = 10^{-5}$; now let us calculate the phase compositions "from one plate to the next" until we get a distillate composition in equilibrium with the feed liquid.

We must also calculate the thermal balance of the process. The results of calculations of the equilibrium and heat balance are given in the table. In the heat calculations, we have adopted the following values for the heats of evaporation r and thermal capacities C [4, 6]:

	TBP	H_2O	CCl_4
r, joule/mole		40,600	29,800
C, joule/mole · deg	456	754	130

The heat contents were calculated relative to the temperature of the upper plate (70°C).

From the above data, it follows that to separate TBP and CCl_4, which have relative volatility 10^4-10^5, five to six theoretical plates are required. The difference between the heats of evaporation of water and carbon tetrachloride is compensated for by the increased heat content of the liquid draining down the column. The "excess" heat is 15% of the intake and will be expended in making good heat losses. Thus, in this case thermal calculations confirm the applicability of the principle of constant molar overflow to a separating system.

The method described above can be used to assess the possibility of continuous separation of any pair of components which do not join to form a true azeotrope, provided that they have appreciably different boiling points. This method is especially important for the separation of systems in which one of the components begins to decompose below its boiling point at atmospheric pressure, while the use of vaccum leads to losses of the more volatile substance.

The form of the above equations is the same as that for normal rectification of a homogeneous mixture, the only difference being that they contain the fictitious component concentrations in the liquid phases. When the less volatile component has an appreciable vapor pressure, it may become necessary to make use of the rectifying section of the column. If the fictitious concentrations are introduced, the calculations for both sections of the column are similar to the usual ones. In the cases when there is appreciable mutual solubility between the components of the aqueous and organic phases, an appropriate correction can be made in the equation of mass balance. The method described can thus be used to analyze either azeotropic or extractive rectification, provided that nonideality of the system can be neglected.

LITERATURE CITED

1. M. F. Pushlenkov, et al., Report No. 344, submitted by the USSR to the Third International Conference on the Peaceful Uses of Atomic Energy, Geneva (1964).
2. Reactor Handbook, 2nd ed., 2, Intersci. Publ., New York (1961), p. 179.
3. Reactor Handbook, 2nd ed., 2, Intersci. Publ., New York (1961), p. 597.
4. Handbook of Chemistry, 1, Goskhimizdat, Moscow (1962).
5. L. Burger, Progr. Nucl. Engng., Ser. 3, 2, Pergamon Press, London (1958), p. 307.
6. H. McKay and T. Healy, Progr. Nucl. Engng., Ser. 3, 2, Pergamon Press, London (1958), p. 506.
7. N. A. Smirnova and A. G. Morachevskii, Vestn. Leningrad. Un-ta, 2, 106 (1959).

ANALYSIS AND GENERALIZATION OF THE CORRELATION METHOD FOR MEASURING PARTICLE LIFETIME DISTRIBUTIONS IN A PHYSICAL SYSTEM

V. G. Zolotukhin, A. A. Kutuzov,
D. L. Broder, L. P. Kham'yanov,
B. A. Efimenko, and A. S. Zhilkin

UDC 539.16.08

Many problems in experimental nuclear physics reduce to measurement of particle lifetime distributions in a physical system. Among them, for example, are the problem of determining neutron spectral distributions by time of flight, measurement of the lifetime of neutron populations in reactors, measurement of the half-lives of radioactive nuclei, and also problems in activation analysis.

In 1961, Balcomb, et al. [1] used the correlation method for the measurement of reactor transfer functions. Stern, et al. [2] made an attempt to study several theoretical aspects of this method applicable to reactor problems. In 1964, A. I. Mogil'ner, O. A. Sal'nikov, and L. A. Timokhin [3] proposed the use of the correlation method for measurement of neutron spectra by time of flight.

In the correlation method, excitation of a source (modulation) is accomplished by random or pseudo-random signals having a spacing (ratio of excitation period T_0 to pulse width Δ) equalling two. A significant reduction of spacing in [2] was interpreted as the corresponding increase in instrumental transmission leading to reduction in the measurement time needed for obtaining the same accuracy.

In this paper, which generalizes the use of the correlation method, a complete statistical analysis is made. It is shown that the ratio of the squares of the errors of the ordinary (periodically pulsed), and statistical methods of excitation for the same total measurement time in the k-th channel of a time analyzer equals

$$q=\frac{T_0}{\Delta}\cdot\frac{1+2\varkappa_k}{2\varkappa_k+\varphi(\tau_k)/\Delta}, \qquad (1)$$

where $\varkappa_k$ is the background-to-signal ratio in the k-th analyzer channel for the ordinary method of excitation; $\varphi(\tau)$ is the distribution of particle lifetimes normalized to unity. In the absence of background ($\varkappa_k = 0$), this formula leads to

$$q=T_0'\varphi(\tau_k),$$

i.e., the correlation method is more accurate than the ordinary method in the region of maximum values of $\varphi(\tau)$ and less accurate for minimum values. Averaged over the $\varphi(\tau)$ spectrum, the accuracy of both methods is the same. The physical reason for the lack of an advantage lies in the fact that although counting statistics are enhanced in the correlation method, an uncertainty arises in the time of arrival in the system of particles which give rise to detector counts.

In the case of very large background ($\varkappa_k \gg 1$) which is not genetically associated with the excitation S(t), we obtain from formula (1)

$$q=\frac{T'}{\Delta},$$

i.e., the gain in measurement time equals the spacing of the ordinary method and, further, the accuracy of the correlation method in the presence of background and of the classical method in the absence of background is approximately the same. Therefore, a significant advantage for the correlation method is only apparent with considerable background.

Translated from Atomnaya Énergiya, Vol. 20, No. 5, p. 422, May, 1966. Original article submitted November 18, 1965.

A new type of statistical modulation is proposed in the paper: one having random spacing which varies from two to T_0/Δ, so that ordinary excitation and the statistical excitation, investigated by Stern, et al., are its limiting cases.

This modulation method has definite advantages in comparison with Stern's method which become apparent in the practical realization of the correlation method.

LITERATURE CITED

1. J. Balcomb, H. Demuth, and E. Gytopoulos, Nucl. Sci. and Engng., 11, 206 (1961).
2. T. Stern, A. Blaquierre, and J. Yalat, J. Nucl. Energy, P. A/B, 16, 499 (1962).
2. A. I. Mogil'ner, O. A. Sal'nikov, and L. A. Timokhin, Pribory i tekhnika éksperimenta, No. 2, 22 (1966).

All abbreviations of periodicals in the above bibliography are letter-by-letter transliterations of the abbreviations as given in the original Russian journal. *Some or all of this periodical literature may well be available in English translation.* A complete list of the cover-to-cover English translations appears at the back of the first issue of this year.

CALCULATION OF YIELD AND OF MEAN-SQUARE ANGLE OF DEVIATION FOR POSITRONS IN THE PENETRATION OF THICK FOILS BY ELECTRONS

A. V. Bautin and O. S. Koifman

UDC 539.172.2:539.124.6:539.121.72

As is well known, the penetration of high-energy electrons and photons through matter is described by cascade-theory equations which have been formulated for the one-dimensional case in the papers of Bhabha and Heitler [1], and Carlson and Oppenheimer [2]. The integro-differential equations of cascade theory are extremely complex even in the one-dimensional case, and they were solved only approximately in [1, 2]. Subsequently, L. D. Landau developed a mathematical method based on Laplace-Mellin transforms for solving the equations of cascade theory [3]. In this method, the unknown distribution functions are obtained in the form of contour integrals in the plane of the complex variable, and the main difficulty lies in the evaluation of these integrals. In the case of large thicknesses of the layers penetrated by the particles, where $t > 1$ (t is the depth in radiation units), it is possible to discard terms falling off exponentially with depth, and then the expressions under the integral sign are simplified to such an extent that it becomes possible to evaluate the integrals by the method of steepest descent [4]. At small depths, the terms falling off exponentially with depth are not small, and give contributions of the same order as those from terms not decreasing with depth, and, therefore, cannot be neglected. The expression for one-dimensional distribution functions in the form of contour integrals has been evaluated accurately [5] in the region of small depths with the inclusions of terms that fall off exponentially with depth.

In some applications (for example, in converter calculations for an electron-positron, colliding-beam device), it is necessary to know the angular deviation of the positrons which are produced by fast-electron bombardment of slabs of matter.

Based on the transport equations of two-dimensional cascade shower theory, the paper derives analytic expressions for the first two moments of the positron distribution function over the angular variable by the method of Laplace-Mellin integral transforms.

The zero-th moment of the distribution function in two-dimensional theory $P_0^{(+)}(t, E) = \int P^{(+)}(t, E, \theta)\, d\Omega$ ($d\Omega$ is the element of solid angle) gives the total number of particles in the range $(E, E + dE)$, and the mean-square

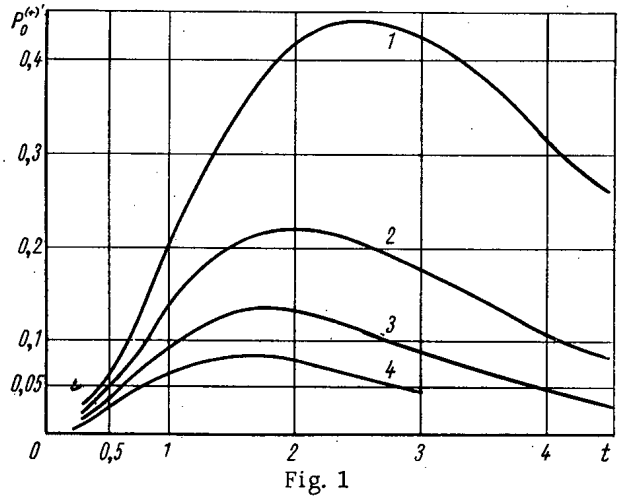

Fig. 1

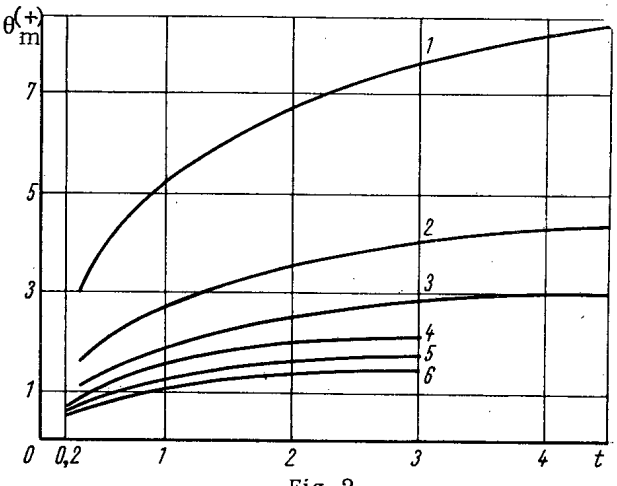

Fig. 2

Fig. 1. The function $EP_0^{(+)} = P_0^{(+)'}$ for values of the parameter E/E_0 equalling: 1) 0.1; 2) 0.2; 3) 0.3; 4) 0.4.

Fig. 2. The function $\theta_m^{(+)} = \frac{E_0}{E_k}\sqrt{\frac{P_1^{(+)}}{P_0^{(+)}}}$ for values of the parameter E/E_0 equalling: 1) 0.1; 2) 0.2; 3) 0.3; 4) 0.4; 5) 0.5; 6) 0.6.

Translated from Atomnaya Énergiya, Vol. 20, No. 5, p. 423, May, 1966. Original article submitted January 21, 1966.

angle of deviation of the particles is $\theta^2_{(+)} = \frac{P_1^{(+)}}{P_0^{(+)}}$, where $P_1^{(+)}(t, E) = \int \theta^2 P^{(+)}(t, E, \theta)\, d\Omega$. The expressions for the functions $P_0^{(+)}(t, E)$ and $P_1^{(+)}(t, E)$ were evaluated on an electronic computer with an accuracy of 1%. The results are given in Figs. 1 and 2 for various values of the parameter E/E_0, where E_0 is the energy of the primary particle producing the shower. In Fig. 1, the quantity $EP_0^{(+)} = P_0^{(+)'}$ is plotted on the ordinate; in Fig. 2, it is the quantity $\frac{E_0}{E_k}\sqrt{\frac{P_1^{(+)}}{P_0^{(+)}}} = \theta_m^{(+)}$.

LITERATURE CITED

1. H. Bhabha and W. Heitler, Proc. Roy. Soc., 159, 432 (1937).
2. I. Carlson and I. Oppenheimer, Phys. Rev., 51, 220 (1937).
3. L. Landau and G. Rumer, Phys. Rev., 166, 213 (1938).
4. B. Rossi and K. Greisen, Interactions of Cosmic Rays with Matter [Russian translation], Izd-vo instr. lit, Moscow (1948).
5. V. S. Synakh, ZhÉTF, 40, 194 (1961).

All abbreviations of periodicals in the above bibliography are letter-by-letter transliterations of the abbreviations as given in the original Russian journal. *Some or all of this periodical literature may well be available in English translation.* A complete list of the cover-to-cover English translations appears at the back of the first issue of this year.

DEPENDENCE OF BUILDUP FACTOR ON DETECTOR POSITION OUTSIDE SHIELDING

Yu. A. Kazanskii, V. I. Kukhtevich,
V. I. Popov, V. V. Tarasov, and B. P. Shemetenko

UDC 539.122:539.121.72

Buildup factors, by means of which one takes into account scattered γ-rays, have been determined for points located inside, or on the surface of, shielding [1]. As has been pointed out in a number of papers [2-4], the buildup factor B* for a detector separated from shielding can be less than that at the surface of the shield because of escape of scattered radiation into space.

The authors measured buildup factors with a radioactive source of Cs^{137} γ-rays for various detector positions and with the source behind an aluminum shield 2.8 mean free paths thick and 40 cm in diameter. The measurements were made with a scintillation detector (stilbene crystal). The distance L from the source to the surface of the shield facing the detector varied from 18 to 150 cm; for each value of L, the distance R from the surface of the shield to the detector varied from 0 to 500 cm. In order to reduce background of radiation scattered from air and ground, the source was placed in a circular shield in the form of a steel cylinder and 40 cm in diameter and 150 cm long with walls 4 cm thick lined internally with lead (0.4 cm). The cylindrical shield was placed in contact with the shield under study.

Results of the measurements are shown in the figure. In addition to the measured quantities, the figure shows calculated values which were computed in accordance with the semiempirical method given in [4].

For calculations of the buildup factor B*, the angular distribution of the intensity of γ-ray flux escaping from the surface of the shield was approximated by $(1/\sin\theta)e^{-k_T\theta}$ for a point isotropic source at the surface of the shield

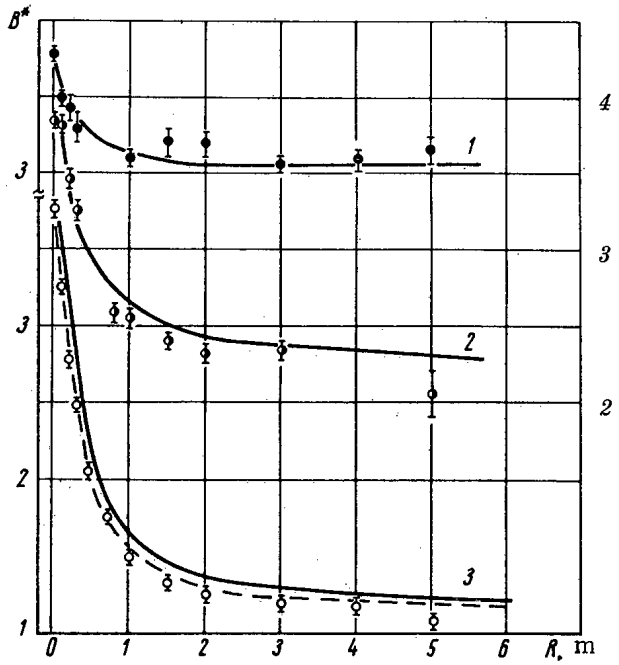

Dependence of buildup factor B* on distance R of detector to shield for various values of L. The plotted points are the measured values; solid lines are calculations for R_0 = 20 cm; dashed lines is calculation for R_0 = 18 cm ; 1) L = 18 cm; 2) L = 35 cm; 3) L = 150 cm (scale is on the right for curve 2).

Translated from Atomnaya Énergiya, Vol. 20, No. 5, p. 424, May, 1966. Original article submitted December 30, 1965.

($L = 18$ cm), and for a plane-parallel beam ($L \geq 100$ cm), the angular distribution of the flux intensity was assumed to be $e^{-k_p\theta}$. In the expressions given for the angular distribution, θ is the angle between the direction of the scattered radiation and the normal to the shielding surface k_T and k_p are experimentally determined constants. The shape of the angular distribution for other source locations is not known. Nevertheless, even for $L \geq 35$ cm, the experimental data is in good agreement with calculated values obtained on the assumption that the angular distribution of the scattered γ-rays was the same as for a plane-parallel beam.

With a plane-parallel source, some difficulties arose in the calculation because the density of the scattered radiation at the surface of the shield decreases at its edges. Therefore, in the calculations, one ought to select an effective radius somewhat less than the actual radius of the shield. Such a correction, as is clear from the figure, improves the agreement of experiment and calculation.

LITERATURE CITED

1. H. Goldstein, Fundamentals of Reactor Shielding [Russian translation], Moscow, Gosatomizdat (1961).
2. J. Moteff and H. Osgood, in Book: "Neutron Dosimetry," 1, Vienna, IAEA (1963), p. 213.
3. G. Langer and B. Shumway, ANS Trans., 6, 437 (1963).
4. Yu. A. Kazanskii, V. I. Kukhtevich, and S. G. Tsypin, Bulletin of Nuclear Data Information Center, No. 2, Moscow, Atomizdat (1965), p. 305.

A METHOD FOR COMPUTING HEAT TRANSFER COEFFICIENTS FOR LONGITUDINAL FLOW OF LIQUID METALS THROUGH FUEL ELEMENTS BUNDLES

M. Kh. Ibragimov and A. V. Zhukov

UDC 621.039.517.3

The temperature field and heat transfer in reactor cores consisting of cylindrical fuel elements depend not only on the physical properties and mode of flow of the coolant, but also on fuel element characteristics (heat conductivity of the cladding and nuclear fuel, cladding thickness, fuel element lattice spacing x). An analytic-solution of the heat transfer problem for fuel element bundles is known only for laminar flow [1, 2]. In the computational methods proposed by some authors for heat transfer in bundles of rods with turbulent flow, no consideration is given to the influence of fuel element characteristics on heat transfer, so that the use of these methods is limited.

The main idea of the described method for calculating heat transfer coefficients in fuel element bundles is that the molecular and turbulent components of the Nusselt number are considered separately, and that the values of these components are determined as a function of the fuel element characteristics and of the velocity profile:

$$Nu = f_1 Nu_s + f_2 Pe. \tag{1}$$

The Nusselt number Nu_s for pulsating flow (smooth velocity profile across a channel cross section with Prandtl number → 0) is determined from the simultaneous solution of heat conductivity and heat transfer equations for the fissionable material (T), the cladding (c), and the coolant (l):

$$\left.\begin{aligned} &\nabla^2 t_T + \frac{q_v}{\lambda_T} = 0; \\ &\nabla^2 t_c = 0; \\ &\nabla^2 t_l = \frac{\bar{w}}{a} \cdot \frac{\partial t_l}{\partial z} \end{aligned}\right\} \tag{2}$$

for the appropriate boundary conditions at the internal (radius R_1) and external (radius R_2) cladding of the fuel elements. The values of Nu_s depend on x and on the fuel element parameters:

$$\Lambda_0 = \frac{\lambda_c - \lambda_T}{\lambda_c + \lambda_T}; \quad \xi = \frac{R_1}{R_2}; \quad \frac{\lambda_c}{\lambda_l}.$$

The function f_1 is found from the analytical solution of the heat transfer problem in fuel element bundles for laminar, turbulent, and pulsed velocity profiles when the Prandtl number → 0. This function depends on the Reynolds number and on x. The empirical function f_2, which is associated with the contribution of turbulence to the heat transfer process, depends on the relative fuel element lattice spacing.

Results obtained with expression (1) agree satisfactorily with experimental data for heat transfer to liquid metals in bundles of rods over a broad range of the Péclet number ($1 \leq Pe \leq 4000$), relative spacing ($1.0 \leq x \leq 1.75$), and rod parameters: $\lambda_c/\lambda_l = 0.67\text{-}16.3$, $\xi = 0.77\text{-}0.93$. This expression replaces the empirical and analytical formulas for calculating the Nusselt number in a narrow range of Péclet numbers, relative spacing, and parameters λ_c/λ_l, λ_T/λ_l, ξ, and can be used for calculations of heat transfer in turbulent, laminar, and transitional modes of liquid metal flow.

LITERATURE CITED

1. M. Kh. Ibragimov and A. V. Zhukov, Atomnaya Énergiya, 18, 630 (1965).
2. E. Sparrow, A. Loeffler, and H. Hubbard, Trans. ASMS, No. 11, 415 (1961).

Translated from Atomnaya Énergiya, Vol. 20, No. 5, p. 425, May, 1966. Original article submitted November 10, 1965.

γ-RAY SHIELDING OF ARTIFICIAL STONE

V. B. Dubrovskii, A. K. Shreiber,
A. F. Mirenkov, and V. N. Solov'ev

UDC 621.039.538.7

Artificial stone is proposed as shielding for γ-radiation from various sources (secondary loops of atomic power stations, γ-irradiation equipment, "hot" cells, electron accelerators).

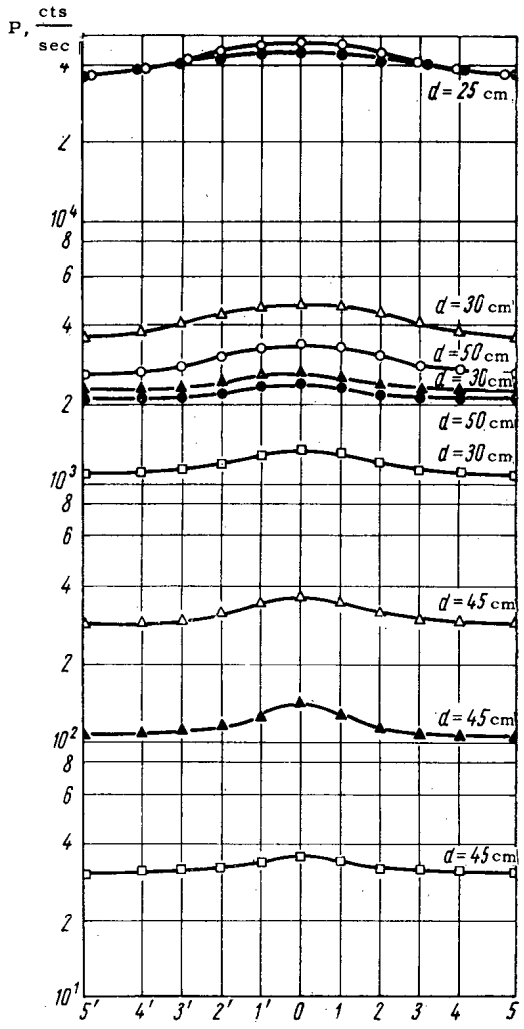

Curves for dose rate distribution behind shields 25, 30, 45, and 50 cm thick: ○) concrete (ρ = 2250 kg/m^3); ●) artificial stone (ρ = 2320 kg/m^3); △) concrete (ρ = 3300 kg/m^3); ▲) artificial stone (ρ = 3775 kg/m^3; □) concrete and artificial stone (ρ = 4600 kg/m^3). Numbers on the abscissa indicate points at which dose rates were recorded behind blocks.

Artificial stone possesses several technical and economic advantages when compared with ordinary concrete and is finding an ever-increasing application in construction [1-4]. Artificial stone is obtained by incorporating stone (ore) into a cement mixture base.

To study shielding properties, blocks were prepared which were made of concrete (densities 2250, 3300, and 4600 kg/m^3) and artificial stone containing limestone and hematite ore as the coarse aggregate. The density of the artificial stone was 2320, 3770, and 4600 kg/m^3.

The experimental studies were carried out with γ-equipment having a Co^{60} source with an activity of 500 gm-equiv Ra.

The γ-ray dose rate behind concrete and artificial stone shields of varying thicknesses was recorded by SBM-10 γ-dosimeters [5](see figure). The results obtained were compared with the results of theoretical calculations for which the linear absorption coefficient μ was computed from the chemical composition of the material and the dose buildup factor B by determining the effective atomic number of the material Z_{eff} in accordance with Goldstein's method [6].

The excellent agreement of calculated and experimental data, and the similarity of the dose rate distribution curves behind concrete and artificial stone shields, is evidence of the high uniformity of the shielding properties of the blocks. Therefore, it is possible to consider artificial stone as a uniform, homogeneous mixture of chemical elements for which the γ-ray shielding parameters can be computed just as for concrete (from chemical composition). The coefficients μ and B for the experimental concrete and artificial stone compositions were calculated over an energy range from 0.1 to 100 MeV, and they can be used in practical shielding calculations.

LITERATURE CITED

1. B. S. Ukhov, et al., Gidrotekhnicheskoe stroitel'stvo, No. 8, 15 (1958).
2. N. N. Danilov and A. K. Shreiber, Building Construction with Lean Concrete [in Russian], Akademiya stroitel'stva i arkhitektury (1959).

Translated from Atomnaya Énergiya, Vol. 20, No. 5, pp. 425-426, May, 1966. Original article submitted December 18, 1965.

3. A. K. Shreiber, et al., A Study of Some Properties of Artificial Stone under Semi-Production Conditions [in Russian], Information Bulletin No. 4, Kuibyshev, Orgenergostroi (1961).
4. V. B. Dubrovskii, et al., Energeticheskoe stroitel'stvo, No. 46, 29 (1963).
5. A. M. Panchenko, Atomnaya Énergiya, 14, 408 (1963).
6. H. Goldstein, Fundamentals of Reactor Shielding [Russian translation], Moscow, Gosatomizdat (1961).

All abbreviations of periodicals in the above bibliography are letter-by-letter transliterations of the abbreviations as given in the original Russian journal. *Some or all of this periodical literature may well be available in English translation.* A complete list of the cover-to-cover English translations appears at the back of the first issue of this year.

γ-RAY PENETRATION THROUGH JOINTS OF BUILTUP CONCRETE SHIELDS

V. B. Dubrovskii, Yu. S. Ryabukhin, A. F. Mirenkov, and V. N. Solov'ev

UDC 621.039.538.7

The construction of biological shields in fixed nuclear installations is done with monolithic concrete as a rule. The use of assembled elements in shielding construction has been held back to the considerable extent by insufficient investigation of the shielding properties of builtup shields and also by the lack of valid methods for calculating the penetration of γ-rays through shields.

The penetration coefficient is proposed as the basic criterion for estimating shielding effectiveness. It is defined as the ratio of the total, or the maximum, dose rate behind builtup and monolithic shielding.

As a rule, the value of the radiation penetration coefficient which is determined from the total dose rate behind a shield is smaller than the value which is determined by the dose rate behind the joints alone. This assertion is illustrated in the paper by two curves for the dose rate distribution from a collimated γ-ray source behind builtup and monolithic concrete shields 75 and 100 cm thick. An analysis of the nature of the variation in γ-ray penetration through the joints of builtup shields indicates that it can be expressed by three different relationships.

From a comparison of the experimental values for radiation penetration coefficients for builtup shields of ordinary and heavy concrete with the calculated data which is obtained from the three relationships, it is clear that the most accurate γ-ray penetration coefficient for joints is described by the formula

$$\varepsilon = 1 + \frac{q-1}{B},$$

where ε is the radiation penetration expressed by the ratio of dose rate through the joint of a builtup shield to that of a monolithic shield; q is the ratio of the dose rates produced by primary γ-rays outside the joints of builtup shields and outside monolithic shields; B is the buildup factor for scattered radiation in a monolithic shield.

Experimental studies of builtup and monolithic shields were carried out with a cobalt source having an activity of 500 gm-equ. Ra in two geometries (collimated and isotropic source). The small SBM-10 counter with improved characteristics, which has practically no energy dependence in the 0.1 to 1.25 MeV energy range, was used as a radiation detector. Joint thickness (2-3 cm) was considerably greater than the counter diameter (0.6 cm); thus, the detector was considered as point isotropic.

As a result of the work that was performed, it was established that the use of builtup shielding does not lead to significant local increase in dose rate behind shielding for practically important situations. The penetration of γ-rays through joints is described by the formula given above with satisfactory accuracy. In cases where the value of the radiation penetration coefficient turns out to be fairly large, one can use the following methods.

1. Take a thickness of builtup shielding such that the dose outside the joints does not exceed the maximum permissible. Such an increase in shielding thickness is usually not significant, and is even obtained automatically if the shielding is designed with standard blocks.

2. Take a maximum permissible value of the radiation penetration coefficient equal to 2, and on the basis of this assumption, calculate the minimum permissible density of the joint filler material from the formula

$$\varrho_i = \varrho_m - \frac{\varrho_m \ln(B+1)}{\mu_m x},$$

Translated from Atomnaya Énergiya, Vol. 20, No. 5, pp. 426-427, May, 1966. Original article submitted December 18, 1965.

where ρ_j and ρ_m are the densities of the joint material and of the monolithic shielding; B is the buildup factor for scattered radiation; μ_m is the mass attenuation coefficient in monolithic shielding for the radiation; x is the thickness of monolithic shielding.

3. If the value of the radiation penetration coefficient exceeds 2, or the value of the required density of the joint filler is greater than actually attainable, it is necessary to turn to blocking off straight-through joints, i.e., to reduce their length. In this case, the builtup shield is made of blocks of several different sizes.

EQUIPMENT FOR RADIOCHEMICAL PROCESSES WITH A REACTION VESSEL GIVING A UNIFORM TEMPERATURE FIELD

L. S. Polak, P. Ya. Glazunov,
B. N. Parfanovich, G. G. Ryabchikova,
V. E. Glushnev, and V. T. Popov

UDC 621.039.83

To perform studies of radiothermal checking of hydrocarbon gases and of liquid petroleum fractions with an electron accelerator, flow equipment was constructed (Fig. 1). The basic unit of the apparatus is a reaction vessel

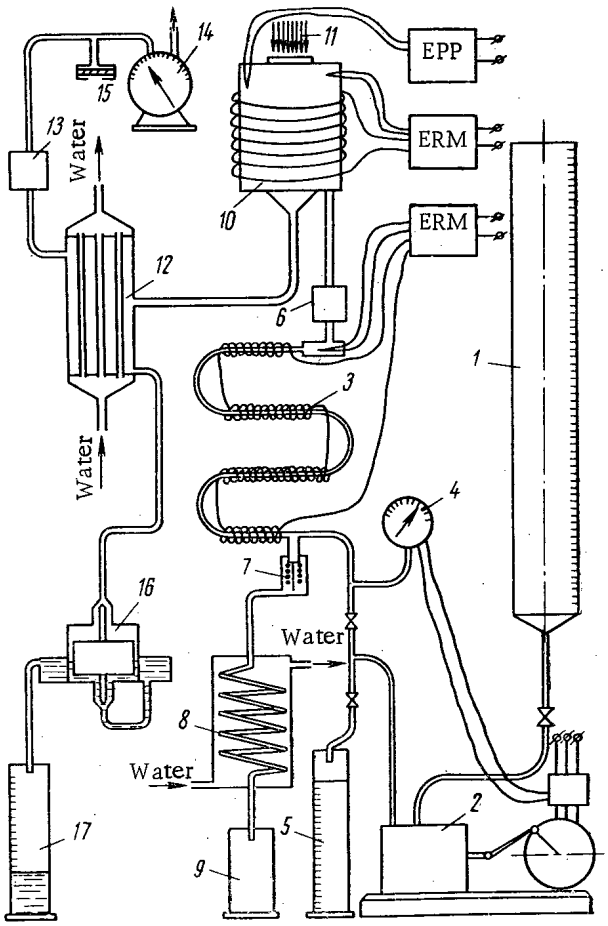

Fig. 1. Diagram of flow equipment: 1) feed material tank; 2) piston regulating pump for supplying feed material to reaction vessel; 3) evaporator (feed material heater); 4) contact monomer for pressure control; 5) measuring tank for establishing a given pump output; 6) automatic reducing valve for maintaining constant pressure in the system; 7) safety valve for relieving excess vapor pressure in the system; 8) coils for condensing vapor from excess pressure; 9) condensate tank; 10) reaction vessel with uniform temperature field; 11) electron flux; 12) condenser for products of radiothermal cracking; 13) automatic regulating valve on gas line; 14) gas meter; 15) sample collector for gas analysis; 16) automatic shutoff float in the liquid products line; 17) measuring vessel for products of radiothermal cracking; EPP) temperature-recording potentiometer; ERM) instrument for automatic temperature control.

Translated from Atomnaya Énergiya, Vol. 20, No. 5, pp. 427-428, May, 1966. Original article submitted July 29, 1965; abstract submitted February 28, 1966.

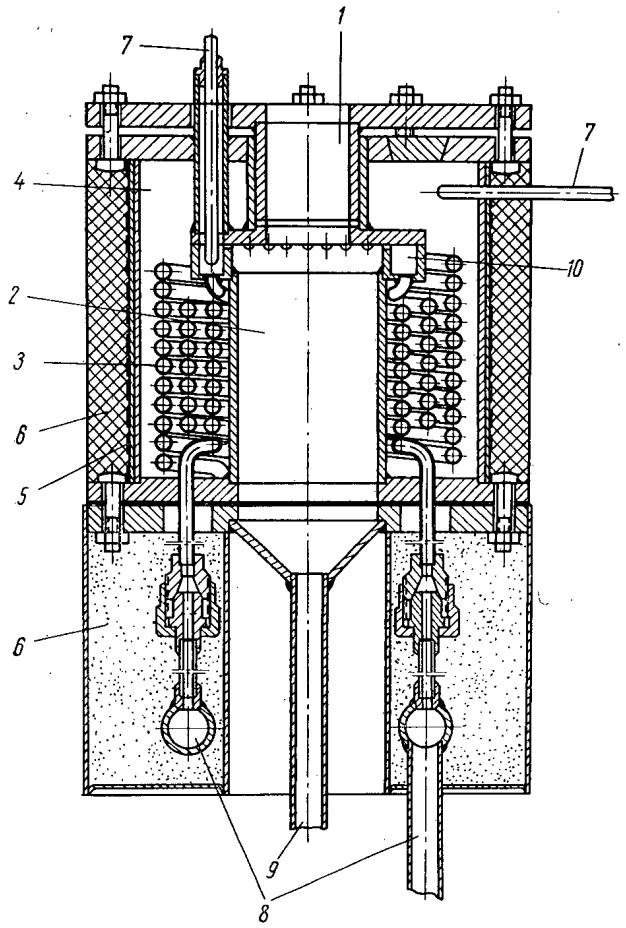

Fig. 2. Diagram of reaction vessel with uniform temperature field: 1) entrance window for electrons (beryllium foil); 2) reaction volume; 3) coils for supplying feed material to the reaction vessel; 4) lead tank; 5) electric heater; 6) thermal insulation; 7) thermocouples for regulating and monitoring temperatures in the reaction vessel; 8) collector for supplying feed material from the evaporator to the reaction vessel coils; 9) pipe for removing reaction products from the reaction vessel; 10) distribution ring with large number of radial openings for the introduction of vapors into the reaction vessel.

(Fig. 2). The use of a lead tank for the reaction vessel and of "heating" coils assures stable heat transfer and permits the production of a uniform, stable temperature field in the reaction vessel.

Vapors from the feed material, fed into the reaction volume through a large number of radial openings in the distribution ring located beneath the entrance window of the reaction vessel, get into the region of greatest radiation intensity and, force the products of radiolysis out of it. Because of the uniformity of the temperature field, a reproducibility of ±1.5% was achieved in the experimental results.

The experiments that were performed made it possible to establish the degree of conversion of the feed material by radiothermal cracking corresponding to true process temperature, given dose rate, and reaction vessel output. The apparatus can be used for investigations of radiothermal cracking and other radiochemical processes with an electron accelerator (oxidation, halogenation, sulfonation, etc.).

LETTERS TO THE EDITOR

A SECTOR CYCLOTRON WITH MAGNET POLES OF DIAMETER 685 mm

A. G. Alekseev, V. N. Barkovskii,
Yu. G. Basargin, V. N. Vasil'ev, R. N. Litunovskii,
O. A. Minyaev, V. N. Nikolaev, and A. V. Stepanov

UDC 621.384.611

This cyclotron with magnet poles of diameter 685 mm is a model for a big accelerator with variable accelerated-particle energy, namely, the 2,4-meter isochronous cyclotron planned at the D. V. Efremov Research Institute for Electrophysical Apparatus [1]. This latter cyclotron will accelerate ions with charge-mass ratios of 1/8-1. The final ion energy will be controllable over a wide range (for example, the energy range of accelerated protons will be 7.5 MeV – 100 MeV, and of deuterons 5 MeV – 65 MeV). The energy ranges for the model are: for protons 2-8 MeV, for deuterons 0.5-4 MeV, and for α-particles 1-8 MeV.

The main characteristics of the accelerator magnet are as follows:

Magnet pole diameter	68.5 cm
Final acceleration radius	29 cm
Air gaps of magnet	7 cm/22 cm
Number of elements of periodicity of magnet structure	3
Maximum magnetic field intensity at center	15 kilo-oersted
Maximum magnetic field intensity at center of "hill"	18.5 kilo-oersted
Maximum magnetic field intensity at center of "valley"	9 kilo-oersted
Amplitude of fundamental harmonic of field variation	$\leq$5.6 kilo-oersted
Maximum spirality of field	$\sim 20°$
Power input to magnet	100 kw
Maximum current in concentric turns	1500 amp
Total power input to concentric turns	100 kw
Weight of electromagnet	12 tons

The amperture of the acceleration chamber is 49 mm. In grooves in the chamber roof are nine pairs of concentric correcting turns with independent supply. One dee with angular extent 180° has aperture 17 mm. The quarter-wave resonance line is at atmospheric pressure, and, therefore, the inner rod of the line is led into the chamber via an insulator. The hf generator has power 7 kW and operates continuously; the voltage on the dees is $\leq$15 kW. The slit-type hot-cathode ion source is introduced into the chamber via a vacuum lock. The cyclotron has three removable target-probes disposed at 60° intervals.

The cyclotron was assembled, magnetic measurements were made and the machine was put into operation in 1963. The topography of the magnetic field (including the field of the concentric correction turns) was investigated with the induction at the center set at 13,895 gauss. Figure 1 shows the magnetic field intensity averaged over azimuth, $\overline{H}$, plotted versus radius: curve 1 was measured with the concentric turns switched off, and curve 2 with them switched on.* The dashed line indicates the theoretical "isochronous" magnetic field for acceleration of deuterons to 4 MeV. The deviation of the corrected field from the "isochronous" field is less than $\pm$6 oersted. The topography of the magnetic field was measured at 2.5° intervals of angle and 1 cm intervals of radius, by means of a Hall effect sensor of area 1 mm^2, made of indium antimonide. The measurement error was below $4 \cdot 10^{-4}$. The lower harmonics of azimuthal perturbations were measured with two induction coils, connected in opposition and spaced by one periodicity element. The accuracy of measurement of the first field harmonic was about 0.5 oersted. Figure 2 shows the measured lower harmonics of azimuthal perturbations of the magnetic field.

*The currents in these turns were determined by means of a "Ural-2" computer.

Translated from Atomnaya Énergiya, Vol. 20, No. 5, pp. 429-430, May, 1966. Original article submitted September 4, 1965.

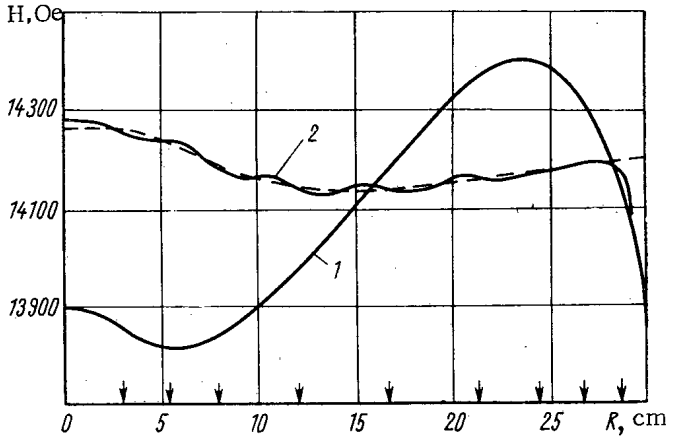

Fig. 1. Magnetic field intensity, averaged over azimuth (arrows indicate positions of concentric turns).

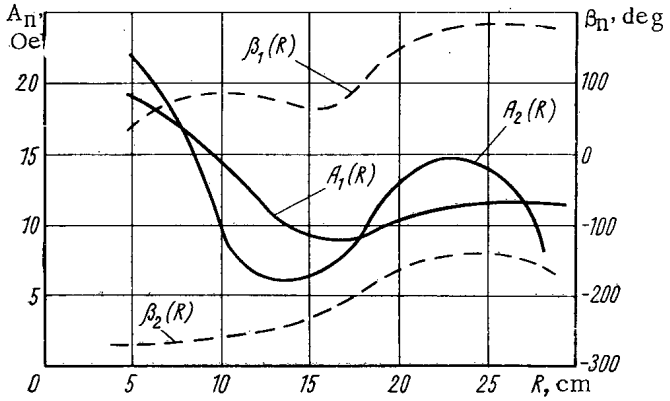

Fig. 2. Amplitudes and phases of lower harmonics of azimuthal perturbations of the magnetic field.

Acceleration of deuterons with 5 kV amplitude on the dees simulated the phase shift of acceleration of protons in the big cyclotron to 100 MeV (for which the amplitude of the hf voltage is 125 kV). Figure 3 plots the target current versus radius. The curves reveal that there is no beam intensity loss due to phase shift of ions. The overall loss of ion-beam intensity accompanying reduction in the voltage amplitude on the dees is due to reduction in the efficiency of ion extraction from the source.*

We studied the phase shifts accompanying acceleration of deuterons up to the final energy for one set of excitation currents in the concentric windings. The graph of sin θ versus R was plotted by analyzing the resonance curves of I versus H for various radii of location of the target-probe [2]. The experimental results agree with the theoretical data based on magnetic measurements. The value of $\Delta \sin \theta$ was about 0.6, which corresponds at the end of acceleration to a cycle efficiency of $\Delta\theta/2\pi \approx 0.16$.

By means of a probe with a narrow (0.5 mm) vertical electrode, we found the position of the initial orbits of low-energy ions. The results of these experiments also agree with those calculated for the initial particle trajectories.

Detailed investigations were made of the influence exerted on the amplitudes of radial ion vibrations by certain parameters of the initial ion optics. The amplitude of these vibrations was found by means of two probes spaced at 120° in azimuth, i.e., one periodicity element.

When we used a slit ion source (slit width 4 mm) without an extracting electrode on the dee, the amplitude of radial ion vibrations near the final radius was 10 mm. When the slit was reduced to 1 mm and an extracting electrode installed 3 mm from the source, the vibration amplitude fell to 3-4 mm.

* When making the measurements plotted in Fig. 3, the beam current was limited to 20 μamp in the interests of radiation safety. However, currents of ~ 50 μamp were obtainable at the final radius.

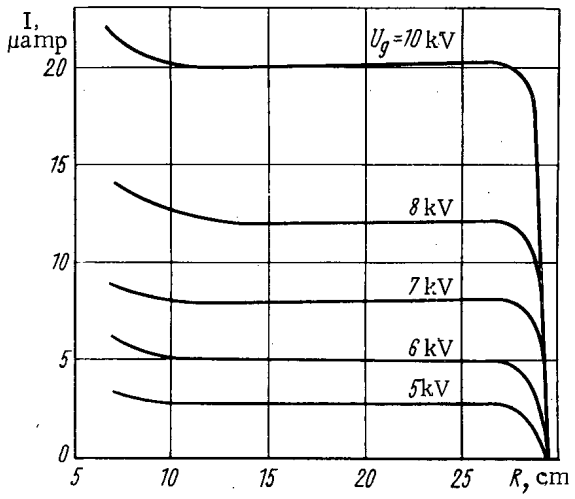

Fig. 3. Intensity of ion current, plotted versus radius of installation of probe, for various values of the accelerating voltage amplitude.

The amplitude of radial vibrations is strongly affected by the choice of position for the ion source relative to the accelerating slit. If the ion source is moved 2-3 mm from the optimum position, there is a "run-away" beam with low energy, due to the action on the particles of a nonlinear resonance $\nu_r = 3/3$. If the source is placed at the center of the chamber, the ion beam vanishes, failing to reach 0.5 MeV. The drift direction of low-energy ions is θ = 60-240°. The amplitude increase observed at the end of acceleration is apparently also due to the action of resonance at the edge of the magnetic field where $\nu_r \approx 1$.

By collimating the ion beam during its first orbits, the amplitude of vibration could be reduced to 1-2 mm. Marked divergence of orbits was observed after 30 revolutions.

Without a collimator the orbits "coalesced" after a few revolutions. The coalescence of separate orbits was apparently caused by time instability of the magnetic field intensity and the amplitude and frequency of the accelerating voltage, and also by variation in the energy gain per cycle for particles with different initial phases. The improvement of initial separation on installation of a collimator was due to the selection of that part of the ions with (theoretical) phases from about −30 to+15°. However, time pulsations of the magnetic field and the amplitude and frequency of the accelerating voltage cause "intermixing" of the orbits at medium and large radii.

The structure of the magnetic field provides axial focusing of the ions throughout acceleration. The measured betatron vibration frequencies agree with the theoretical values [3].

During acceleration of ions of molecular hydrogen (H_2^+) we noticed that an important effect was produced by their dissociation into protons. In the conditions prevailing in a sector cyclotron, in which the ions execute several hundred revolutions, this process may prevent the formation of an intense H_2^+ ion beam at the final energy if the vacuum in the accelerating chamber is below $1 \cdot 10^{-5}$ mm Hg.

The experiments were performed with the internal ion beam. We are now finishing the preliminary work on extracting the beam. This will be achieved by means of an electrostatic deflector of overall length 60° and maximum potential 30 kV.

LITERATURE CITED

1. A. G. Alekseev, et al., in: "Proceedings of International Conference on Accelerators" (Dubna, 1963). Moscow, Atomizdat (1964).
2. A. Garren, Smith Lloyd, CERN 63-19, 18 (1963).
3. Yu. G. Basargin and V. P. Belov, Electrophysical Apparatus. Symposium. Issue 3, Moscow, Atomizdat (1965), p. 3.

MEASUREMENT OF FAST NEUTRON ABSORPTION CROSS SECTIONS WITH A RESONANCE DETECTOR IN WATER*

Yu. Ya. Stavisskii et al.†

UDC 539.172.4:539.17.02

Integration of moderated neutron densities is extensively used in nuclear physics problems [1, 2]. This method also finds use in measurements of fast neutron absorption cross sections by the transmission method in spherical geometry [3], since it makes it possible to create detectors independent of neutron energy. In this case, the neutron source, surrounded by a spherical layer of the material under study, is located inside a cavity in the moderator in which the radial distribution of moderated neutrons is measured. Since the absorption of thermal neutrons by the material investigated is usually large, it is considerably more advantageous to measure the distribution of resonance neutrons.

In this work, a practically convenient method was used for monitoring the intensity of the neutron source, which was a variation on the "manganese bath" proposed by Amaldi some time ago [4]. The features of the method developed (use of a hermetically sealed volume containing the solution, the use of indium as a resonance absorber, the suppression of thermal neutrons, etc.), made it possible to use it successfully for accurate monitoring of small changes in fast neutron flux during absorption cross section measurements.

The experimental apparatus for cross section measurement consisted of a water-filled tank 3 (Fig. 1) 2 × 2 m in size with a spherical cavity 2, 1 m in diameter, at the center of which the photoneutron source 1 and sample was located. A portion of the water-filled volume of the tank bounded by the conical surface 5, with vertex at the center, in the form of a thin-walled Plexiglas cone 4, is filled with an aqueous solution of the resonance absorber to be activated. An evaluation of the energy independence of this system showed that the neutron detection efficiency varied by hundredths of a percent in the 0.001-10 MeV range.

The activity A of a solution in the cone is proportional to the source intensity a and is expressed by

$$A \sim \int_{r_0}^{\infty} q(r, E)\, r^2\, dr, \qquad (1)$$

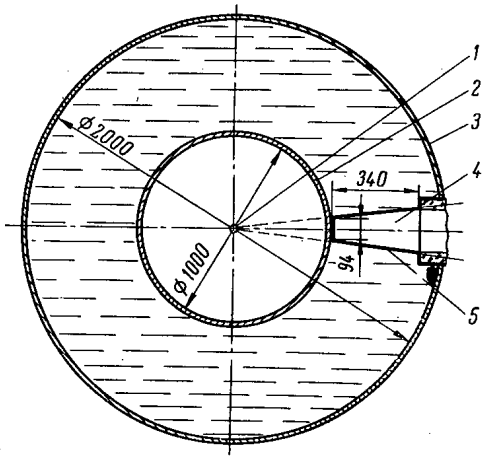

Fig. 1. Cross section of water-filled tank.

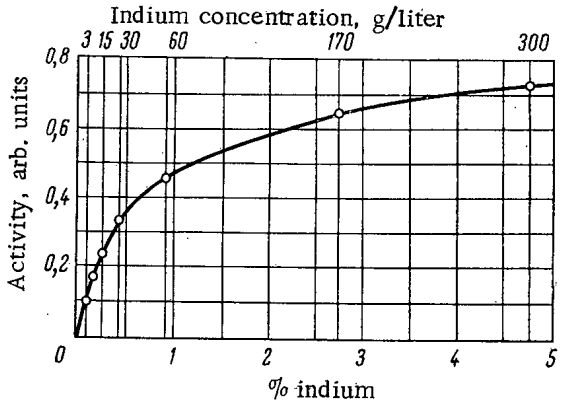

Fig. 2. Activity of solution in cone as a function of indium concentration.

* Letter received from the journal Yadernaya fizika where it was submitted June 7, 1965.

† Name of coauthor illegible in original—Publisher's note.

Translated from Atomnaya Énergiya, Vol. 20, No. 5, pp. 431-432, May, 1966. Original article submitted October 21, 1965.

Absorption Cross Sections σ_a, mb, for Isotopes Studied

Material	Detection		
	cone in tank (this work)	fission chamber in tank and long counter[6]	long chamber [7]
$_{29}Cu$	59±6	59±8	42±15
$_{42}Mo$	188±15	192±12	—
$_{49}In$	778±79	776±66	823±60
$_{90}Th$	611±40	615±25	—
$_{92}U^{238}$	380±20	412±18	—

where q(r, E) is the neutron slowing-down density; r_0 is the radius of the air cavity. Thus, by measuring the γ-activity of the solution in the cone with an external detector and assuming complete mixing, we directly obtain a quantity proportional to the total number of neutrons in the tank.

Indium was chosen as the neutron resonance absorber because it has a large resonance integral, suitable half-life, and good stability in solution. The indium was used in the form of the chloride salt at metal concentrations from 3 to 300 g/liter.

A curve giving solution activity as a function of indium concentration is shown in Fig. 2. The working concentration of indium was 60 g/liter which made it possible to obtain a statistical accuracy of 0.1% with a photoneutron source giving $\sim 3 \cdot 10^8$ n/sec for irradiation and counting after 15 min. In order to avoid thermal neutron activation of the indium, cadmium acetate in the amount of 200 g/liter was added to the solution. Supplementary experiments were performed to check the absence of boundary effects arising from the fact the cone was surrounded by water and not by the same solution of indium salt.

By means of the cone, the value of the transmission

$$T = \frac{A_1}{A_0}, \qquad (2)$$

was measured, where A_1 is the activity of the solution in the cone for the case where the source was surrounded by the sample under study; A_0 is the activity of the solution in the cone for the case of a bare source. At the time of irradiation, the solution was thoroughly mixed with a spiral vane by means of a system of permanent magnets. The gamma-activity of the solution in the cone was measured with three scintillation counters having 60 × 70 mm NaI(Tl) single crystals and FÉU-11 photomultipliers. The stability of the γ-counters was no worse than 0.5% in 12 h. To reduce background, the scintillation counters were surrounded by lead shielding ~15 cm thick. Background from the three counters was 500 cts/min for a 150 keV discrimination level which corresponded to 6% of the activity of the solution in the cone when working with a source having a yield of $\sim 3 \cdot 10^8$ n/sec. As a rule, a single cone was irradiated not more than two times in succession.

The table gives values of the absorption cross section which were obtained by this method for a Sb–Be source producing 24±1.5 keV neutrons [5], and for absorption cross sections obtained in [6, 7].

Calculation of the absorption cross sections from the transmission T was accomplished by the Monte-Carlo method in the one-velocity transport approximation which was developed by A. A. Van'kov and F. F. Mikhailus for similar problems. In the treatment of the results, corrections were introduced for the finite dimensions of the source for moderation of the neutron spectrum in the beryllium cladding of the source, and allowance was also made for the effect of absorption in the source of neutrons reflected from the sample and for the absorption of 380 keV neutrons by the sample.

As can be seen from the table, the results are in agreement within experimental error. The errors shown for σ_a are the sum of the mean-square error in the transmission measurements and of the uncertainties in the constants used for the calculations.

The method developed makes it possible to measure the attenuation (1–T) with an accuracy of ~1%. The accuracy of the resulting cross sections is determined mainly by the accuracy of the constants used in the calculations (chiefly σ_{tr}), and may amount to 3-5% at most. One deficiency of the method is the high sensitivity of the detection system to background from extraneous sources.

In conclusion, the authors express their deep gratitude to A. A. Van'kov, A. I. Abramov, and T. S. Belanova for valuable discussions and assistance, and also to L. E. Fedorov, N. N. Mamontova, and A. A. Stognii for help in performing the experiments.

LITERATURE CITED

1. M. A. Bak, et al., Uspekhi fiz. nauk, 58, 667 (1956).
2. R. Macklin, et al., Nucl. Sci. and Engng., 8, 210 (1960).
3. K. Litner, Acta Physica Austriaca, 3, 353 (1950).
4. E. Amaldi and E. Fermi, Phys. Rev., 50, 899 (1936).
5. Yu. Ya. Stavisskii, et al., Atomnaya énergiya, 15, 489 (1963).
6. T. S. Belanova, et al., Atomnaya énergiya, 19, 3 (1965).
7. H. Shmitt and C. Cook, Nucl. Phys., 20, 202 (1960).

ANALYSIS OF MATERIAL COMPOSITION BY INELASTIC SCATTERING OF FAST CHARGED PARTICLES

S. S. Vasil'ev, T. N. Mikhaileva,
Yu. A. Vorob'ev, and D. L. Chuprunov

UDC 539.106

This paper proposes the use of the inelastic scattering of fast charged particles for analysis of the composition of materials. By analyzing the spectra of inelastically scattered charged particles obtained at several angles to the direction of the incident beam, one can determine the composition of the sample under study sufficiently reliably because isotopic identification is accomplished through mass and through several values of nuclear excitation energy with supplementary checking of those values at various scattering angles. Knowing the inelastic scattering cross section, or comparing with a standard, it is also possible to determine the percentage content of the components. In order to make an analysis of a material under study, a thin (fractions of a mg/cm^2) scattering target is prepared. The proposed method was used for the determination of impurities in aluminum. The 6.6 MeV proton beam of the 120-centimeter cyclotron at the Institute of Nuclear Physics, Moscow State University, was used. A diagram of the experimental equipment is shown in Fig. 1. The protons which are scattered by the target made of the sample being investigated are detected by an ordinary scintillation spectrometer with 100-channel analyzer.* A thin CsI(Tl) crystal out from a standard Khar'kov factory crystal, was used as a scintillator. Calibration of the energy scale of the spectrometer was obtained by elastic scattering of the protons by gold with variation in the energy of the incident protons produced by gold filters [3]. The time for obtaining a scattered proton spectrum at one angle over an energy range of 2-6.5 MeV was ~10 min for a proton current at the target of several tens of microamperes. As an example, the spectra of protons scattered by pure aluminum and by aluminum containing impurities are shown in Fig. 2.

Analysis of the spectra obtained was accomplished in the following manner: first, the peaks corresponding to protons elastically and inelastically scattered by nuclei of the main component were determined; this was aluminum

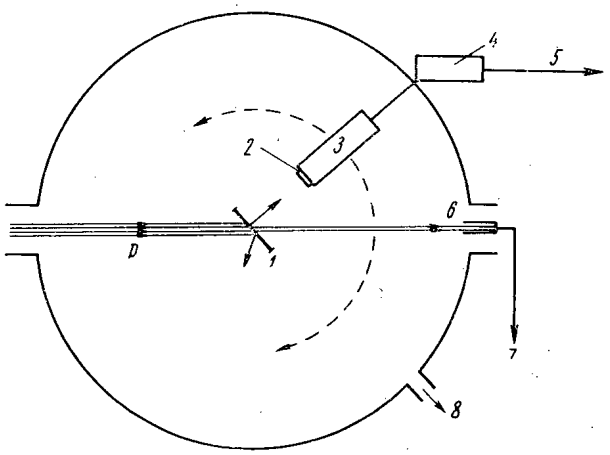

Fig. 1. Diagram of experimental arrangement: 1) target; 2) scintillator; 3) photomultiplier; 4) preamplifier; 5) to multichannel analyzer; 6) Faraday cup; 7) to integrator; 8) to pump.

*The experimental material presented below is illustrative, having been obtained more than three years ago. The use of detectors with better resolution, i.e., semiconductor detectors, or a scintillation detector with a resolution of 2% for 6.6 MeV protons [1], and also a scintillation spectrometer for separate recording of the products of nuclear reactions [2], would undoubtedly expand the range of analyzable materials.

Translated from Atomnaya Énergiya, Vol. 20, No. 5, pp. 432-434, May, 1966. Original article submitted September 18, 1965.

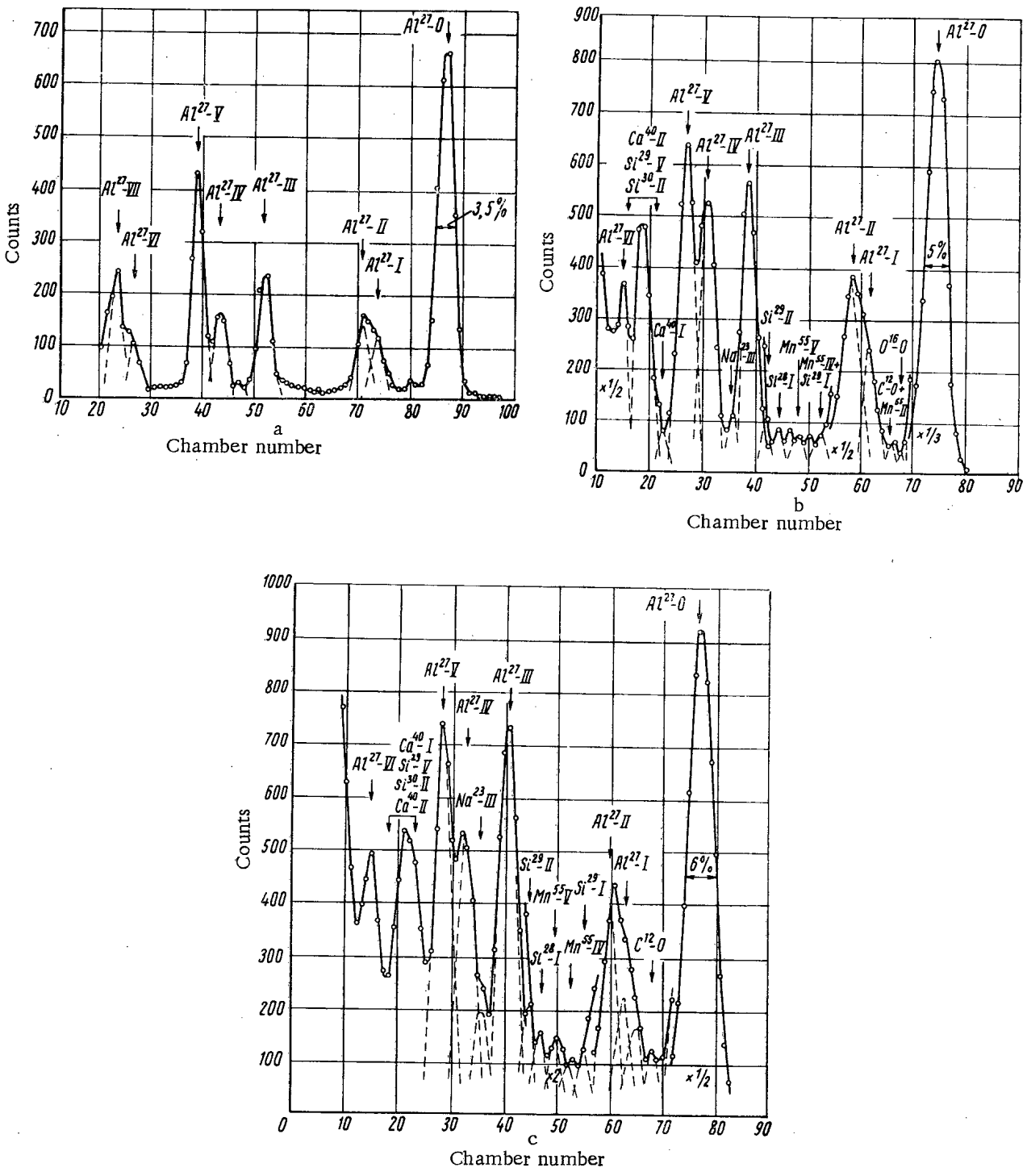

Fig. 2. Experimental spectra of elastically and inelastically scattered protons by targets made of pure aluminum (a) and of aluminum containing impurities (b, c). Roman numerals indicate the number of the excited level of the scattering nucleus (a, b— $\theta = 120°$; c—$\theta = 120°$).

in the case under discussion. In this way, the peaks belonging to other components were separated out. Peaks corresponding to protons scattered elastically by impurities, in this case, practically merged with the peaks corresponding to protons elastically scattered by aluminum. Inelastically scattered protons were spread over a larger energy range. Therefore, the peaks corresponding to them can be separated out by decomposition of the curves and their energy $E_i(\theta)$ determined.

Excitation Energy Values and Identification of Corresponding Isotopes

keV, degrees					Mass of scattering nucleus	Q_i, average of five values, keV	Q_i, tabulated, keV	Deviation from tabulated value, keV	Isotope and excited level number
60	90	105	120	90					
867	839	798	795	849	27	829	834	—5	Al^{27} — I
989	1022	1010	1009	1040	27	1014	1013	1	Al^{27} — II
1226	1358	1324	1388	1270	29	1313	1280	33	Si^{29} — I
1626	1691	—	—	1651	55	1656	1650	6	Mn^{55} — IV
1807	1839	1815	1905	1851	55	1843	1840	3	Mn^{55} — V
1837	1832	1728	1870	1829	28	1812	1780	32	Si^{28} — I
2027	1993	1986	2064	2073	29	2028	2027	1	Si^{29} — II
2289	2204	2192	2191	2276	27	2228	2212	16	Al^{27} — III
—	—	2372	—	—	29	—	2425	—	Si^{29} — III
2412	2407	2500	2292	2475	23	2417	2391	26	Na^{23} — III
2753	2659	2678	2725	2810	27	2725	2731	—6	Al^{27} — IV
3030	2962	2919	2937	3043	27	2978	2976 3000	2 —22	Al^{27} — V
3335	3361	3421	3359	3338	40	3363	3350	13	Ca^{40} — I
3543	3395	3449	3518	3515	30	3521	3520	1	Si^{30} — II
3527	3587	3589	3503	3507	29	3542	3621	—79	Si^{29} — V
3707	3670	3726	3625	3670	40	3680	3730	—50	Ca^{40} — II
3645	3647	3740	3741	3647	27	3684	3674	10	Al^{27} — VI

Determining the values $E_i(\theta)$ at various scattering angles θ for peaks which correspond to the same excitation energy Q_i, we found the most probable value of the mass of the scattering nucleus from several expressions for the excitation energy Q_i (at various angles):

$$-Q_i = \left(1 - \frac{m_I}{m}\right) E_I + 2\frac{m_I}{m}\sqrt{E_I E_i(\theta)} \times \cos\theta - \left(1 + \frac{m_I}{m}\right) E_i(\theta), \quad (1)$$

where E_I is the incident particle energy; m_I is the incident particle mass. Because the energy value $E_i(\theta)$ is determined with an accuracy of ±1-2 analyzer channels, the resulting mass values can have considerable spread. From the average value of the mass and $E_i(\theta)$, the excitation energy of the scattering nucleus is determined by formula (1). Through the derived approximate mass value and excitation energy, the nucleus in which the scattering occurred is selected from published tables [4-6]. The results obtained by the authors were reduced to a table from which it is clear that silicon, sodium, manganese, and calcium were contained in the aluminum investigated.

Activation analysis of a portion of the impurity-containing aluminum sample irradiated in a reactor, which was done by means of γ-radiation, positively indicated the presence of sodium and manganese in the aluminum and showed traces of silicon. The presence of calcium was not established because of unsuitable half-life and type of radiation.

In the determination of silicon by neutron activation analysis, the sensitivity is 7-10%, the "interfering" element with similar activation characteristics being aluminum [7], while in the proposed method, silicon in the amount of 1% is easily detected even when the basic component is aluminum, and the silicon is only an impurity (the proton inelastic scattering cross sections for silicon and aluminum were taken from [8]). From what has been discussed above, it follows that the method described can be used in addition to existing methods for analysis of materials.

LITERATURE CITED

1. S. S. Vasil'ev, et al., Izv. AN SSSR, ser. fiz., 29, 181 (1965).
2. T. N. Mikhaileva, et al., Izv. AN SSSR, ser. fiz., 30, 343 (1966).
3. S. V. Starodubtsev and A. M. Romanov, Penetration of Charged Particles through Matter [in Russian], Izd-vo AN UzSSR (1962).
4. B. S. Dzhelepov and L. K. Peker, Decay Schemes of Radiative Nuclei [in Russian], Moscow-Leningrad, Izd-vo AN SSSR (1956).

5. E. A. Ajzenberg-Selove and T. Lauritsen, Nucl. Phys., 11, 1 (1959).
6. P. Endt and C. Vander Leum, Nucl. Phys., 34, 91 (1962).
7. D. I. Leipunskii, Z. E. Gauer, and G. N. Flerov, Atomnaya Énergiya, 6, 315 (1959).
8. J. Kokane, J. Phys. Soc., Japan, 16, 2108 (1961); G. Greenless, et al., Proc. Phys. Soc., (L), 71, 342 (1958).

All abbreviations of periodicals in the above bibliography are letter-by-letter transliterations of the abbreviations as given in the original Russian journal. *Some or all of this periodical literature may well be available in English translation.* A complete list of the cover-to-cover English translations appears at the back of the first issue of this year.

MEASUREMENT OF LARGE γ-RAY DOSES AND FLUXES BY PHOTOACTIVATION OF ISOMERIC NUCLEAR STATES

I. A. Abrams, L. L. Pelekis,
and I. Ya. Taure

UDC 541.15

The operation of powerful γ-sources requires reliable and accurate methods for measuring γ-ray doses and fluxes. Chemical dosimetry, the most promising method in this respect, offers no possibility of determining very high dose rates (10^8 rad/sec). In the following, there is discussed the activation method for measuring high γ-ray dose rates and fluxes based on γ-ray excitation of isomeric states of stable nuclei through the nuclear interaction $A(\gamma, \gamma')A^m$.

Between the γ-ray flux Φ(photons/cm^2 · sec) of an irradiator and the counting rate N of the induced activity in a sample (dosimeter), there exists the following realation:

$$\Phi = \frac{NA}{6{,}02 \cdot 10^{23} m a \sigma \Omega \varepsilon k (1 - e^{-\lambda t_1}) e^{-\lambda t_2}}, \quad (1)$$

where m is the sample mass, g; a is the content of excited nuclei in the sample; σ is the γ-ray activation cross section; Ω is the relative solid angle; ε is the efficiency of γ-ray detection; k is the γ-ray yield per decay; λ is the decay constant of the isomer; t_1 is the irradiation time; t_2 is the time from end of irradiation to measurement; A is the nuclear mass number.

The relationship between counting rate N from induced activity and dose rate P can be obtained from expression (1), if one takes into account the relation

$$P = \frac{\Phi \gamma E}{6{,}88 \cdot 10^4} \text{ R/sec}, \quad (2)$$

where γ is the electron conversion coefficient for γ-rays of energy E.

From experiments, indium and cadmium are most suitable for γ-ray dosimetry. With the use of indium or cadmium dosimeters of definite geometrical shape and weight, and fixed conditions of measurement, expression (1) takes a simple form:

$$\Phi = Z \frac{N}{\sigma (1 - e^{-\lambda t_1}) e^{-\lambda t_2}}, \quad (3)$$

where Z is a constant characteristic of the dosimeter and the measuring equipment.

In the case of measurements of induced activity with radiometers having scintillation detectors with well-type NaI(Tl) crystals, $Z_{In} = 9.05 \cdot 10^{-22}$ for an indium dosimeter in the form of a sphere weighing 1 g and $Z_{Cd} = 1.78 \cdot 10^{-22}$ for a cadmium dosimeter in the form of a cylinder with a base 5 mm in radius and weighing 20 g. The activation cross sections for Co^{60} γ-rays are $\sigma_{In} = 8.3 \cdot 10^{-5}$ mb and $\sigma_{Cd} = 1.4 \cdot 10^{-5}$ mb; for an irradiator in a radiation loop with an In^{116m} γ-ray source, they are $\sigma_{In} = 1.5 \cdot 10^{-4}$ mb and $\sigma_{Cd} = 6.9 \cdot 10^{-6}$ mb [1, 2].

It is convenient to use γ-activation dosimeters for the relative determination of flux or dose by calibrating such dosimeters through chemical, calorimetric, or other methods. Because of their small dimensions and independence of measuring equipment during time of irradiation, λ dosimeters are indispensable for use in monitoring variations in radiation dose during prolonged experiments. An indium γ-activation dosimeter was used by the authors to

Translated from Atomnaya Énergiya, Vol. 20, No. 5, pp. 434-435, May, 1966. Original article submitted August 21, 1965; revised November 9, 1965.

determine the γ-ray dose and flux distribution along the irradiator channel in a radiation loop of the IRT reactor. The results obtained were in good agreement with calculated data and with thimble chamber measurements.

The gamma-activation method of measuring γ-ray flux and dose can be used for γ-ray fluxes $\Phi \geq 10^{10}$ photons/cm^2 · sec and doses $D \geq 10^5$ R. The γ-ray energy must be at least equal to, or greater than, the energy of the metastable level; furthermore, the greatest sensitivity with indium is achieved at γ-ray energies $E \geq 935$ keV and at $E \geq 610$ keV for cadmium.

It is most advantageous to use γ-activation dosimeters for measuring pure γ-ray fields; however, by using neutron filters, it is possible to measure γ-ray fields in the presence of low neutron fluxes (for example, in the core of a shut down reactor).

Gamma-activation dosimetry has definite advantages over other methods of dosimetry:

1) the use of γ-activation dosimeters does not require their destruction, and subsequent use is possible through half-lives of the isomer;
2) measurements of induced activity, and, therefore of dose, can be made with standard radiometric equipment supplied with well-type crystals;
3) gamma-activation dosimeters can be used for monitoring γ-ray fluxes and dose distributions.

LITERATURE CITED

1. A. Veres, Appl. Rad. and Isotopes, 14, 123 (1963).
2. I. A. Abrams, L. L. Pelekis, and I. Ya. Taure, Neutron Activation Analysis [in Russian], Riga, Zinatne (1966).

EFFECT OF γ-IRRADIATION ON SCALE FORMATION

V. N. Vasina, V. N. Aleksandrova, and V. V. Gerasimov

UDC 621.039.544.5

It is well known that in atomic power installations, the surfaces of the fuel elements operate under extreme conditions. Acting upon them simultaneously are thermal flux, radiation, mechanical stresses, and coolant. The results of the actions of these factors are corrosion of the fuel element surfaces and the formation of deposits upon them. A study of the effect of various combinations of the factors mentioned on scale formation and corrosion of the materials used for fuel element cladding is of considerable interest. These problems have received some slight attention in the literature [1-3].

This paper presents the results of a study of the simultaneous effect of thermal flux and γ-irradiation on scale formation. The study was carried out on apparatus which is sketched in Fig. 1. The equipment consisted of an open tank made of 1Kh18N9T steel, which was filled with an aqueous solution into which the sample was lowered. The sample was heated electrically by a current carried to it from the control unit over buses. The thermal flux was regulated from the control unit by changing current and voltage values. Constancy of level and water temperature in the tank (40°C) was provided by a cooling system of 1Kh18N9T steel in the form of a coil arranged around the sample.

The scale-producer selected was calcium sulfate—a slightly soluble salt having a negative solubility coefficient. The tests were carried out with supersaturated solutions in order to avoid reduction in solution concentration in the neighborhood of the sample because of scale formation. The scale-formation process was monitored through sample temperature. To do this, a 1.5-2 mm groove was milled in the sample into which a chromel-copel thermocouple was sealed. A sample with thermocouple is shown in Fig. 2. A type PP potentiometer acted as the secondary instrument. Before each experiment, the sample was thoroughly cleaned with No. 100 emery paper. A check on the effect of roughness showed that a permanent scale was formed on a rough surface; on a smooth surface, a layer of deposit was loosely bound to the surface.

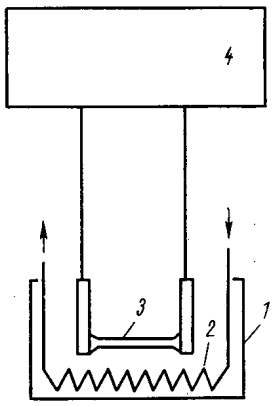

Fig. 1. Diagram of the apparatus: 1) tank; 2) cooling system; 3) 1Kh18N9T steel sample; 4) control unit.

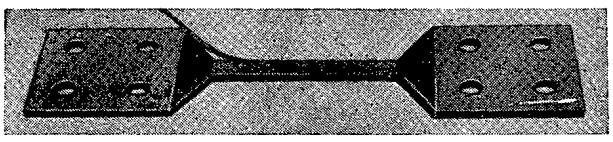

Fig. 2. Sample.

Two sets of experiments were performed, and each experiment was repeated no less than three times.

In the first set of experiments, a study was made of the effect of thermal loadings from $0.23 \cdot 10^6$ to $1.9 \cdot 10^6$ W/m^2 on scale formation and corrosion. The results are given in Fig. 3. The tests showed that the rate of scale formation rose with increase in thermal flux. Similar relations have already been noted [1-3]. Iron concentration in solution in all the experiments was 0.05 mg/liter. Chemical analysis of the scale showed that only calcium sulfate was deposited on the sample. No effect on the intensity of scale formation was observed for pH values in the range 3.8-10 (produced with HNO_3 or NH_4).

In the second set of experiments, a study was made of the effect of simultaneous thermal flux and γ-irradiation on scale formation. The tests were performed at a thermal loading of $1.4 \cdot 10^6$ W/m^2 and a radiation dose rate of 19.5 R/h at the sample surface. The γ-ray source was Co^{60} (2 g-equ Ra). The γ-ray flux was directed on the sample through a quartz window located in a side wall of the tank. The results are shown in Fig. 4.

Translated from Atomnaya Énergiya, Vol. 20, No. 5, pp. 435-436, May, 1966. Original article submitted November 29, 1965.

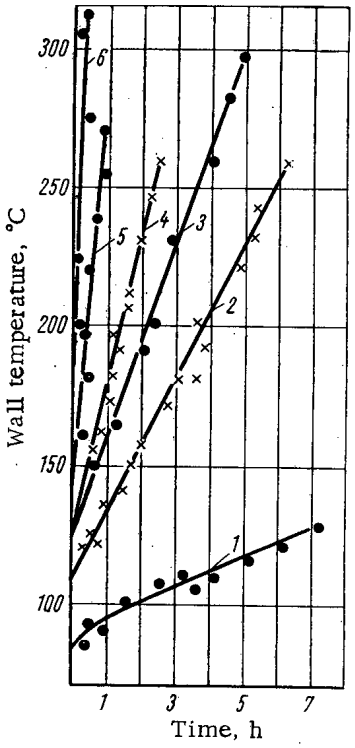

Fig. 3. Dependence of the scale-formation process on the amount of thermal loading (W/m^2) in $CaSO_4$ solution: 1) $0.23 \cdot 10^6$ W; 2) $0.52 \cdot 10^6$; 3) $0.6 \cdot 10^6$; 4) $0.7 \cdot 10^6$; 5) $1.16 \cdot 10^6$; 6) $1.9 \cdot 10^6$.

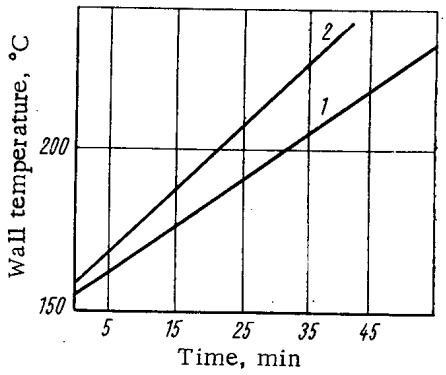

Fig. 4. Effect of γ-irradiation on scale-formation process: 1) wall temperature in saturated solution of $CaSO_4$, without irradiation; 2) the same, with irradiation.

The experimental data obtained were treated by the least squares method. For each straight line, about 30 points were analyzed. The direct increase in sample wall temperature (see Fig. 4), shows that the process of scale formation is speeded up by the action of γ-irradiation on fuel element surfaces for identical thermal loading and identical solution parameters.

Visual observation showed that the deposits on the sample surface had a reddish color, whereas they were white in the first set of experiments. From chemical analysis of the scale, it developed that corrosion products from stainless steel were deposited on the sample along with calcium sulfate. Composition of the scale was the following: $CaSO_4$—50%, Fe_2O_3—45% , the remainder—oxides of chromium, and nickel. The rate of deposition of corrosion products, calculated from analysis of the scale taken from the sample surface, was 2 g/m^2-day.

The results obtained for the effect of thermal flux values, pH, and irradiation on the scale-formation process are verified by published data [1, 4, 5] (for conditions where the main mass of water is only heated to boiling).

From what has been said above, one can conclude that γ-irradiation increases the rate of scale formation on fuel element surfaces.

LITERATURE CITED

1. A. A. Kot, Water Treatment and Water Cycle in Atomic Power Stations [in Russian], Moscow, Atomizdat (1964).
2. N. N. Man'kina, Élektricheskie stantsii, No. 2, 13 (1962).
3. N. N. Man'kina, Teploénergetika, No. 3, 8 (1960).
4. G. Simon, et al., Bettis Technical Review, 1, No. 3. Reactor Chemistry and Plant Materials, Westinghouse Electric Corp., Bettis Plant, Pittsburgh, UC-4 (1957).
5. G. Simon, Bettis Technical Review, 1, No. 3. Reactor Chemistry and Plant Materials, Westinghouse Electric Corp., Bettis Plant, Pittsburgh; UC-4 (1958).

APPARATUS FOR OSCILLATOR MEASUREMENTS IN A REACTOR

A. I. Efanov, L. V. Konstantinov,
V. V. Postnikov, I. P. Sadikov, and M. P. Sokolov

UDC 621.039.5 16.2:621.039.564

In certain experimental work associated with the study of reactor reactivity effects and also of reactor kinetic characteristics, the oscillator method [1] is employed. Further, in order to produce fluctuations in the reactivity, most often there is introduced into the reactor core special oscillator equipment which consists of strongly absorbing material and a drive mechanism for periodically changing the effective area of the absorber [2]. However, it is not always possible to introduce such equipment into the core. Therefore, in practice and particularly in experiments on power reactors, one often uses as oscillator a control rod whose drive mechanism operates in a reversible mode produced by the experimental equipment.

For physical measurements on the reactor of the first unit of the I. V. Kurchatov Atomic Power Station at Beloyarsk, oscillator equipment was developed and assembled which was used in combination with the regular system of manual control and ionization chambers to measure the differential and integral effectiveness of the manual control rods for different modes of operation and also to determine the frequency characteristics of the reactor. Through a relay circuit for controlling manual regulation, the apparatus can be connected with the drive of any of the manual control rods, whose selection is accomplished by an operator at the control panel. Because of this, it is a very convenient instrument for mass measurements of the effectiveness of a large number of rods in 1-1.5 h without disturbing the normal operating mode of the reactor. It should be pointed out that the amplitude of the periodic power oscillations during measurement was no more than 0.5-1% of the steady level.

The equipment consists of a fluctuation sensor and harmonic analyzer (see figure). The fluctuation sensor contains a frequency divider and a two-position relay which controls the output pulses from the frequency divider. At the input of the frequency divider, there is a scaling circuit which supplies a sinusoidal voltage with a frequency of 50 Hz. The scaling factor can be set at 128, 256, 512, 1024, or 2048. Periodic switching of the fluctuation sensor relay is determined by the operation of the relay circuit for controlling manual regulation. With equal rates of rod displacement upwards and downwards, rod motion in the oscillator mode is described by the function $x(t)$ with period T, where $x(t) = t$ for $\frac{\pi}{2} \leq t \leq \frac{\pi}{2}$. In order to prevent drift of the central point of rod oscillation, which arises when

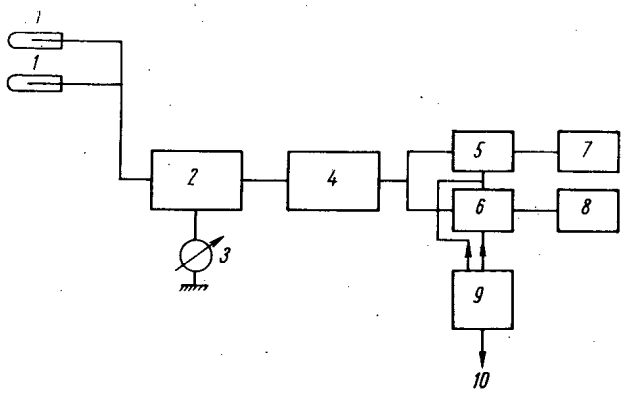

Diagram of oscillator equipment: 1) ionization chamber; 2) bandpass filter section; 3) dc microammeter; 4) dc amplifier; 5) u(t) multiplier; 6) v(t) multiplier; 7) I_1 integrator; 8) I_2 integrator; 9) fluctuation sensor; 1) signal controlling manual regulation.

Translated from Atomnaya Énergiya, Vol. 20, No. 5, pp. 437-438, May, 1966. Original article submitted July 7, 1965.

there is some inequality in the rate of rod displacement upwards and downwards, the sensor is provided with a delay circuit which permits a change in the time of rod motion in one of the directions.

The output pulses from the frequency divider are also used (with a quarter-period phase shift) for periodic switching of two relay-multiplier in the harmonic analyzer. The fluctuation sensor also includes a delay circuit and automatic shutdown of the harmonic analyzer for a time equal to an integral number of fluctuations cycles.

Current from the ionization chamber, J(t), is fed into the harmonic analyzer which consists of a band-pass filter tuned to the oscillation frequency, a dc amplifier, two multipliers, and two integrators. The signal J(t) can be represented in the form

$$J(t)=J_0+\sum_{n=1}^{\infty} J_n \sin(n\omega t+\theta_n)+J_g(t),$$

where J_0 is the dc component of the signal, whose magnitude is determined by the value of the neutron flux density at the chamber position; J_n is the amplitude of the n-th harmonic of the ac component of the signal, whose amplitude is proportional to the product $k_n |G(\omega)|$ (k_n is the amplitude of the n-th harmonic of the reactivity fluctuations; $G(\omega)$ is the modulus of the reactor transfer function); θ_n is the phase shift of the n-th harmonic of the signal with respect to the phase of rod oscillation; J_g is the signal component produced by drift in the steady reactor power level; ω is the frequency of rod oscillation ($\omega = 2\pi/T$).

Expanding k(t), the function for periodic variation in reactivity, ($k(t) \sim x(t)$), we obtain

$$k(t)=k_0\left(\sin\omega t+\frac{1}{3^2}\sin 3\omega t+\frac{1}{5^2}\sin 5\omega t+\ldots\right),$$

where

$$k_n=\frac{k_0}{(2n+1)^2}, \qquad n=0, 1, 2, \ldots$$

Consequently, with a given law for reactivity variation, the signal from an ionization chamber will contain mainly odd harmonics. The band-pass filter removes the dc component J_0 from the signal, and sharply attenuates the values of $J_g(t)$, $J_3(t)$, $J_5(t)$, ... in comparison with J_1. For example, a filter tuned to a frequency of 0.1 Hz, with which the majority of the measurements were made, has a band pass Δf = 0.05 Hz and attenuates the magnitude of the amplitude of the third harmonic by a factor of four in comparison with the attenuation for the first harmonic. Therefore, the first harmonic predominates in the signal supplied to the dc amplifier after filtration. A simple calculation, making use of the frequency dependence of the modulus of the reactor transfer function, showed that $J'_3/J'_1 \approx 0.03$, where J'_1 is the amplitude of the first harmonic of the signal at the filter output and J'_3 is the corresponding value of the third harmonic.

The dc amplifier of the harmonic analyzer has a symmetric, two-phase output which is connected through the contacts of the relay-multipliers to the inputs of the integrators. The output voltage of the amplifier is multiplied by functions u(t) and v(t) with period T where

$$u(t)=\begin{cases}1\left(0<t<\frac{T}{2}\right)\\ -1\left(\frac{T}{2}<t<T\right)\end{cases},$$

$$v(t)=\begin{cases}1\left(-\frac{T}{4}<t<\frac{T}{4}\right)\\ -1\left(\frac{T}{4}<t<\frac{3}{4}T\right)\end{cases}.$$

Expansion of the functions u(t) and v(t) in Fourier series gives the following expressions:

$$u(t)\sim\sin\omega t+\frac{1}{3}\sin 3\omega t+\frac{1}{5}\sin 5\omega t+\ldots,$$

$$v(t)\sim\cos\omega t-\frac{1}{3}\cos 3\omega t+\frac{1}{5}\cos 5\omega t-\ldots$$

The two signals resulting after multiplication are independently integrated by two integrators which are electromechanical follower systems.

The integrators produce output signals I_1 and I_2, which are proportional, respectively, to

$$\int_0^m \sum_{n=1}^{T\infty} J'_n(t)\, u(t)\, dt \sim J'_1 \cos\theta'_1,$$

$$\int_0^m \sum_{n=1}^{T\infty} J'_n(t)\, v(t)\, dt \sim J'_1 \sin\theta'_1, \quad m=4,\ 8,\ 16.$$

The contribution to the values of I_1 and I_2 from higher harmonics does not exceed 0.5-1% roughly.

In conclusion, the authors thank B. I. Bazunov, V. Ya. Mizik, V. Yu. Kammerer, and V. K. Gladkov for assembling and adjusting the equipment.

LITERATURE CITED

1. P. Liewers, Kernenergie, No. 8, 593 (1961).
2. J. Pottier, L'Onde Electrique, 35, 847 (1955).

CROSS SECTION AVERAGING IN THE THERMAL REGION FOR MEDIA CONTAINING ZIRCONIUM HYDRIDE

L. M. Gorbunov, F. M. Mitenkov, O. B. Samoilov, and V. V. Farmakovskii

UDC 539.125.52:539.17.02

It is well known that it is impossible to use a Maxwellian spectrum [1] for averaging cross sections in the thermal region for media containing zirconium hydride. The deviation of spectral shape in the thermal region from a Maxwellian spectrum for zirconium hydride results from the features of the crystalline structure, notably because of the fact that energy can be transferred only in amounts of the order of 0.13 eV during interaction of a neutron with a hydrogen atom in the lattice; therefore, this determines the shape of the thermal spectrum.

Values of the cross section in the thermal region were calculated in this paper as functions of temperature and absorption per hydrogen nucleus; they were obtained by averaging over the spectrum for an infinite, homogeneous zirconium hydride medium poisoned by absorber.

The scattering cross sections for zirconium hydride were computed from Nelkin's model [2]. The calculations were performed on the Ural-2 computer by the multigroup method for twenty groups of equal width with the boundary of the thermal region at 0.4 eV on the assumption that absorption in the medium varied in accordance with the 1/v law.

A comparison of results with experimental data [3] demonstrated the feasibility of such considerations (Fig. 1).

Shown in Fig. 2 are average absorption cross sections in the thermal region, varying in accordance with the 1/v law, as functions of the absorption per hydrogen nucleus and the temperature. (For convenience, the averaged cross sections were normalized to unity at 0.03 eV.)

Shown in Figs. 3 and 4 are the average absorption and fission cross sections in the thermal region for U^{235} located in a medium of zirconium hydride. From the curves given, one can calculate the average cross sections in the thermal region for cases where absorption in the medium obeys the 1/v law and does not exceed 20 barns per hydrogen nucleus for a temperature range of 293-773°K. Inclusion of the deviation of the U^{235} absorption cross

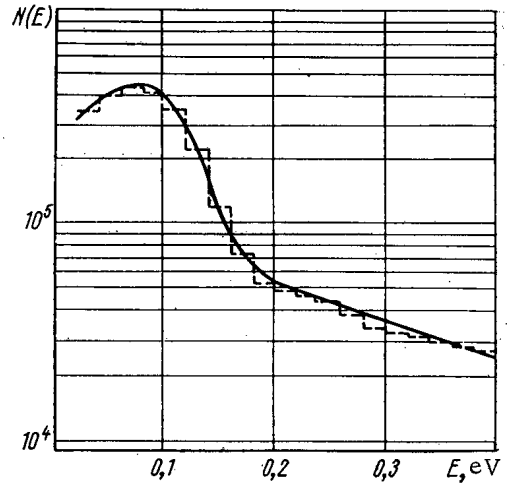

Fig. 1. Thermal neutron spectrum in medium with zirconium hydride (absorption is 4 barns per hydrogen nucleus; temperature of the medium, 293°K): – – – –) calculation; ———) experiment.

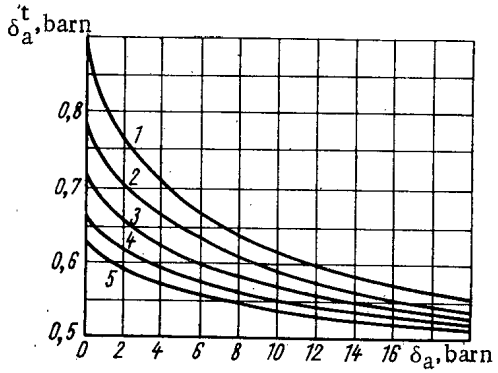

Fig. 2. Dependence of the average absorption cross section in the thermal region, varying like 1/v, on the absorption per hydrogen nucleus at 0.03 eV and on temperature: 1) 293°K; 2) 473°K; 3) 573°K; 4) 673°K; 5) 773°K.

Translated from Atomnaya Énergiya, Vol. 20, No. 5, pp. 438-439, May, 1966. Original article submitted August 14, 1965.

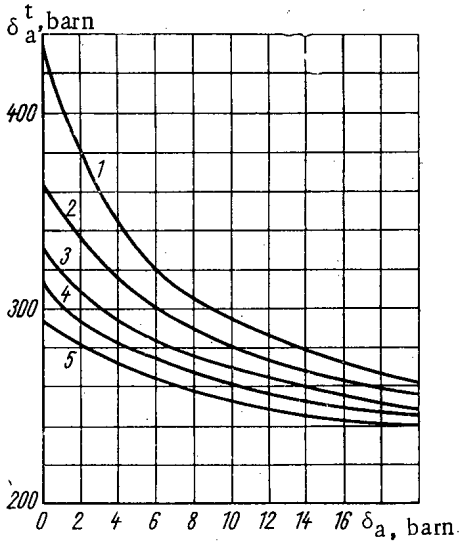

Fig. 3. Average U^{235} absorption cross section in the thermal region as a function of absorption per hydrogen nucleus for E = 0.03 eV and various temperature values. (See Fig. 2 for meaning of symbols on curves).

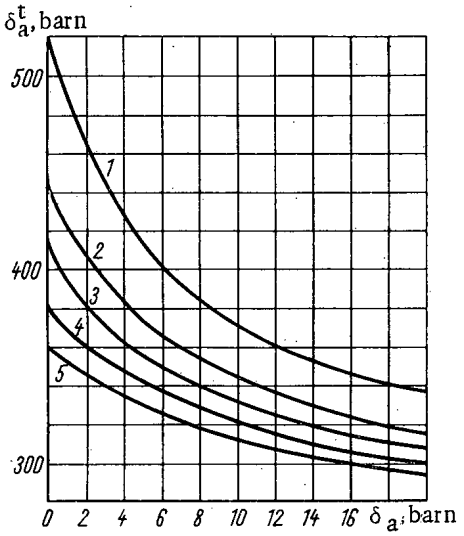

Fig. 4. Average U^{235} fission cross section in the thermal region as a function of absorption per hydrogen nucleus at E = 0.03 eV and various temperature values. (See Fig. 2 for meaning of symbols on curves).

section from the 1/v law does not lead to significant changes in the spectrum or in the average cross sections in the thermal region.

The results shown can be used for calculations of the effect of thermalization and of temperature effects.

LITERATURE CITED

1. L. V. Maiorov, V. F. Turchin, and M. S. Yudkevich, Report 360 presented by the USSR at the Third International Conference on the Peaceful Uses of Atomic Energy, Geneva (1964).
2. A. MacReynolds, et al., Proceedings of the Second International Conference on the Peaceful Uses of Atomic Energy (Geneva, 1958) [in Russian], Izbr. dokl. inostr. uchenykh, 2, Moscow, Atomizdat (1959).
3. V. F. Turchin, Slow Neutrons [in Russian], Moscow, Gosatomizdat (1963).

All abbreviations of periodicals in the above bibliography are letter-by-letter transliterations of the abbreviations as given in the original Russian journal. *Some or all of this periodical literature may well be available in English translation.* A complete list of the cover-to-cover English translations appears at the back of the first issue of this year.

THERMIONIC EMISSION OF URANIUM DODECABORIDE

S. V. Ermakov and B. M. Tsarev

UDC 621.032.273:546.791 + 546.271

Following the synthesis of uranium dodecaboride [1], we were able to study this compound's thermoelectric emission. The measurements were made by the method described in [2]. The substrate was a tungsten strip on which was deposited a thin layer (30-50 μ) of a dense suspension of UB_{12} powder in methyl alcohol.

Like the hexaborides of the rare earth metals [3], UB_{12} reacts with tungsten, and this causes buckling of the tungsten strip and the appearance of a deposit of uranium metal on the sides of the bulb (opposite the interelectrode space).

TABLE 1. $\varphi_{eff}(T)$ for Uranium Dodecaboride

Cathode No.	T, °K								
	1100	1200	1300	1400	1500	1600	1700	1800	1900
1	3,12	3,18	3,19	3,19	3,19	3,18	3,19	3,23	3,33
4	3,22	3,27	3,26	3,26	3,26	3,23	3,25	3,27	3,35
5	3,19	3,19	3,22	3,26	3,28	3,30	3,31	3,32	3,36
6	3,06	3,09	3,12	3,17	3,19	3,19	3,22	3,27	3,33
φ_{eff} (mean)	3,15	3,18	3,20	3,22	3,23	3,22	3,24	3,27	3,34
j_e, amp · cm^{-2} (mean)	$5\cdot10^{-7}$	$7\cdot10^{-6}$	$8\cdot10^{-5}$	$6\cdot10^{-4}$	$4\cdot10^{-3}$	$2\cdot10^{-2}$	$8\cdot10^{-2}$	$3\cdot10^{-1}$	$6\cdot10^{-1}$

TABLE 2. Comparison of Work Functions of UB_{12}, UB_4, and UB_2

Type of boride	$\varphi_{eff} = \varphi_0 + \frac{\partial\varphi}{\partial T} T$	Value of φ_{eff} at T°K		
		1500	1800	1900
UB_{12}	$2,89+2,38\cdot10^{-4}\,T$	3,25 (3,23)	3,32 (3,27)	3,35 (3,34)
UB_4	$3,4-0,8\cdot10^{-4}\,T$	3,28	3,26	3,25
UB_2	$3,3+0,2\cdot10^{-4}\,T$	3,33	3,336	3,34

Note: Figures in brackets are experimental values of the work function.

Table 1 gives our results for the work function at various measured temperatures and current densities, and also the mean effective work function of UB_{12} (for $A_0 = 120{,}4$ amp/cm^2 · deg^2). The effective work function obeys the equation

$$\varphi_{eff} = \varphi_0 + \frac{d\varphi}{dT} T = 2{,}89 + 2{,}38\cdot10^{-4}T.$$

The deviation from linearity towards lower work functions at 1500-1900°K is apparently due to the onset of reaction between the UB_{12} and the tungsten near 1450°K. Unfortunately, it proved impossible to plot the UB_{12} work function above 1900°K, owing to severe overloading of the anode by the emission current. We attempted to measure the thermionic emission of UB_{12} on a tungsten strip covered with a layer of iridium powder, as was done in [3] in a study of the hexaborides of the rare earths; however, this was unsuccessful, because a strong exothermic reaction set in at ~1600°K, causing overheating of the cathode. We did not discover the nature of this reaction.

Translated from Atomnaya Énergiya, Vol. 20, No. 5, pp. 439-440, May, 1966. Original article submitted October 1, 1965.

Table 2 gives our results, together with data from [4] on the emission of uranium diboride and tetraboride. Comparison of the work functions at 1800°K reveals that the deviation from linearity at high temperatures can be explained by a gradual conversion, by reaction with tungsten, of UB_{12} to UB_4 and then to UB_2, accompanied first by a decrease and then an increase in the work function.

The authors would like to thank Yu. B. Paderno and G. V. Samsonov for letting them have the sample of uranium dodecaboride.

LITERATURE CITED

1. Yu. V. Paderno, Atomnaya Énergiya, 10, 396 (1961).
2. B. V. Bondarenko and S. V. Ermakov, Radiotekhnika i élektronika, 7, 2099 (1962).
3. S. V. Ermakov and B. M. Tsarev, Radiotekhnika i élektronika, 10, 972 (1965).
4. G. Haas and J. Jansen, J. Appl. Phys., 34, 3451 (1963).

All abbreviations of periodicals in the above bibliography are letter-by-letter transliterations of the abbreviations as given in the original Russian journal. *Some or all of this periodical literature may well be available in English translation.* A complete list of the cover-to-cover English translations appears at the back of the first issue of this year.

EFFECT OF ULTRASOUND ON THE PLASTICITY OF HIGH-BORON STAINLESS STEEL*

L. E. Al'shevskii, Yu. S. Kuz'michev,
L. M. Kurochkina, I. S. Lupakov,
V. E. Neimark, and I. I. Teulin

UDC 621.789.2:669.15

Steels with high-boron content are widely used in nuclear power production, and also find applications in nuclear geophysics. However, it is extremely difficult to fabricate thin sheets and tubes of this material, owing to its low plasticity: the boron forms many hard, brittle and thermally stable borides with chromium, iron and other elements, and these sharply reduce the plasticity. Furthermore, in steels of types 1Kh18N15, Kh18N10, and Kh18N6G9, when the boron content exceeds 1.8% coarse hyper-eutectic borides form, and these reduce the plasticity even further. It can be improved by reducing the amount of the boride phase and breaking up the particles of hyper-eutectic borides. The amount of boride phase can be reduced by adding transition metals, which form boride phases of the type Me_2B_3 or MeB_2, more concentrated in boron content than the borides of type $Me_2B(FeCr)_2$ which they replace [1].

The form and degree of dispersion of the primary borides can apparently be altered by the action of ultrasound waves on the alloy during crystallization. In the present letter, we give some results on how ultrasound affects the dispersity of the boride phase and the plasticity of high-boron stainless steels of types Kh18N15, Kh18N10, Kh18N6G9, and Kh17, which contain 2-3.7% boron. The plasticity was assessed during the fabrication of tubes by extrusion. The steels were treated with ultrasound of frequency 8.8 kc/sec in the apparatus of the N. P. Bardin Central Research Institute for Ferrous Metallurgy [2]. It was found that with relatively low-temperature casting (~1380°C) there was little difference from the structure of untreated steel. This can be explained by the thesis that in low-temperature casting activated impurities arise in the melt and act as crystallization centers [3]. When the casting temperature was raised to 1500°C, we obtained a marked change in the structure of steel Kh18N6G9, which contains 3.5% boron (Fig. 1).

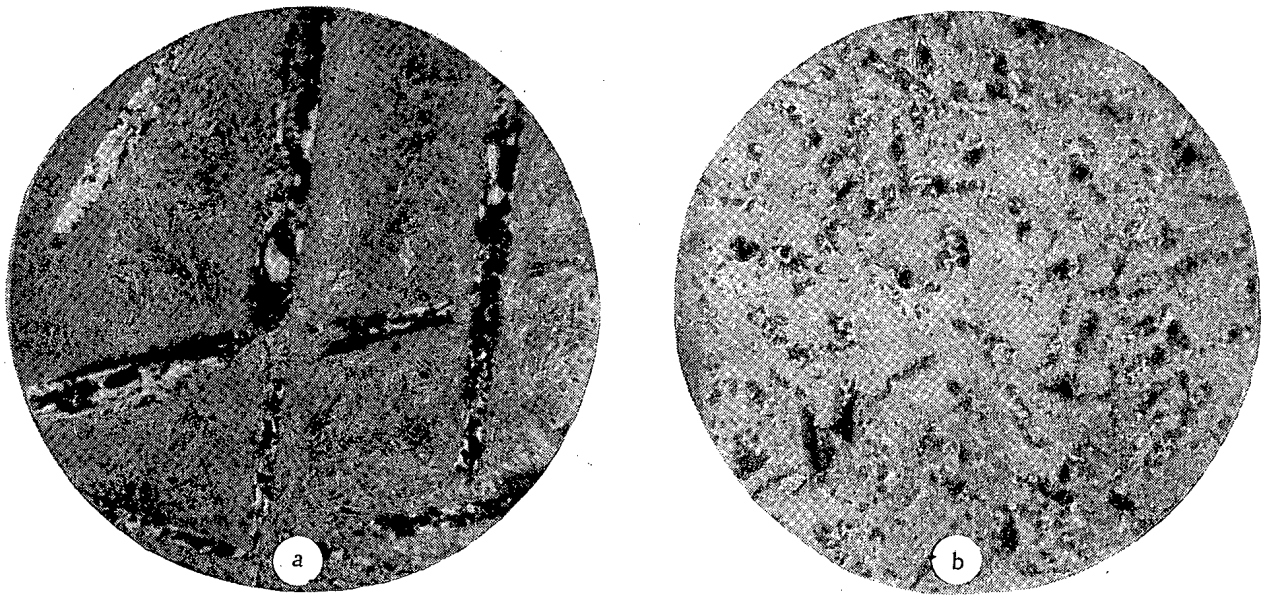

Fig. 1. Microstructure of cast steel Kh18N6G9; a) not exposed to ultrasound; b) exposed to ultrasound.

*V. I. Lomakin and N. D. Mel'nichenko helped in the work.

Translated from Atomnaya Énergiya, Vol. 20, No. 5, pp. 440-442, May, 1966. Original article submitted August 14, 1965.

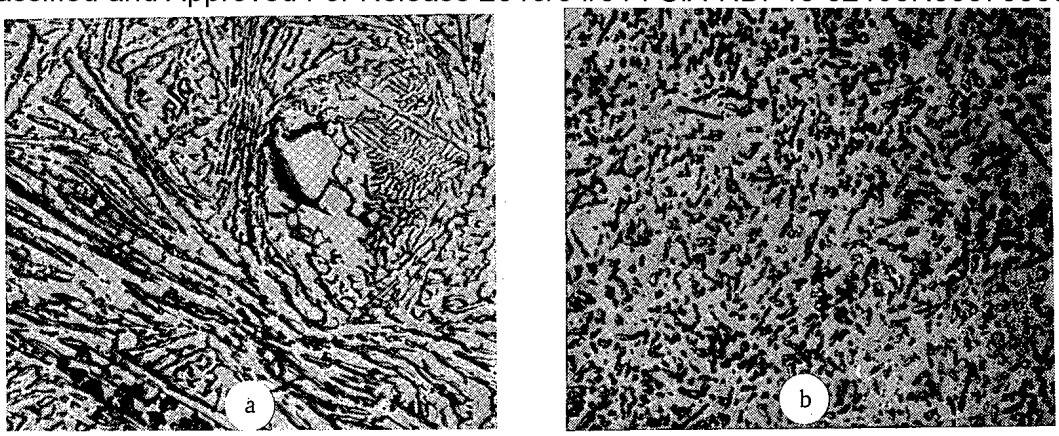

Fig. 2. Microstructure of cast steel Kh18N15. a) Not subjected to diffusion annealing; b) after diffusion annealing.

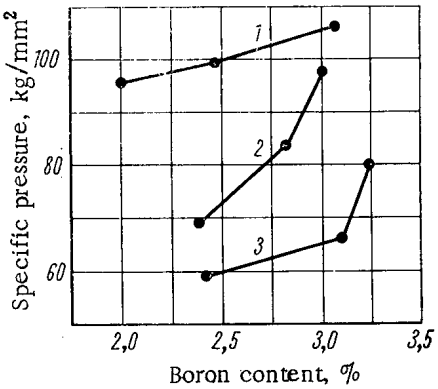

Fig. 3. Specific pressure of extrusion versus boron content of steel. 1) 1500-ton press, coeff. of extension 5; 2) 1500-ton press, coeff. of extension 7.4; 3) 800-ton press, coeff. of extension 5.3.

Similar structural changes were obtained in steels Kh18N15, Kh18N10, and Kh17, which contain about the same amount of boron. To assess the effect of ultrasound on the composition of the boride precipitates, we separated them electrolytically and subjected them to chemical analysis: it was found that ultrasound treatment does not alter the composition of the borides, and that the separated boride phase is a compound of type $(FeCr)_2B$. The amount of iron in the borides is about the same as the amount of chromium, while the nickel content in the boride phase separated from austenitic steels is small, varying from 2-3%. The manganese content in precipitates separated from steel Kh18N6G9 was 4-6%.

As well as ultrasound treatment, we studied the effect of diffusion annealing at 1200-1250°C on the structures of the high-boron steels. It was found that diffusion annealing at 1200°C for 1 h leads to marked changes in the microstructure of steel Kh18N15, which contains 2.5% boron (Fig. 2).

We observed similar changes in the microstructure of steels Kh18N10T and Kh18N6G9 after high-temperature annealing. As seen in Fig. 2, after high-temperature annealing for 1 h, the boride phase becomes spheroidized. We can assume that this improves the plasticity of the steel. Rolling and forging reveal that after ultrasound treatment the plasticity of the steel is appreciably increased. Particularly marked improvement was found on rolling, and a somewhat less marked improvement on free forging: this may be explained as due to the more favorable stress pattern in forging.

We also assessed the effect of ultrasound on the extrudability of ingots of hyper-eutectic steels. Billets were pressed on an 800-ton vertical hydraulic press and a 1500-ton horizontal hydraulic press. For the 800-ton press, the billets had diameter 77 and length 120-200 mm. For the 1500-ton press they had diameter 106 and length 150-225 mm. From the results of high-temperature tension tests, and also of rolling wedge-shaped specimens,* we chose an optimum extrusion temperature in the range 1050-1140°C. The rate of extrusion was varied from 40-250 mm/sec. Before extrusion, the machine was loaded to 200-400°C. The matrix and billet were lubricated with vitreous lubricant. The coefficient of extension during pressing was 5.0-4.4 (shrinkage 80-86%). It was found that in every case the extrusion of billets of non-ultrasound-treated steel gave unsatisfactory results. However, by extruding steel which had been treated with ultrasound, we obtained tubes of satisfactory quality, of diameters 50 and 71 mm, with wall thickness 5-6 mm and length up to 800 mm. The force required for extrusion increased with the coefficient of extension and the boron content. Figure 3 plots the relative pressure on the press plate versus the boron content of the steel.

We can thus conclude that ultrasound treatment of hyper-eutectic steels of types Kh18N10, Kh18N15, and Kh18N6G9, containing up to 3.5% boron, leads to breakup of the boride phase on high-temperature casting. This increases the plasticity of cast high-boron steel and thus makes it possible to fabricate tubes by extrusion.

*This work was done by Ya. B. Gurevich.

LITERATURE CITED

1. I. S. Lupakov and Yu. S. Kuz'michev, Fizika metallov i metalloved., 18, 1 (1964).
2. I. I. Teulin and A. M. Zubko, Tekhniko-informatsionnyi byulleten' Osobogo konstruktorskogo byuro ul'trazvukovykh i vysokochastotnykh ustanovok [Technical Information Bulletin of the Special Construction Office for Ultrasonic and High-Frequency Equipment], No. 3, (15), 3 (1960).
3. V. E. Neimark, Problems in Metallurgy and Metal Physics, Moscow, Metallurgizdat (1962).

All abbreviations of periodicals in the above bibliography are letter-by-letter transliterations of the abbreviations as given in the original Russian journal. *Some or all of this periodical literature may well be available in English translation.* A complete list of the cover-to-cover English translations appears at the back of the first issue of this year.

IONIZATION-MECHANICAL DETECTOR FOR IONIZING RADIATIONS

O. A. Myazdrikov, V. N. Demidovich, and A. P. Suslov

UDC 621.376.577.391

The macrocharge self-oscillation condition established in an electromechanical model of a diode [1] may be used in setting up a detector for high-intensity fluxes of radiation [2]. Let us suppose that a spherical particle of radius r with an electrically-conducting surface is in contact with one of the plates of an air condenser (Fig. 1). As a result of the electrical contact the particle will acquire a charge Q given by [3]

$$Q=\frac{\pi^2 D^2}{24d}v, \tag{1}$$

where v is the voltage applied to the electrodes of the detector, D = 2r is the diameter of the macroparticle, and d is the interelectrode distance.

An electric force equal to

$$F_e=\frac{B\pi^2 D^2}{24d^2}v^2, \tag{2}$$

will act on the particle, where B = 0.84.

If the repulsive force is greater than the weight of the particle p, i.e.,

$$F_e > p=mg, \tag{3}$$

then the particle will enter into self-oscillatory motion between the electrodes. Each act of charge transfer at the electrodes will correspond to a voltage pulse, which may be taken from the load resistance R_L.

When there is a field of ionizing radiation in the interelectrode space, the concentration of ions formed will depend on the strength of the dose or the intensity of the radiation. Hence, as the particle moves there will be a partial neutralization of the charge Q during its flight; this will lead to a reduction in the electric force and, hence, in the frequency of the oscillations. This in turn will reduce the repetition frequency of the output pulses. The time variation in the charge Q resulting from its neutralization by ions of opposite polarity may to a first approximation be represented by an exponential relationship of the form

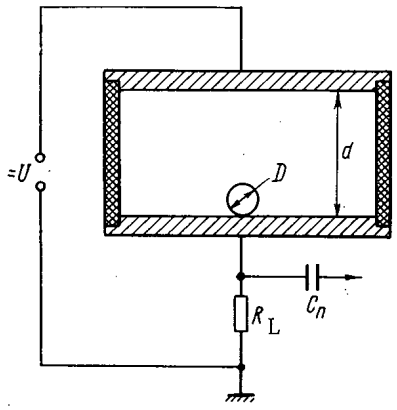

Fig. 1. Arrangement of detector.

$$Q_{(t)}=Q_0 e^{-\alpha\frac{\bar{k}eN}{\varepsilon}}, \tag{4}$$

where α is a coefficient allowing for the efficiency of neutralization, k is the average mobility of the positive and negative ions, c is the charge of an ion, N is the concentration of the ions, and ε is the dielectric constant of the medium.

The coefficient α takes into consideration the effect of space charge of the same sign as the macrocharge. This factor may be determined either theoretically or experimentally. To each value of voltage will correspond a certain critical intensity, on reaching which the self-oscillatory motion will stop. In order to restore the oscillations, it is sufficient to raise the voltage on the electrodes of the detector; this is the same thing as transforming to a higher measuring range.

Translated from Atomnaya Énergiya, Vol. 20, No. 5, pp. 442-444, May, 1966. Original article submitted October 16, 1965.

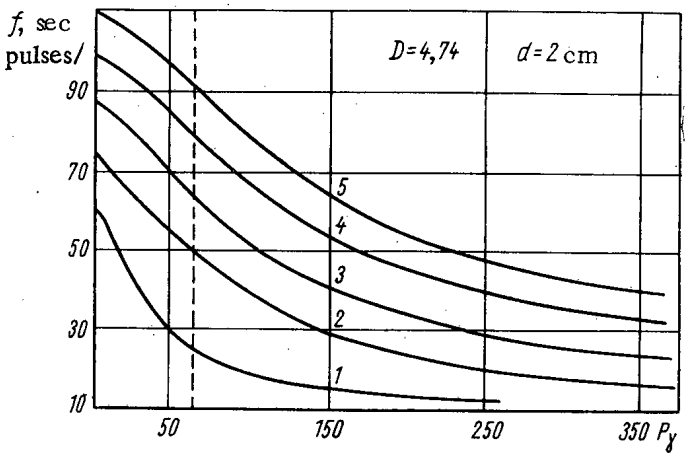

Fig. 2. Counting characteristics of the IMD (ionization-mechanical detector). 1) v = 4.5 kV; 2) 5.5 kV; 3) 6.5 kV; 4) 7.5 kV; 5) 8.5 kV.

Analysis of the equivalent circuit of the detector shows that the formation of the output signal takes place as the result of the excitation of an R_eC_e circuit by a quantity of electricity Q, where R_e is the equivalent input resistance of the recording device and C_e is the equivalent capacitance. The pulse length determined by the time constant R_eC_e lies between 2 and 50 μsec.

In the majority of cases the weight of the particle may be neglected in steady-state conditions of self-oscillation. Then the principal equation of motion of the particle in the interelectrode space will take the form

$$m\frac{d^2x}{dt^2}+A\left(\frac{dx}{dt}\right)^2-BQ_{(t)}E=0, \tag{5}$$

where m is the mass of the particle, A is a quantity defined by the aerodynamic-resistance formula:

$$A=\frac{\pi D^2}{4}\cdot\frac{C_x}{2}\rho;\quad F_a=A\left(\frac{dx}{dt}\right)^2;\quad B=0.84;$$

and E is the electric field.

Determination of the aerodynamic-resistance force F_a for a wide range of particle velocities and diameters showed that F_a was always much smaller than F_e under the operating conditions and could therefore be neglected. The error in solving Eq. (5) in this case is no greater than 1-2% and falls for higher dose values.

The solution of Eq. (5), even without counting F_a, involves an implicit relationship between the oscillation frequency f and the dose strength P_γ

$$d'=\frac{B_1}{\alpha\beta P_\gamma}\left(1-\frac{1-e^{-\frac{\alpha\beta P_\gamma}{f}}}{k-1}K\right)\frac{1}{f}-\frac{B_1}{\alpha^2\beta^2P_\gamma^2}\left(1-e^{-\frac{\alpha\beta P_\gamma}{f}}\right), \tag{6}$$

where d' is the reduced interelectrode distance (d' = d−D), E is the coefficient of restitution of momentum when the particle strikes the electrode, $B_1 = F_e/m\varepsilon$, and β is a constant factor ($\beta = 2.08\cdot10^9$ ke). Thus, in general form the frequency f depends on the parameters P_γ, B_1, d, K.

Equation (6) in f and P_γ may be solved by means of an electronic computer. Unequivocal information on the dose strength or radiation intensity can only be obtained when operating the detector under saturation-current conditions. This condition is automatically satisfied, since the operating voltage is always higher than the voltage

corresponding to the beginning of self-oscillatory motion is given to a fair accuracy by the formula

$$v_b = 513 \frac{d}{D} \sqrt{p}, \tag{7}$$

where p is the weight of the particle. If p is in mg and d and D in cm, then v_b is given in volts.

In order to reduce the operating voltage, spherical particles obtained from foamed polystyrene of the PS-5B type were used in experiments. The particles were covered with graphite dissolved in a mixture of alcohol and benzene; this ensured an electrically-conducting surface. All the detectors used were of cylindrical form, the bases of the cylinders constituting the electrodes. The sides were made a dielectric (glass or organic materials).

The amplitude of the pulses in the ionization-mechanical detector is a function of the supply voltage v, the interelectrode distance d, and the particle diameter D: $V_A = \varphi$ (v, d, D) (for R_L = const); it may reach 10 V or over. Stabilization of the frequency and the amplitude spectrum of the pulses is achieved by giving spherical form to one or both electrodes. The count statistics may be improved and the measurements made more accurate by increasing the number of particles in the working space. The relative error in the count will be expressed by the following relation:

$$\frac{f'}{f_0} = \frac{n}{(1 + f_0 t_r)}, \tag{8}$$

where f' is the number of pulses from several particles per unit time, f_0 is the number of pulses from one particle per unit time, t_r is the resolution time of the detector, and n is the number of particles.

The IMD was studied experimentally in conjunction with a K-2000 cobalt system in the dose range 0 to 380 R/sec. The IMD pulse frequency is shown as a function of γ-radiation dose in Fig. 2.

Theoretical calculation of P_γ from Eq. (6), carried out on the "Minsk-2" electronic computer gave results differing from experiment by 15-25%, the error falling with increasing dose.

Analysis of Eq. (6) shows that the second term may be neglected for $P_\gamma \geq 50$ R/sec. In this case we have a hyperbolic relationship between f and P_γ:

$$f = \frac{B_1}{\alpha\beta\, d P_\gamma} \left(\frac{K}{1 - K} + 1 \right), \tag{9}$$

and this agrees satisfactorily with the experimental results presented.

The stability and reliability of operation of the IMD for large doses is determined entirely by the radiation and mechanical stability of the materials used.

Leaks of various kinds due to radiation damage of the insulators have no effect on the indications of the detector, owing to the pulse form of the signal.

The ionization-mechanical detector clearly has its uses in solving some special problems involving the measurement of various kinds of high-intensity fluxes, especially fluxes of low-energy radiation.

LITERATURE CITED

1. O. A. Myazdrikov, Author's Certificate No. 155049.
2. O. A. Myazdrikov and V. N. Demidovich, Author's Certificate No. 168805.
3. J. Maxwell, Treatise on Electricity and Magnetism, Cambridge (1872).
4. N. I. Lebedev and I. P. Skal'skaya, ZhTF, 32, No. 3 (1960).

EXPRESS METHOD OF DETERMINING THE CONCENTRATION OF AN RaA AEROSOL AND THE LATENT ENERGY IN THE AIR

N. P. Kartashov

UDC 543.52: 546.296

In order to eliminate radiation hazard in uranium mines, it is essential to have methods of rapidly and accurately measuring the quantities of radon and its short-lived decomposition products, RaA, RaB, and RaC, in the atmosphere of the mine. The disrupted radioactive equilibrium [1, 2] makes a quantitative estimate of these products from the concentration of radon very difficult. Hence, the perfection of existing express methods [3-6] of directly determining the specific activity of an aerosol and the development of new methods constitute an important problem. We shall now consider a highly efficient method of determining the concentration of RaA and the "latent energy"* E (MeV/liter); this is no less accurate than the method given in [6], but has a much lower apparatus measuring time.

Theory of the Method

Let us suppose that the air being studied is drawn through a filter from some instant of time $\tau = 0$; the air contains a chain of short-lived decomposition products RaA → RaB → RaC with a displacement of radioactive equilibrium between them (defined by the coefficients $\xi_1 = C_B/C_A$ and $\xi_2 = C_C/C_A$), the concentration of the first of these being $C_A = Q_A\lambda_A$, where Q_A and λ_A are the number of atoms in a liter of air and the decomposition constant of RaA respectively.

For a filtration time τ, the α activity of the filter, allowing for the decomposition of the radioactive materials taking place in the period t which has elapsed since the filtration period ended, is

$$N(\tau, t) = N_A + N_C, \tag{1}$$

where the activities of RaA and RaC are respectively equal to

$$N_A = v\eta \frac{C_A}{\lambda_A}(1 - e^{-\lambda_A \tau})\, e^{-\lambda_A t}; \tag{2}$$

$$\begin{aligned} N_C = v\eta \frac{C_A}{\lambda_A} \Bigg\{ & \frac{\lambda_B\lambda_C(1 - e^{-\lambda_A\tau})\, e^{-\lambda_A t}}{(\lambda_B - \lambda_A)(\lambda_C - \lambda_A)} \\ & + \frac{\lambda_A\lambda_C(\lambda_B + \xi_1\lambda_A - \xi_1\lambda_B)(1 - e^{-\lambda_B\tau})\, e^{-\lambda_B t}}{\lambda_B(\lambda_A - \lambda_B)(\lambda_C - \lambda_B)} \\ & + \frac{\lambda_A[(\lambda_A - \lambda_C)(\xi_1\lambda_C - \xi_2\lambda_C + \xi_2\lambda_B) + \lambda_B\lambda_C] \times (1 - e^{-\lambda_C\tau})\, e^{-\lambda_C t}}{\lambda_C(\lambda_A - \lambda_C)(\lambda_B - \lambda_C)} \Bigg\}. \end{aligned} \tag{3}$$

Here v is the air flow rate (volume) and η is the capture coefficient of the aerosol in the filter.

In contrast to the complicated mathematical apparatus considered in [3] and [6], Eq. (3) enables us to obtain exact numerical values of the function $N_C(\tau, t, \xi_1, \xi_2)$ by a single-stage solution after substituting the values of the four arguments.†

*The energy released on complete decomposition of the short-lived derivatives of radon contained in one liter of air.

†In particular, at radioactive equilibrium $\xi_1 = \xi_2 = 1$ with $\tau = \infty$ and t = 0, formula (3) gives $N_C = v\eta(Q_A + Q_B + Q_C)$; for a maximum displacement $\xi_1 = \xi_2 = 0$ and the same values of τ and t we have $N_C = N_A = v\eta Q_A$.

Translated from Atomnaya Énergiya, Vol. 20, No. 5, pp. 444-448, May, 1966. Original article submitted October 15, 1964; revised October 11, 1965.

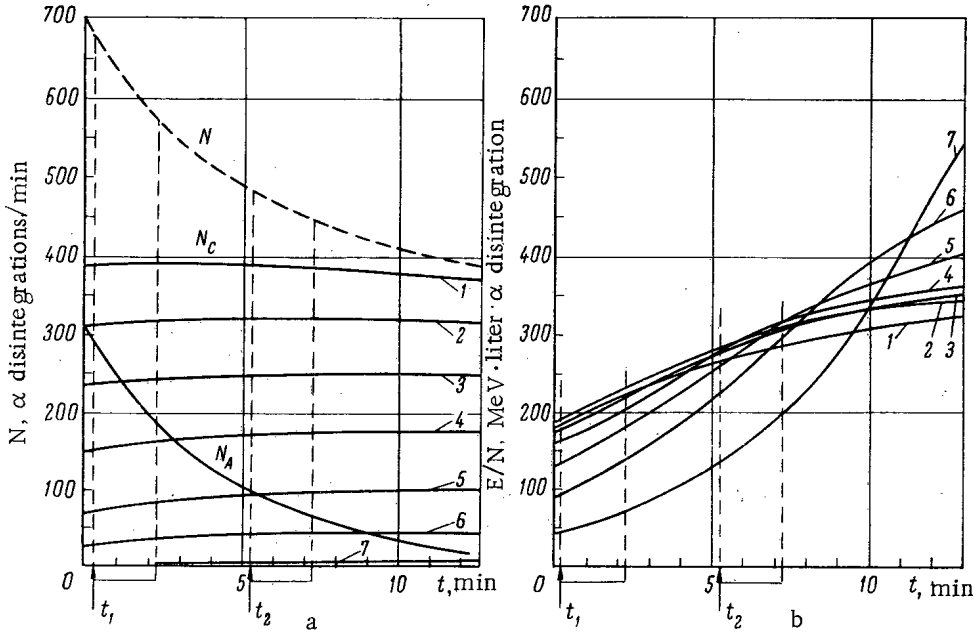

Fig. 1. Group of differential functions calculated with respect to parameters ξ_1 and ξ_2; a) specific activity of the filter; b) information energy capacity of α-particles; 1) $\xi_1 = 1$, $\xi_2 = 1$; 2) $\xi_1 = 1$, $\xi_2 = 0.8$; 3) $\xi 1 = 0.8$, $\xi_2 = 0.6$; 4) $\xi_1 = 0.6$, $\xi_2 = 0.4$; 5) $\xi_1 = 0.4$, $\xi_2 = 0.2$; 6) $\xi_1 = 0.2$, $\xi_2 = 0.1$; 7) $\xi_1 = 0$; $\xi_2 = 0$ ($C_A = 1 \cdot 10^{-10}$ Ci/liter, $\tau = 1$ min 45 sec).

Analysis of Eq. (3) shows that, for a brief filtration period ($\tau \leq 1/\lambda_A$), and as a result of the development of radioactive equilibrium between RaB and RaC, the function $N_C(t)$ remains practically constant for all values of argument t within the limits $0 \leq t \leq 8$ min. Hence, the fall in the activity of the filter in the time period indicated is due solely to the change in the function $N_A(t)$. Using Eqs. (1) and (2), we obtain

$$C_A = K_1 \Delta N_A = K_1 [N(t_1) - N(t_2)], \quad (4)$$

where K_1 is a coefficient depending on t_1 and t_2. For disrupted equilibrium, the condition N_C = const is not satisfied quite so well. Hence, for unknown values of ξ_1 and ξ_2, a certain systematic error appears in the concentration of RaA determined from formula (4), and the value of this depends on the measuring arrangement.*

Under conditions of radioactive equilibrium, the latent energy E can be determined exactly from the obvious relation

$$E = K_2 N(t), \quad (5)$$

where K_2 (MeV/liter·disintegration) is the so-called information energy capacity of the α-particles, which represents the amount of latent energy causing one α-disintegration in the filter (for a given time τ) in the period between t and $t + \Delta t$.

Since $K_2 = f(\xi_1, \xi_2)$, a systematic error also appears in the value of E determined from formula (5) (for unknown arguments); this may be determined numerically for the particular measuring arrangement used.

Selection of Optimum Measuring Method and Analysis of Systematic Errors

A measuring method may be considered optimum if the errors introduced into the quantities E and C_A being determined by the displacement of equilibrium are minimal as compared with other methods of similar efficiency and economy.

The numerical values of the errors associated with various displacements of equilibrium were preliminarily estimated from a series of graphs of differential functions of the specific activity of the filter $N(\tau, t) = \varphi(\xi_1, \xi_2)$ and the information energy capacity of the α-particles $E/N(\tau, t) = \varphi(\xi_1, \xi_2)$, a group of which (optimal with respect to τ) appears in Fig. 1. Analysis of these graphs enabled us to select the following measuring method as

*In [6] this error is unfortunately called "methodical."

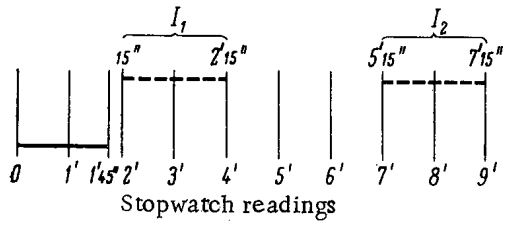

Fig. 2. Principle of the IEM: ——— section of samples; – – – – measurement of filter. Time reckoned from the moment of starting the stopwatch.

optimum (allowing for all the other requirements): air passed through the filter for τ = 1 min 45 sec, radiometry of the filter begun at t_1 = 15 sec and t_2 = 5 min 15 sec, measurements lasting for periods of $\Delta t_{1.2}$ = 2 min. The general principle of this method, called IEM (improved express method) for short, is shown in Fig. 2.

We see from Fig. 1, that the relative change in the function $N_C(t)$ over the intervals chosen, $\psi = \frac{N_C(t_1) - N_C(t_2)}{N_C(t_1)}$, is fairly small for all values of the parameters ξ_1 and ξ_2 from 1 to 0. Moreover, at first (curves 1, 2) $\psi > 0$, and then (curves 4-7) $\psi < 0$. This symmetry, in particular, determines the optimum time for passing air through the filter: for larger τ this change in the function $N_C(t)$ is solely negative for any arbitrary displacement, while for very small values ($\tau \leq$ min), it is positive, increasing the systematic errors made in determining C_A. Moreover, for $\tau \geq 2$ min, the absolute value of N_C is considerably greater than N_A, which is undesirable in view of the increase in the statistical error in measuring the difference ΔN and the fall in the accuracy of determining the concentration of RaA. Thus, for example, with the method proposed in [6] (τ = 5 min for $C_A = 1 \cdot 10^{-11}$ Ci/liter), the statistical error corresponding to the actual apparatus parameters equals 40% and exceeds the maximum systematic error of determining C_A by a factor of 3.1. A peculiar node in the function E/N(t) (see Fig. 1) for different values of the parameters ξ_1 and ξ_2 within the region of which the information energy capacity of the α-particles depends very little on the equilibrium displacement, determines the choice of interval t_2. For this the systematic errors in determining E will clearly be smallest (an exception is curve 7 in Fig. 1, which corresponds to the limiting displacement, but this circumstance is not decisive, as we shall show later).

The choice of t_1 = 15 sec is imposed by technical considerations. Theoretically the best value would be $t_1 = 0$, since this increases ΔN_A and the accuracy of determining C_A. The measuring time $\Delta t_{1.2}$ = 2 min is also optimum since (as calculations confirm), it gives the highest absolute values of N and ΔN and, hence, the smallest statistical errors, without greatly increasing the systematic errors of determining C_A and E.

Integration of the function N(t) over the count limits indicated for unit values of the parameters v and η and unit concentration of equilibrium RaA equal to $1 \cdot 10^{-10}$ Ci/liter gives the following number of α-particles:

$N_1 = \int_{t_1}^{t_1+\Delta t} N(t)\,dt = 1262$, $N_2 = 926$. Knowing these quantities and using Eq. (4), we find $K_1 = \frac{C_A}{N_1 - N_2} = \frac{1}{336}$.

The concentration of RaA is related to the number of pulses I_1 and I_2 recorded in the first and second count intervals by the relation

$$C_A = \frac{1}{336} \cdot \frac{I_1 - I_2}{\varepsilon \eta v} 10^{-10} = 3 \frac{I_1 - I_2}{\varepsilon \eta v} 10^{-13} \qquad (6)$$

where ε is the efficiency of the α-radiometer used.

In order to estimate the systematic error in determining the concentration of RaA from formula (6) for various displacements of equilibrium, a graphical integration of function N was carried out with respect to its components N_A and N_C. The results of the integration and values of the relative systematic errors $\delta C_A = \Delta N_C / \Delta N_A$ are shown in Table 1.

The computed values of component N_A equal $N_A(t_1)$ = 486 pulses, N_A = 162 pulses and ΔN_A = 324 pulses. We see that for actual cases of departure from equilibrium the value of relative systematic error does not exceed 6% (it only reaches a maximum of 23.4% in the case $\xi_1 = 1$, $\xi_2 = 0$, which never occurs in practice). The algebraic error values are distributed nearly symmetrically with respect to a certain mean displacement 0.5:0.35. Hence, there is no need to vary the coefficient K_1, as the authors of [6] do, operating with arbitrary figures.

Using Eq. (5) and known values of N_1 and N_2 for unit concentration of equilibrium RaA, which, as we know, corresponds to a latent energy of $E = 1.28 \cdot 10^5$ MeV/liter, it is not hard to obtain simple relations between I_i and E:

$$E = 138 \frac{I_2}{\varepsilon \eta v} = 101 \frac{I_1}{\varepsilon \eta v}. \qquad (7)$$

TABLE 1. Systematic Errors in Determining C_A

ξ_1	ξ_2	$N_C(t_1)$	$N_C(t_2)$	ΔN_C	δC_A, %
1	1	776	764	+12	+3,7
1	0,8	627	639	—12	—3,7
0,8	0,6	475	486	—11	—3,4
0,6	0,4	316	333	—17	—5,2
0,4	0,2	161	180	—19	—5,7
0,2	0,1	81	90	—10	—3,1
0,1	0,05	40	46	—6	—1,8
0	0	1	3	—2	—0,6

In order to calculate the systematic error in determining E due to a displacement of equilibrium, we use the value of the information energy capacity of the α-particles, E/N_i, in the count intervals chosen. The results of such a calculation for unit concentration of RaA and the indicated values of equilibrium-displacement coefficients are shown in Table 2. Since $\lambda_A > \lambda_B \cong \lambda_C$, we find that, as the equilibrium displacement increases and approaches its maximum, for which $C_B = C_C = 0$, the value of E falls more rapidly than N (for all $t < 10/\lambda_A$). The information energy capacity of the α-particles naturally falls, and the systematic error at first positive, as indicated in Table 2, changes its sign to negative and then rises in absolute value, producing an overestimate in the measured values of E. This physically obvious result contradicts the numerical material in the table of [6], where the systematic errors for two extreme cases (equilibrium and maximum displacement) have the same sign and are almost equal in absolute magnitude.

The results show that, by using the second measurement I_2, made after 9 min of apparatus time, the value of the latent energy is determined to a fair accuracy for any displacement of equilibrium. The use of I_1 in examining surface objects, where a displacement of radioactive equilibrium close to the limiting value may occur, is inadmissible: the systematic error could in this case exceed 200%. In underground workings and shafts, for any practical rate of air exchange, the limiting displacement of equilibrium cannot arise. For the greatest practically-observed displacement [1, 3], equal to $\xi_1 = 0.15$ and $\xi_2 = 0.07$, we find by interpolating from the data of Table 2 $\delta_1 E = -109.8\%$. We note that this displacement of equilibrium nevertheless leads to an impermissibly large overestimate of E. If, however, we take the coefficient of I_1 in Eq. (7) as equal to 81.0 (which corresponds to a displacement of equilibrium 0.3, 0.15), then systematic errors of both signs are almost equally probable. For these conditions the value of the latent energy in underground workings may be found in 4 min of apparatus time with an error no greater than ±55%. Suitable choice of the coefficient of I_2 leads to the possibility of determining E with no error greater than ±35% in 9 min of apparatus time, both in underground and surface objects. Thus, finally the methodical formula (7), takes the following form:

$$E = 122\frac{I_2}{\varepsilon\eta v} = 81\frac{I_1}{\varepsilon\eta v}. \qquad (7')$$

Given a measuring scheme similar to that recommended in [5], we can show that the latent energy found by the Kusnetz method is determined by an expression analogous to formula (7):

$$E = 138{,}4\frac{I_3}{\varepsilon\eta v}, \qquad (8)$$

TABLE 2. Systematic Errors in Determining the Latent Energy E

ξ_1	ξ_2	E, MeV/liter	E/N_1, MeV/liter·disintegration	$\delta_1 E$, %	E/N_2, MeV/liter·disintegration	$\delta_2 E$, %
1	1	128 200	101,5	0	138,4	0
1	0,8	118 500	106,4	+4,6	148,0	+6,5
0,8	0,6	95 660	99,6	—1,9	147,5	+6,2
0,6	0,4	72 500	85,1	—19,3	146,0	+5,2
0,4	0,2	49 580	76,6	—32,5	145,0	+4,6
0,2	0,1	31 480	55,7	—82,2	125,0	—10,7
0,1	0,05	21 510	42,7	—137,4	108,4	—27,6
0	0	13 400	27,6	—268,0	82,0	—68,7

TABLE 3. Accuracy of the IEM

Parameters	C_A, Ci/liter		
	$1 \cdot 10^{-11}$	$1 \cdot 10^{-10}$	$5 \cdot 10^{-9}$
$\pm\delta C_A$, %	42,1	17,3	7,6
$\bar{E}_2$, MeV/liter	$1,3 \cdot 10^4$	$1,3 \cdot 10^5$	$6,5 \cdot 10^6$
$\pm\delta E_2$, %	41,0	36,9	35,9

where I_3 is the number of pulses recorded in the course of Δt_3 = 5 min at t_3 = 60 min after the end of the sample-taking process. A check comparison of the E values obtained from formulas (7') and (8), was made for industrial samples; this showed satisfactory agreement between the two (±25%). The validity of the above IEM calculation is thus confirmed.

Working Formulas and Accuracy of the IEM

The sensitivity and accuracy of the method depends greatly on the apparatus parameters. Taking the rate of driving air through the filter as v = 20 liter/min, and the efficiency of recording the collimated beam of ε = 0.15, and supposing that the aerosol capture coefficient for modern molecular filters is close to unity [7], we obtained the following simple working formulas from expressions (6) to (8):

$$\left.\begin{aligned} C_A &= (I_1 - I_2) \cdot 10^{-13} \text{ Ci/liter} \\ E &= 27I_1 = 41I_2 = 46I_3 \text{ MeV/liter} \end{aligned}\right\} \quad (9)$$

For the apparatus parameters indicated, unit concentration of RaA, $1 \cdot 10^{-10}$ Ci/liter, corresponds to the following number of recorded pulses: I_1 = 3786 and I_2 = 2779. Using these figures and a known method of calculating the statistical dispersion [8], we can find the total (statistical plus systematic) errors in determining the values of C_A and E for any given concentration of the active aerosol. Table 3 contains the values of such errors for three concentrations of RaA, referred to the apparatus parameters indicated.

The error in the determination of E was calculated on the assumption that the latent energy was found from I_2, the coefficients of the displacement of equilibrium being arbitrary.

If we take the maximum permissible error in determining C_A and E as 40%, then the sensitivity of the IEM for the apparatus parameters indicated is $1 \cdot 10^{-11}$ Ci/liter with respect to RaA and $1.3 \cdot 10^4$ MeV/liter with respect to the latent energy, which is equivalent to a concentration of equilibrium RaA equal to $1 \cdot 10^{-11}$ Ci/liter (see Table 3). The upper limit of measurable quantities is determined by the resolving power of the electronic part of the apparatus.

LITERATURE CITED

1. D. A. Holaday, et al., Problems of Radon in Uranium Mines [Russian translation], Moscow, Gosatomizdat (1961).
2. Yu. P. Bulashevich and N. P. Kartashov, Atomnaya énergiya, 6, 584 (1958).
3. E. Tsivoglon, H. Ayer, and D. Holaday, Nucleonics, No. 9, 40 (1953).
4. H. Lucas, Rev. Scient. Instrum., 28, 83 (1957).
5. H. Kusnetz, Amer. Industr. Hyg. Assoc. Quart., 17, 85 (1956).
6. K. P. Markov, N. V. Ryabov, and K. I. Stas', Atomnaya énergiya, 12, 315 (1962).
7. B. I. Ogorodnikov, et al., Atomnaya énergiya, 15, 230 (1963).
8. A. K. Mitropol'skii, Technique of Statistical Calculations [in Russian], Moscow, Fizmatgiz (1961).

HOW TO CALCULATE CHANGES IN THE CONCENTRATION OF A RADIOACTIVE ISOTOPE IN THE WATERS OF A NONCIRCULATING RESERVOIR WITH ISOTOPE ABSORPTION BY THE BOTTOM LAYER

V. M. Prokhorov

UDC 621.039.7:628.515

The absorption of radioactive contaminants gaining access to reservoir water by the bottom layer of a noncirculating water reservoir is described by Rovinskii [1] on the basis of kinetics equations. The treatment of adsorption of radioactive isotopes by the reservoir bottom layer as a first-order chemical reaction enabled the author to apply kinetic equations to data obtained for natural conditions, and thereby to forecast changes in the concentration of isotopes in the water.

A more rigorous mathematical description of the process of adsorption of radioactive contaminants by the reservoir bottom layer should reflect the assumption that the adsorption rate is governed by the rate of diffusion of the isotopes into the surface layer of the reservoir bottom. The reader should recall that the kinetics of the process are also diffusion-controlled in adsorption on ion exchange resins [2].

By considering two cases: batch access and continuous access (at a constant rate) of the isotope to the water of a flat noncirculating reservoir, we can assume that the total amount of isotope contained in the reservoir water at any instant of time is uniformly distributed throughout the volume of the water. The isotope concentration c(0, t) in the surface layer of the reservoir bottom is determined by the isotope concentration u in the water:

$$c(0, t) = ku, \tag{1}$$

where k is the distribution coefficient.

Batch ingress of isotope can be described by the solution of the diffusion equation under the following initial and boundary conditions:

$$\left.\begin{array}{l} x > 0, \quad t = 0, \quad c = 0; \\ x = 0, \quad t > 0, \quad \dfrac{\partial c}{\partial x} = \dfrac{h}{D} \cdot \dfrac{du}{dt}; \\ t = 0, \quad u = u_0. \end{array}\right\}$$

Here h = V/S is the average reservoir depth; V and S are the volume and surface area of reservoir and reservoir bottom respectively; D is the actual diffusion coefficient; $u_0 = A/V$ is the initial concentration of isotope in the water; A is the amount of isotope gaining access to the reservoir.

Under these conditions, the solution appears in the form [3]:

$$c(x, t) = u_0 k e^{\frac{kx}{h} + \frac{k^2 Dt}{h^2}} \operatorname{erfc}\left(\frac{x}{2\sqrt{Dt}} + \frac{k\sqrt{Dt}}{h}\right), \tag{2}$$

and hence,

$$\frac{u}{u_0} = e^{y^2} \operatorname{erfc} y, \tag{3}$$

where

$$y^2 = \frac{k^2 Dt}{h^2}. \tag{4}$$

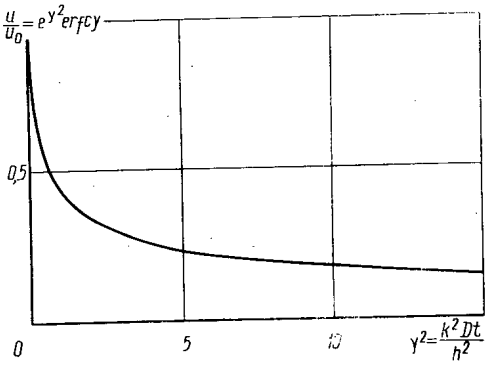

Fig. 1. Adsorption kinetics of isotope: adsorption by reservoir bottom layer in batch ingress of isotope to reservoir water.

Translated from Atomnaya Énergiya, Vol. 20, No. 5, pp. 448-449, May, 1966. Original article submitted November 1, 1965.

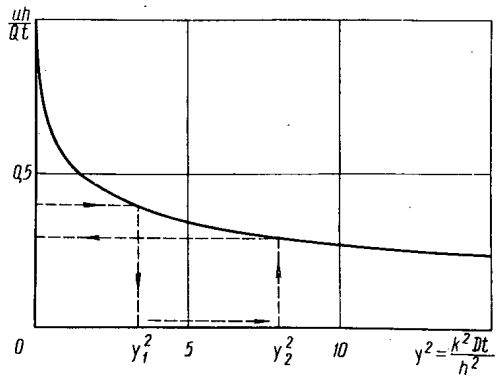

Fig. 2. Kinetics of adsorption of isotope by reservoir bottom layer in continuous ingress of isotope to reservoir water at a constant rate.

The shape of this function is seen in Fig. 1. All quantities included in y^2 have an obvious physical significance and can be found experimentally by independent measurements. Once the applicability of formula (3) to the experimental data has been demonstrated, then it becomes possible to predict changes in the isotope concentration in the reservoir water without recourse to empirical formulas.

For the case of continuous ingress of the isotope, the following initial and boundary conditions are typical:

$$\left.\begin{aligned} &x>0, \quad t=0, \quad c=0; \\ &x=0, \quad t>0, \quad \frac{\partial c}{\partial x}=\frac{h}{D}\cdot\frac{du}{dt}-\frac{Q}{D}. \end{aligned}\right\}$$

Here Q = const is the amount of isotope gaining access to the reservoir from outside in unit time through unit surface area.

The solution of the diffusion equation for these conditions is given by the formula

$$\frac{uh}{Qt}=\frac{1}{y^2}\left(\frac{2y}{\sqrt{\pi}}-1+e^{y^2}\operatorname{erfc} y\right), \tag{5}$$

which is shown graphically in Fig. 2. The right-hand side of this equation, as in the case of formula (3), depends solely on the parameter y. But if the isotope is not absorbed by the bottom layer of the reservoir, then the isotope concentration in the water would be U = QSt/V = Qt/h. Hence, the left-hand side of (5) can be restated differently:

$$\frac{u}{U}=\frac{1}{y^2}\left(\frac{2y}{\sqrt{\pi}}-1+e^{y^2}\operatorname{erfc} y\right). \tag{6}$$

Once the concentration u_1 at time t_1 is known, we can compute the concentration for any other time t_2 by using Fig. 2. (The reader should bear in mind that the average reservoir depth h and the rate of ingress Q of the isotope are also known.) To do this, we first read off the graph the value of y_1^2 corresponding to the known value of the ratio u_1h/Qt_1, and then find, from this, the numerical value of $k^2D = y_1^2h^2/t_1$. Next, substituting k^2D into formula (4), we get y_2^2 for a specific time t_2 and find the corresponding ratio u_2h/Qt_2 from the graph, using this in turn to arrive at the concentration u_2.

The case of batchwise contamination of the reservoirs is handled in similar manner, using the graph in Fig. 1, to find the concentration at any time, once the initial concentration u_0 is known.

Formulas (3) and (5) can be used for determining the total amount P of isotope absorbed by the reservoir bottom layer cumulatively up to a specific instant of time.

In the batch ingress case

$$P=(u_0-u)V, \tag{7}$$

and in the continuous ingress case

$$P=\left(\frac{Qt}{h}-u\right)V.$$

For these formulas to be useful, we have to substitute into them the formulas for u from Eqs. (3) and (5) respectively.

In the case of need we can introduce a correction for radioactive decay of the isotope during the adsorption process, multiplying the right-hand members of Eqs. (3) and (5) by the factor $e^{-\lambda t}$, where λ is the decay constant.

LITERATURE CITED

1. F. Ya. Rovinskii, Atomnaya énergiya, 18, 379 (1965).
2. F. Helferich, Ion Exchange Resins [Russian translation], Moscow, Foreign Lit. press (1962), p. 237.
3. M. Carslaw and J. Jaeger, Heat Conductivity in Solids [Russian translation], Moscow, Nauka press, (1964), p. 301.

CONFERENCE ON RESEARCH REACTOR PHYSICS AND TECHNOLOGY

G. Zhemchuzhnikov

In November 1965, the Fourth Working Conference on Research Reactor Physics and Technology was held in Budapest. Participating in the work of the conference were delegations from Bulgaria, Hungary, GDR, Poland, Roumania, USSR, Czechoslovakia, and from the Joint Institute for Nuclear Research; a delegate from the Chinese People's Democratic Republic was present at the conference.

The conference discussed 102 reports which contained: 1) reviews presented by the Soviet delegation in accordance with a resolution of the Third Working Conference (Prague, 1963); 2) the problems of rebuilding IRT and VVR research reactors with an increase in power to 4-5 MW and future increases to 10-12 MW; 3) descriptions of experimental equipment; 4) discussions of nonstationary processes (for example, reactor dynamics, critical assembly research, mechanism for the formation of explosive mixtures, and others).

S. M. Feinberg (USSR), gave a report on the prospects for research reactor development in which he noted that research reactor thermal neutron fluxes have increased during the past decade from $3 \cdot 10^{14}$ to $3 \cdot 10^{15}$ n/cm^2 · sec and now questions of future increases to $2\text{-}5 \cdot 10^6$ n/cm^2 · sec are being raised. Specific power in the core was ~ 50 kW/1 liter 10 years ago; now it has gone up to 2500 kW/liter (in the SM-2 reactor). The report discussed the problems associated with the construction of "loop" and "beam" reactors, presented some data on the MIF research beam reactor with a flux of about 10^{11} n/cm^2 · sec at the beam channel exit, and covered the features of a plan for a neutrino generator in which a favorable ratio between the desired signal and cosmic and radioactive background can be achieved by pulsed operation with high power per pulse, thus making it possible to use research reactors in a new field—research into neutrino properties.

The report given by M. N. Nikolaev (USSR), "Physical Problems in the Development of Fast Power Reactors," aroused great interest. It discussed the status and basic problems of neutron and reactor yields which have emerged in the present stage of producing fast power reactors.

Interesting reports on operating experience with the MR and SM-2 research reactors were given by V. V. Goncharov and V. A. Tsykanov. The reports described test results for individual reactor systems, presented operating results for experimental loop and channel facilities, and gave data on the radiation resistance of reflector materials, internal structures, and horizontal channels of the SM-2 reactor, etc.

A large group of problems were discussed at the conference dealing with an increase in the power of operating IRT and VVR reactors to 5-10 MW and higher. G. N. Zhemchuzhnikov and P. M. Egorenkov (USSR) presented considerations on power increase in a typical IRT reactor by using new types of fuel elements and a new system for removing heat from the reactor core. The experimental facilities of these reactors were also discussed.

K. A. Konoplev (USSR) told of a plan for modernization of the VVR-M reactor in order to expand its experimental capabilities. It is proposed to construct a special hot cell beneath the reactor which will be furnished with a viewing system and manipulators.

E. Aleksandrovich (Poland) reported on work connected with the rebuilding of the EVA reactors, which operates at 4 MW. It is proposed to increase the power to 10 MW, and a group of VVR-M fuel elements will be installed in the core for this purpose. He described their operating experience with the reactor and the changes in its construction. Reports by the Czechoslovak and Hungarian delegations were devoted to similar problems; they proposed to rebuild the core using rough fuel elements and also pipes to direct coolant flow, etc.

Several of the reports reflected the status of experimental work being done at the IRT and VVR reactors. Methods for measuring fuel element temperatures were discussed in reports presented by Hungarian and Bulgarian scientists. The measurements were made with the help of experimental fuel elements. They gave a description of the components of the technical and structural parts of the experiments, and discussed various modes of reactor operation. Several reports were devoted to the construction of experimental facilities, to the methods of working with them, and to the problems connected with their operation.

Translated from Atomnaya Énergiya, Vol. 20, No. 5, pp. 450-451, May, 1966.

Some of the reports reflected work done in connection with the use of recent advances in the production of instrumentation systems for the automatic control and protection of reactors. In the report "Automatic Control System for the VVR-S Reactor," (Roumania), they discussed the operation of a set of standard functions for the cases of power increase, power setting at a given level, power level reduction, and manual regulation. For expanding the range of system operation, stepping switches are used. The main distinguishing feature is the use of standard time functions for setting power and assuring exponential law variation, thus avoiding logarithmic and differential operation. The standard time function set is made up in the form of two operational amplifiers—an integrating amplifier and a summing amplifier. Feedback in the integrating amplifier circuit, initial conditions, and the amplification constant are different for different modes of operation. The report "New, Simplified, Transistorized Instrumentation for Control and Protection of Experimental Reactors" (Poland) discussed the dynamics of system operation in various modes. Basically, the system is composed of transistors and magnetic amplifiers. The block diagram of the system is of undoubted interest since it contains several functional units which permitted an increase in start-up safety and improvement in static accuracy and dynamic characteristics.

A Hungarian report discussed the use of pulse counters as sensors for period measurements. The instrument consists of a counting circuit, built of transistor multivibrators, and a time interval measure. As the power increases, the counters record the times when it is increased by factors of 2, 4, . . . , 2n; in this way, the instrument measures the time interval corresponding to the passage of power through these points. The instrument measures the period for doubling the number of pulses. The readings of the instrument are printed out on a special form.

A part of the reports was devoted to the development and testing of methods for investigating the physical characteristics and parameters of research reactors and critical assemblies. D. Albert, et al., (GDR) reported on measurements of neutron gas temperatures in a reactor score by means of resonance detectors of Lu^{176}, Eu^{151}, Pu^{239}, and others. The report of S. Ishmaev, et al. (USSR) presented the results of an experimental study of the process of neutron thermalization in time within hydrogen-containing moderators.

Several reports gave the results of measurements of neutron noise in reactors for the purpose of determining transfer functions and other reactor characteristics.

One of the Polish reports discussed the possibilities of controlling reactor power through the activity of N^{16} which is produced in the coolant water. It was shown that the thermal power of a reactor could be controlled by this method with an accuracy of $\pm 3\%$ regardless of the neutron flux distribution within the core.

SEMINAR AT THE USSR NATIONAL EXHIBITION

T. I. Nezhel'skaya

At the "Atomnaya Énergiya" Pavilion of the National Exhibition, a seminar was held in February 1966 on an exchange of experiences in the operation of the Luch-1 teletherapy unit with a 4000 Ci Co^{60} source which is intended for fixed irradiation of malignant tumors. Radiologists from various cities in the country and representatives of other organizations participated in the work of the seminar.

The Latvenergo factory has produced more than 30 Luch-1 teletherapy units.

Radiologists at cancer dispensaries and clinics where these units have been installed have expressed complete satisfaction with the construction of the units.

In Moscow municipal hospitals No. 40 and No. 62, the doctors received practical instruction in the methods and techniques of working with the Luch-1 unit. E. V. Pampe, chief radiologist of the Latvian SSR, told of his three-year experience in operating this unit. G. Ya. Linde and G. E. Kublyn'sh, Latvenergo factory representatives, gave instruction on the construction, assembly features, and installation of the Luch-1 unit.

A. G. Sul'kin (All-Union Research Institute for Radiation Technology) gave a report on prospective developments of teletherapy units. He reported that there are plans for the development of a new, universal teletherapy unit for rotational and fixed therapy in which the diameter of the radiation source should be reduced by a factor of 1.5-2, reducing the width of the penumbra and reducing the radiation exposure of healthy tissue. Together with the development of a universal unit for rotational and fixed therapy, there is envisaged, in creative collaboration with the leading clinics of the country, the development of new types of equipment for beam therapy of specific pathological sites. There are plans for the development of equipment for internal therapy using sources of low-energy γ-rays and bremsstrahlung and equipment for surface therapy using γ-ray sources, and for the development of other equipment.

Participants in the seminar became acquainted with other domestic equipment also: a 5 MeV linear electron accelerator, the Rokus and Volfram rotational and convergent γ-units, a 25 MeV betatron, and a modernized GUT-Co-1000 γ-unit.

At the conclusion of the meeting, seminar participants expressed the wish that further improvement of the Luch-1 unit would be accelerated, that it would be furnished with a medical table, dosimeters, centering device, a complete set of isodose curves, etc.

Translated from Atomnaya Énergiya, Vol. 20, No. 5, pp. 454-455, May, 1966.

THE UNIT OF MEASUREMENT FOR BIOLOGICAL DOSE OF IONIZING RADIATION

Yu. V. Sivintsev

In connection with the need for regulating terminology in the field of ionizing radiation dosimetry, a commission was created in 1961 under the Committee for Scientific and Technical Terminology, Division of Technology and Science, USSR Academy of Science, which recommended the introduction of a new unit of measurement for biological dose of ionizing radiation, the biological equivalent of the rad (rem), and the replacement by it of the unit, biological equivalent of the roentgen (rep) [1, 2].

As is well known, the main object of measurement in ionizing radiation dosimetry is the so-called absorbed dose, i.e., the energy transferred to unit mass of irradiated medium. The quantity, measured in rads (1 rad = 100 erg/gm), expresses the result of the interaction of the ionizing radiation field and the irradiated medium. In some cases, the absorbed dose can be determined by direct methods, for example, calorimetrically. Unfortunately, this method is characterized by low sensitivity, and is inapplicable for living tissue, in principle, which is particularly important in connection with the problems of practical dosimetry.

In the particular case of x and γ-rays of medium energy (from 200 keV to 3 MeV), there exists a simple relation between absorbed dose and ionizing radiation field which makes it possible to use an indirect method for determining the absorbed dose [3]. Such a field is quantitatively characterized by the ionizing power of the radiation or the so-called exposure dose. Its unit of measurement is the roentgen, equal to $2.08 \cdot 10^9$ ion pairs per cm^3 of dry air at 0°C and 760 mm Hg pressure. At quantum energies less than 200 keV, the same exposure dose, measured in roentgens, corresponds to different absorbed doses in soft tissue and bone. Because of the higher atomic number Z, the photoelectric effect plays a greater role in bone than in soft tissue, and the corresponding absorbed doses can differ by factors of 4-5. At quantum energies greater than 3 MeV, electron equilibrium in the irradiated medium sets in at greater depths, which has an important effect on the attenuation of the primary radiation. As a result, the exposure and absorbed doses are not comparable.

In the dosimetry of thermal, fast, or intermediate neutrons, the concept of exposure dose is generally inapplicable because of the practical absence of interactions between neutrons and air atoms. At the same time, the high ionizing power of the recoil protons produced in living tissue by the neutrons leads to a sharp rise in the recommended values for the relative biological efficiency of these radiations.

The biological effect of ionizing radiations depends not only on absorbed dose but also on dose rate, type of radiation, linear energy loss, irradiated organ, and other parameters [4]. Despite this, no objection has been raised at the present time to the natural assumption that the biological effect correlates more with the energy transferred to the tissue by ionizing radiation, i.e., with absorbed dose, than with the radiation field itself which acts upon the medium.

From this point of view, it would appear more correct to put the unit of measurement for this phenomenon in a logical relationship similar to: radiation field, interaction of radiation with matter, biological effect. However, both outside [1] and local [2] recommendations try to create a connection between the outside links of this chain, omitting the middle, uniquely and strictly physical concept. The unit, biological equivalent of the roentgen (rep), was proposed and used at a time when the concept of absorbed dose and the means for measuring it were lacking. Then, attempts to compare biological effect and ionization field (particularly x- or γ-ray fields) were justified to some degree. At the present time, when the determination of absorbed dose, i.e., the physical result of the interaction of ionizing radiation field and irradiated medium, has become the main problem of radiation dosimetry, it is necessary to look for a correlation between the energy transferred to the irradiated tissue and expressed in rads and the biological effect of that irradiation. From that point of view, it is a natural proposal to replace the unit, biological equivalent of the roentgen (rep), by the new unit, biological equivalent of the rad, which is given the definition: the biological equivalent of the rad is the amount of energy from any kind of ionizing radiation absorbed

Translated from Atomnaya Énergiya, Vol. 20, No. 5, pp. 455-456, May, 1966.

per unit mass of the irradiated biological tissue whose biological effect is equivalent to the effect of 1 rad of x-radiation with a limiting energy of 200 keV.

LITERATURE CITED

1. Recommendations of International Commission on Radiological Protection (adopted September 9, 1958), London, Pergamon Press (1959).
2. Health Rules for Working with Radioactive Materials and Sources of Ionizing Radiation [in Russian], Moscow, Gosatomizdat (1960).
3. Yu. V. Sivintsev, Atomnaya Énergiya, 9, 39 (1960).
4. Evans, Biological Effects of Ionizing Radiation, Radiation Dosimetry, G. Hine and G. Brownell, eds., [Russian translation], Moscow, Izd-vo inostr. lit., Moscow (1958).
5. W. Russell, Science, 128, 1546 (1958).

All abbreviations of periodicals in the above bibliography are letter-by-letter transliterations of the abbreviations as given in the original Russian journal. *Some or all of this periodical literature may well be available in English translation.* A complete list of the cover-to-cover English translations appears at the back of the first issue of this year.

STUDIES OF NUCLEAR REACTIONS

"Trudy" Volume 33 of the Lebedev Physics Institute Series

Edited by Academician D. V. Skobel'tsyn

Director, Lebedev Physics Institute
Academy of Sciences of the USSR

Translated from Russian

Contains nine articles prepared by leading research workers at the Lebedev Physics Institute, one of the largest research centers of the Soviet Union, on such topics as the elastic scattering of charged particles on some light nuclei, interactions of protons and tritium, and inelastic scattering of neutrons on light and medium nuclei. Other articles deal with quantum mechanics and the theory of particle interactions, scattering, and nuclear reactions.

CONTENTS: Investigation of the interaction of protons with tritium at energies below the threshold of the (p,n)-reaction, *A. B. Kurepin* • Investigation of elastic scattering of charged particles on several light nuclei at low energies, *Yu. G. Balashko* • Analysis of the *p*—T interaction above the threshold of the T (p,n) He^3 reaction, *Yu. G. Balashko and I. Ya. Barit* • Investigation of inelastic scattering of 14 Mev neutrons on light and medium nuclei, *B. A. Benetskii* • Theory of nuclear reactions and the many-body problems, *G. M. Vagradov* • Quantum-mechanical fundamentals of the theory of nuclear reactions, *V. I. Serdobol'skii* • On the phases of the elastic n—d-scattering process, *V. N. Efimov and S. A. Myachkova* • Method of time correlation functions in the description of the interaction of various particles with a complex system, and its applications, *M. V. Kazarnovskii* • Some possible ways of increasing the yield of nuclear reactions, *L. N. Katsaurov.*

222 pages 1966 $22.50
87 ill., 28 tables

Previously published in the Lebedev Physics Institute series:

Volume 25: Optical Methods of Investigating Solid Bodies
188 pages 1965 $22.50

Volume 26: Cosmic Rays
254 pages 1965 $27.50

Volume 27: Research in Molecular Spectroscopy
205 pages 1965 $22.50

In preparation:

Volume 28: Radio Telescopes
173 pages 1966 $22.50

Volume 29: Quantum Field Theory and Hydrodynamics
Approx. 240 pages 1967 $27.50

Volume 30: Physical Optics
Approx. 250 pages 1966 $27.50

Volume 31: Quantum Radiophysics

Volume 32: Plasma Physics

Volume 34: Photomesonic and Photonuclear Processes

Volume 36: Photodisintegration of Nuclei in the Giant Resonance Region

Volume 37: Electrical and Optical Properties of Semiconductors

---

OF INTEREST TO: nuclear physicists and theoretical and mathematical physicists investigating nuclear interactions.

CONSULTANTS BUREAU 227 West 17th Street, New York, New York 10011

A DIVISION OF PLENUM PUBLISHING CORPORATION